

# 博士論文

## Development of Phenylboronic Acid-Based Ligand Strategies for Intratumorally Activated Sialic Acid Targeting and Drug Delivery Enhancement

(フェニルボロン酸リガンドによる腫瘍内活性化シアル酸を標  
的とした新規ドラッグデリバリー増強戦略の開発)

東京大学大学院バイオエンジニアリング専攻

カーン タホミナ タレク

## Preface

This dissertation is the collection of studies conducted during three years of doctoral course program at The University of Tokyo (2017-2020). The aim of the study was to develop phenylboronic acid-based ligand strategies for intratumorally activated sialic acid targeting and drug delivery enhancement.

The author would like to express her heartfelt gratitude to Associate Professor Horacio Cabral for giving her the opportunity to pursue her studies at his laboratory, immense support, positive advice and great encouragement.

The author conveys her profound gratitude to Professor Kazunori Kataoka for his constructive guidance. The author also wants to express her acknowledgement to members of Kataoka Lab at Innovation Center of NanoMedicine (iCONM) specially Dr. Sabina Quader and Dr. Yuki Mochida for their support during her work at iCONM. The author is also deeply grateful with Associate Professor Akira Matsumoto of Tokyo Medical and Dental University for his precious advice.

The author is profoundly grateful to Mrs. Hiroko Koyama for all the secretarial assistance and encouragement and all the members of Cabral laboratory for their support. Finally, the author wants to express her wholehearted thankfulness and love to her family who have always encouraged and supported her.

Thahomina Tareque Khan

*Department of Bioengineering*

*School of Engineering*

*The University of Tokyo*

*June, 2020*

## Table of Contents

<b>Chapter 1: General Introduction .....</b>	<b>1</b>
1.1 Nanomedicine .....	1
1.2 Polymeric micelle as nanomedicine.....	3
1.3 Ligand installed nanomedicine .....	4
1.4 Targets.....	6
1.4.1 Cancer specific gene or protein.....	6
1.4.2 Intratumoral triggers .....	7
1.4.3 Overexpressed factors .....	9
1.5 Sialic acid as targeted epitope .....	10
1.6 Cancer stem cells .....	12
1.7 Strategies for targeting sialic acid .....	13
1.8 Nanomedicine design for sialic acid targeting .....	15
1.9 Aim and outline of thesis.....	18
1.10 References .....	19
<b>Chapter 2: Ligand validation .....</b>	<b>33</b>
2.1 Introduction .....	34
2.2 Experimental .....	36
2.2.1 Materials.....	36
2.2.2 Cell line and animals.....	37
2.2.3 Quantification of sialic acid on cancer cells .....	38
2.2.4 Analysis of expression of sialic acid in patient sample.....	38
2.2.5 <i>In-vitro</i> evaluation of 5-BPA and sialic acid binding.....	39
2.2.6 <i>In vitro</i> evaluation of 5-BPA-rhodamine.....	39
2.2.7 Conjugation of 5-BPA to acetal-PEG-amine.....	40
2.2.8 Binding constant of 5-BPA-PEG <sub>5.5K</sub> -acetal.....	40
2.2.9 Conjugation of 5-BPA and PBA to 8-arm-PEG <sub>40K</sub> -amine .....	42
2.2.10 <i>In vitro</i> cellular uptake.....	43
2.2.11 <i>In vivo</i> tumor accumulation and biodistribution .....	43
2.3. Result .....	43
2.3.1 Quantification of Sialic acid.....	43
2.3.2 Sialic acid expression in patient sample.....	46
2.3.3 <i>In-vitro</i> binding of 5-BPA.....	47
2.3.4 Polymer characterization of 5-BPA-PEG <sub>5.5K</sub> -acetal .....	51
2.3.5 Binding constant of 5-BPA-PEG <sub>5.5K</sub> -acetal.....	51
2.3.6 Polymer characterization of 8-arm-PEGs .....	53
2.3.7 Cellular uptake of 8-arm-PEGs.....	55
2.3.8 <i>In vivo</i> tumor accumulation and biodistribution of 8-arm-PEGs .....	56
2.4 Discussion.....	57
2.5 Conclusion .....	58
2.6 References.....	59
<b>Chapter 3: Preparation of DACHPt loaded 5-BPA installed polymeric micelle .....</b>	<b>63</b>
3.1. Introduction .....	64

<b>3.2 Experimental .....</b>	<b>67</b>
3.2.1 Materials.....	67
3.2.2 Synthesis of block co-polymers .....	67
3.2.3 Conjugation of 5-BPA.....	71
3.2.4 Conjugation of PBA.....	72
3.2.5 Confirmation of boron diol presence on conjugated polymer .....	72
3.2.6 Conjugation of Alexa 647 and alexa 555 to MeO-PEG <sub>10K</sub> -b-PLGA .....	73
3.2.7 Preparation of DACHPt loaded micelles.....	73
<b>3.3 Result .....</b>	<b>75</b>
3.3.1. Characterization of polymers .....	75
3.3.2 Quantification of 5-BPA conjugation.....	78
3.3.3 Quantification of PBA conjugation .....	79
3.3.4 Confirmation of presence of boron diol on conjugated block-copolymer.....	80
3.3.5 Micelle Characterization .....	81
<b>3.4. Discussion .....</b>	<b>82</b>
<b>3.5 Conclusion .....</b>	<b>83</b>
<b>3.6 References .....</b>	<b>83</b>
<b>Chapter 4: Biological activity of 5-BPA installed polymeric micelle.....</b>	<b>89</b>
<b>4.1 Introduction .....</b>	<b>90</b>
<b>4.2 Experimental .....</b>	<b>92</b>
4.2.1 Materials.....	92
4.2.2 Cell line and animals.....	93
4.2.3 Confirmation of SA cleavage from cell surface by sialidase treatment .....	93
4.2.4 Analysis of stemness in different pH.....	94
4.2.5 <i>In vitro</i> cellular uptake .....	94
4.2.6 <i>In vitro</i> cytotoxicity.....	96
4.2.7 Effect of micelles on CSCs <i>in vitro</i> .....	96
4.2.8 <i>In vivo</i> blood circulation.....	97
4.2.9 <i>In vivo</i> tumor accumulation and biodistribution .....	97
4.2.10 Antitumor activity and survival study .....	98
4.2.11 Evaluation of CSCs after treatment.....	98
<b>4.3 Result .....</b>	<b>99</b>
4.3.1 Confirmation of SA cleavage from cell surface by sialidase treatment .....	99
4.3.2 Analysis of stemness in different pH.....	100
4.3.3 <i>In vitro</i> Cellular uptake.....	101
4.3.4 <i>In vitro</i> cytotoxicity .....	106
4.3.5 <i>In vitro</i> effect of micelle in CSCs .....	107
4.3.6 <i>In vivo</i> blood circulation of micelles .....	109
4.3.7 Plasma clearance of micelles.....	111
4.3.8 Interaction of the micelles with the cellular components of blood.....	112
4.3.9 <i>In vivo</i> tumor accumulation and biodistribution .....	113
4.3.10 Antitumor activity and survival study .....	117
4.3.11 <i>In vivo</i> assessment of CSCs.....	119
<b>4.4 Discussion.....</b>	<b>121</b>
<b>4.5 Conclusion .....</b>	<b>123</b>
<b>4.6 References .....</b>	<b>123</b>
<b>Chapter 5: PBA installed polymer as immunomodulator .....</b>	<b>129</b>
<b>5.1 Introduction .....</b>	<b>129</b>



<b>5.2 Experimental .....</b>	<b>132</b>
5.2.1 Materials.....	132
5.2.1 Cell line and animals.....	132
5.2.3 Conjugation of 5-BPA and PBA to 8-arm-PEG (40k)-amine .....	133
5.2.4 <i>In vitro</i> proliferation of Jurkat cells.....	134
5.2.5 <i>In vitro</i> proliferation of mouse T cells .....	134
5.2.6 CD4 and CD8 staining of mouse T-cells.....	135
<b>5.3 Result .....</b>	<b>135</b>
5.3.1 Characterization of polymers .....	135
5.3.2 T cell proliferation assay .....	137
5.3.3 Staining of CD4 and CD8 .....	140
<b>5.4 Discussion.....</b>	<b>142</b>
<b>5.5 Conclusion .....</b>	<b>142</b>
<b>5.6 References.....</b>	<b>143</b>
<b><i>Chapter 6: Conclusion.....</i></b>	<b><i>146</i></b>
<b>6.1 Conclusion .....</b>	<b>146</b>
<b>6.2 Future Perspectives .....</b>	<b>148</b>
6.2.1 5-BPA installed polymeric micelle.....	148
6.2.2 PBA installed polymer as immunomodulator.....	149
<b>6.3 References .....</b>	<b>150</b>
<b><i>Publications.....</i></b>	<b><i>151</i></b>

# **Chapter 1**

## **General Introduction**

# Chapter 1: General Introduction

## 1.1 Nanomedicine

## 1.2 Polymeric micelle as nanomedicine

## 1.3 Ligand installed nanomedicine

## 1.4 Targets

1.4.1 Cancer specific gene or protein

1.4.2 Intratumoral triggers

1.4.3 Overexpressed factors

## 1.5 Sialic acid as targeted epitope

## 1.6 Cancer stem cells

## 1.7 Strategies for targeting sialic acid

## 1.8 Nanomedicine design for sialic acid targeting

## 1.9 Aim and outline of thesis

## 1.10 References

## 1.1 Nanomedicine

Cancer nanomedicine can be defined as the implementation of nanotechnology for the treatment and diagnosis of cancer<sup>1</sup>. Recent progress in the field of nanomaterials including organic and inorganic nanoparticles have steered the rising attention in nanomedicine area<sup>2</sup>. Nanoparticles (NPs) are defined as any shape of particles with dimensions between 1nm-100nm of any shapes. Among NPs platforms, organic NPs (e.g. layer by layer and polymer assembly<sup>3,4,5,6</sup>, lipid based<sup>7</sup> and cell membrane derived<sup>8</sup>) and inorganic NPs (eg. iron oxide<sup>9</sup>, silicon<sup>10</sup>, silver and gold<sup>11</sup>) are getting enormous attention (**Fig. 1**) and some have been approved for the treatment of cancer and are in different phases of clinical trials<sup>12</sup>. The

advantages of these NPs range from improved pharmacokinetics to reduce side effects of cytotoxic drugs. Some of the notable benefits of NPs comprise from improvement of solubility issue to pharmacokinetics<sup>13</sup>. NPs can be loaded with hydrophobic drug<sup>14,15</sup> and genes (e.g. siRNA<sup>16,17</sup>). The shell of the particle also solves stability and blood circulation issue. They are in the size range of biomolecules like nucleic acids and antibodies. NPs can be functionalized with various ligands and can be used for targeted cancer therapy thus improving efficiency and reducing unwanted toxicity<sup>18</sup>. High therapeutic payloads can be loaded in the core shell structure which protects the drug from being released until it reaches the desired target sites; once recognized by the receptor it can release the drug and cause extensive damage. NPs are accumulated in the tumor site due to enhanced permeability and retention (EPR) effect<sup>19</sup>. EPR effect is attributed to the leaky tumor vasculature and faulty lymphatic drainage system. Enhanced permeability of the tumor vasculature allows NPs to enter tumor interstitial space and defective lymphatic drainage enables retention of NPs inside the tumor thus increasing the accumulation inside tumor microvasculature. It has been evident that EPR differs from patients to patients and types of tumor. EPR may also alter with time in the same patient.

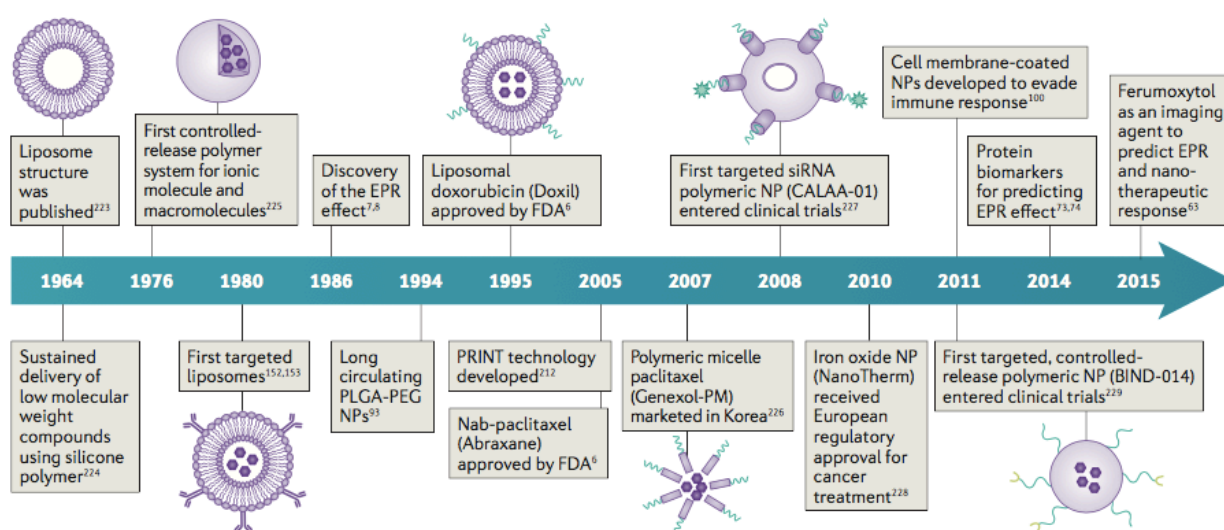


**Figure 1:** Key progresses of different NPs in the field of cancer nanomedicine<sup>13</sup>

## 1.2 Polymeric micelle as nanomedicine

Among all the NPs polymeric micelles have some unique advantages over others and is being tested in clinical trials<sup>20,21,22,14</sup>. Polymeric micelles normally have core shell structure and are an efficient cargo system to deliver poorly water soluble hydrophobic anticancer drugs. The shell can be made up of hydrophilic biodegradable materials like poly(ethylene glycol) (PEG), Poly(N-vinyl pyrrolidone) (PVP)<sup>23</sup> or poly(N-isopropyl acrylamide)(pNIPAM)<sup>24</sup> and core of the micelles can be loaded with drug. Their physical characteristics like size, shape, drug loading and chemical composition can easily be controlled<sup>25</sup>. Among all the polymers PEG is the most widely used shell forming hydrophilic part of the micelle. The sheath properties of the PEG shell reduces the recognition of NPs in blood thus prolonging blood circulation<sup>26</sup>. The benefits of using PEG is that it is biocompatible, highly water soluble, neutral charge and non-toxic. In our laboratory, we have expertise in developing self-assembled polymeric micelles using PEG. These polymeric micelles are prepared by self-assembly of PEG-poly(amino) block-copolymers<sup>5</sup> (**Fig. 2**). For example, PEG block copolymer with poly-(L-glutamic acid) side chain can form polymer-metal complexation with platinum anticancer drugs (e.g. cisplatin) in water<sup>27</sup>. As discussed earlier, the major advantages of core-shell structure are due to the shielding of hydrophobic core by PEG shell which reduces the interaction of drug with proteins and also avoids recognition by macrophages and reticuloendothelial systems (RES). This ensures prolonged blood circulation of polymeric micelles, consequently achieving higher accumulation in the tumor through EPR effect. Polymeric micelles are being designed to deliver cytotoxic agents, nucleic acids and other molecule for diagnosis and treatment of cancer<sup>14,28</sup>. One of the key advantages of our polymeric micelles is the manipulation of size which can be engineered as required<sup>29</sup>. Furthermore, specific tumor targeting and elevated accumulation can be achieved through installing ligands on the surface of the polymeric micelles<sup>30</sup>.

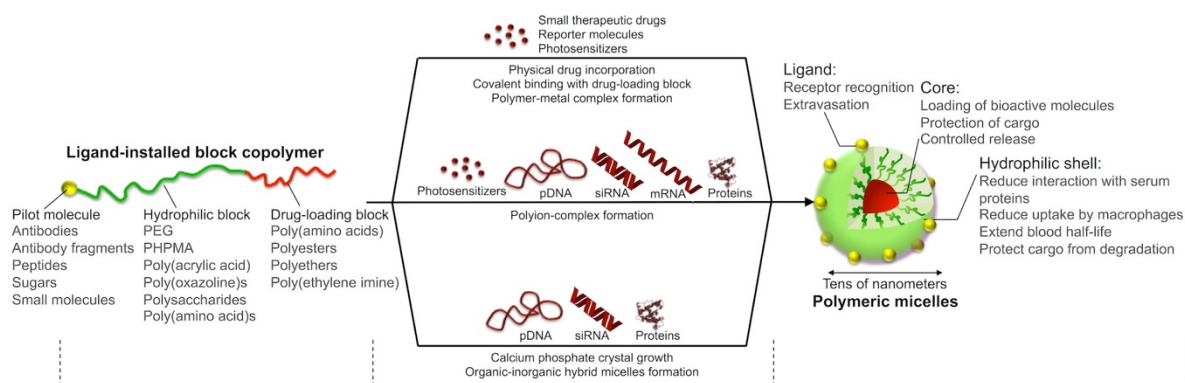


**Figure 2:** Self-assembly of polymeric micelle from PEG-*b*-poly(amino acid) copolymer which can carry biomolecule pay loads to target site<sup>5</sup>

### 1.3 Ligand installed nanomedicine

Cancer cells share many common traits with the host cells from which they are originated. So the cytotoxic drugs administered to kill cancer cells not only affect mutated cells but also the normal host cells, which is the cause of extreme side effects due to the toxicity of anti-cancer drugs. This particular reason makes administration of high doses of cytotoxic reagents necessary to exterminate the whole tumor unattainable. Even though the accumulation of nanomedicine in tumor is much higher due to EPR effect than free drug, but it is still not enough to eradicate the cancer cells completely. Targeted cancer nano-therapy can be developed by installing an antibody<sup>31</sup> or ligand (peptides<sup>32,33</sup>, nucleic acid<sup>34</sup>, aptamers<sup>35,36</sup>, small molecule<sup>37,38</sup>) on the surface of NPs which can then selectively bind with the antigens or receptor that are only present or overexpressed on cancer cells. Such targeting strategies (**Fig. 3**) can not only improve accumulation of NPs in tumor, but also avoid unspecific affect to normal cells. As discussed above, multiple NPs have been approved by FDA and are being tested in different clinical trials thus the efficacy of standard NPs can be improved by simply decorating it with specific ligand. The main concern of using antibody as targeting molecule is that they have very high binding affinity and antigens differ greatly in different types of cancer. For example, HER2 is a well-known overexpressed factor in most of the patients with breast

cancer and is a marker for targeted therapy. But the overexpression is mostly abundant for breast cancer only and the targeted treatment outcome is not as successful with other types of cancer<sup>39</sup>. Thus, the more realistic approach would be to design a system to target a universal marker that is abundant in all types of cancer. Ligand installation can improve transport of nanoparticles through tumor vasculature and increase cellular uptake by receptor mediated pathways by interacting with the target molecule. Such interaction with the cancer cells will also allow better retention of NPs inside the tumor. Moreover tumor specific ligand can not only target primary tumors, but also recognize and diminish circulating cancer cells which are responsible for metastasis. To design a ligand decorated NPs tumor related factors like cancer specific gene or protein (e.g. HER2), intratumoral triggers (e.g. acidic pH) and overexpressed factors (e.g. GLUT1, sialic acid) are of great importance. Peptides, antibodies, Fab, proteins and small molecules are being installed on the surface of NPs to target the specific molecule in tumor. Researchers have reported improved and better treatment efficacy of ligand mediated NPs compared to non-ligand NPs.

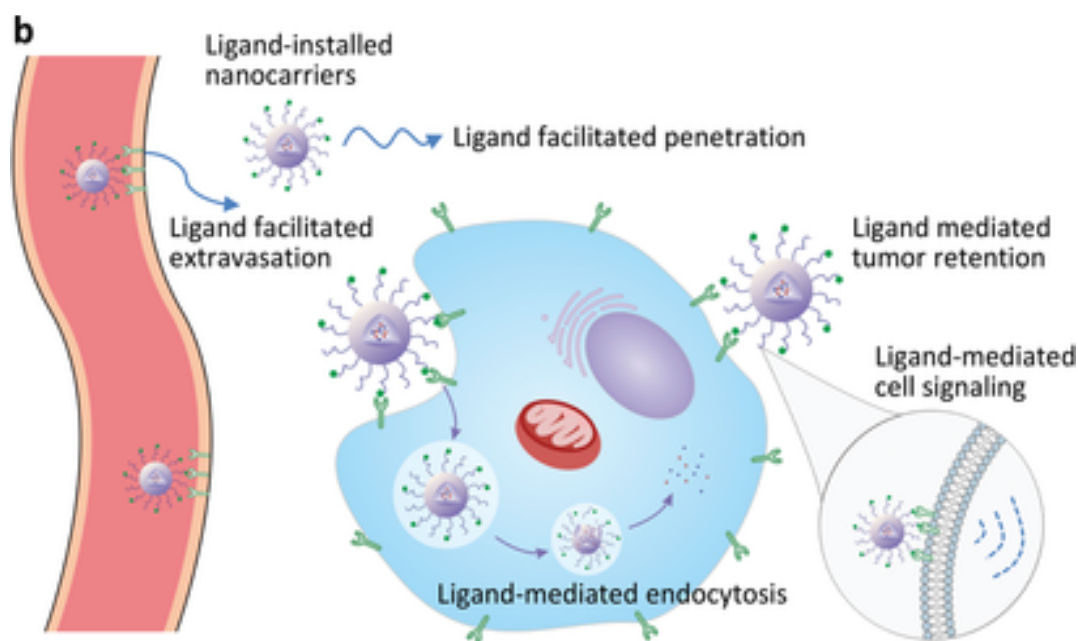


**Figure 3:** Selective targeting of ligand installed NPs

## 1.4 Targets

For the development of precise targeted tumor treatment first we need to identify specific tumor markers that distinguish them from the normal tissue. As cancer cells basically originate from the normal cells due to gene mutation and uncontrollable cell multiplication, they share similar traits with the normal cells. Years of in depth research in tumor biology have enabled us to identify numerous characteristics unique to cancer cells only. These are cancer specific genes or proteins, distinctive intratumoral condition such as acidic pH and low oxygen level and factors that are either upregulated or downregulated in tumor microenvironment to favor tumor growth. These features exclusive to tumors only have driven development of many ligand mediated therapy including NPs that are specific for treating cancer cells.

### 1.4.1 Cancer specific gene or protein

Genes are the governor of accurate cell function and does so through making proteins. Mutation in one or more genes in cell is the reason of beginning of all cancers. Gene mutation can generate abnormal protein or even hinder synthetization of proteins. Thus, the altered information provided by the abnormal protein induces uncontrollable cancerous cell division. Many of the mutated genes and abnormal proteins have been identified to play key roles in cancer formation. Transmembrane proteins (TMEM) TMEM48 or TMEM97<sup>40</sup>, human epidermal growth factor receptor 2 (HER2)<sup>39</sup>, tumor protein p53/TP53<sup>41</sup>, breast cancer type 1&2 (BRCA1 or BRCA2)<sup>42</sup> and RAS<sup>43</sup> are some of the most well-studied mutated genes or proteins in cancer. They are being studied as cancer biomarkers for targeted cancer therapy due to their specificity to tumor only. The augmentation of HER2 gene is associated with aggressiveness of breast cancer<sup>44,45</sup>. HER2 have been designated as a vital biomarker for identifying lymph node metastasis and progressiveness of breast cancer<sup>46,47</sup>. There have been efforts in developing targeted therapy towards HER2<sup>48</sup>. But the expression of HER2 is limited



to 20-25% among all the breast cancer<sup>49</sup>. Similarly, 80% BRCA1 positive breast cancers are triple-negative breast cancer (TNBCs)<sup>50,51</sup>, which is only 10% of the total TNBCs<sup>52</sup>. For targeting BRCA 1 or 2 positive breast cancer poly(ADP-ribose) polymerase (PARP) inhibitors are being investigated<sup>42</sup>. Mutation of RAS gene is much more widely seen in 27% of all type of cancers and regarded as the utmost generally mutated gene. But targeting RAS have been challenging due to the absence of drug binding sites and farnesyltransferase inhibitors are being used to directly target them<sup>43</sup>. Thus, targeting a cancer specific gene or protein can only be applied for a particular type of tumor only and a universal targeting moiety is more practical for ligand based therapy.

### 1.4.2 Intratumoral triggers

The condition of intratumoral microenvironment are of great importance for designing targeted nanomedicine. Tumors have some unique characteristics compared to healthy tissues due to their abnormal proliferation capability, angiogenesis and high requirement of ATP. Moreover, such unusual properties lead the tumor microenvironments to have low pH, decreased glucose concentration and hypoxia. These are all interrelated and are being exploited for targeted cancer therapy. Cancer therapy that can be activated at low pH<sup>53</sup> or hypoxic condition<sup>54</sup> are being developed thus highlighting their importance.

In general tumor tend to have lower pH than the normal tissues due to aberrant aerobic glycolysis; this phenomenon is known as Warburg effect<sup>55</sup>. Such low pH of tumor have been branded as the culprit for local invasion of cancer<sup>56</sup>. Due to increased glycolysis, tumor cells generate increased amount of lactic acid and protons in cytoplasm compared to normal cells. Produced lactic acid and protons are constantly flashed out of cells to keep the intracellular pH near neutral. Moreover, titration of intracellular acid with bicarbonate and release of CO<sub>2</sub> by pentose phosphate from cells also contributes to the acidic microenvironment of tumor<sup>57</sup>.

Moreover, poor perfusion of tumor debilitates its ability to transport produced acid through diffusion. Due to this the extracellular pH of cancer cells is typically lower than the intracellular pH<sup>58</sup>. The pH gradient in tumor is opposite to that of the normal tissues. This low pH phenomenon of tumor has been validated by researchers<sup>59</sup>. Extracellular pH is lowest near the cell membrane<sup>60</sup> and progressively rises with distance from the cell surface. Peritumoral acidic pH has also been proved to associate in metastasis<sup>61</sup> and lowest pH region in tumor contributed to the highest tumor invasion<sup>56</sup>. Researchers have long been taking advantage of this unique acidic nature of tumor to design cancer targeted nanomedicine like pH sensitive polymeric nanocarriers<sup>53</sup>. The acidic pH of tumor is of great importance in this research. As, pH plays a significant role in interaction of sialic acid (SA) with different sugar. We have recently identified a boronic acid ligand that has very specific binding to SA in acidic pH (intratumoral pH).

Tumor hypoxia is considered as one of the core problems in cancer treatment as it makes the tumor resistant to chemotherapy and radiation thus paving the way for more aggressive and metastatic tumor<sup>62</sup>. Moreover, hypoxia related features like hypoxia-inducible factor 1a (HIF-1a) and enzyme CAXII have been confirmed to play key roles in tumor prognosis and metastasis. HIF-1 is also a major target for mapping tumor hypoxia<sup>63</sup>. Hypoxic condition in solid tumor have been correlated with poor survival outcome. Measurement of oxygen in tumors collected from patient have been quantified between 1.3 – 3.9% (10 – 30 mmHg). The measurement was recorded as low as 0.01% (0.08 mmHg) in some tumors. The amount of oxygen tensions was considerably higher 3.1 – 8.7% O<sub>2</sub> (24 – 66 mmHg) in normal tissue<sup>64</sup>. It is reported that severe hypoxia (pO<sub>2</sub><0.33%, 2.5 mmHg) observed in some tumor does not happen in normal tissue thus making low oxygen as an excellent trigger for targeted cancer therapy<sup>65</sup>. One of the main drawback is that the distance of hypoxic region from blood vessels makes it difficult to deliver cytotoxic drugs in the area. Furthermore, cancer cells in the

severe hypoxic area are mostly nondividing cells thus requiring extraordinary cytotoxicity and specificity of delivered drugs. As under reduced O<sub>2</sub> condition proliferation of cancer cells is seized, which hinders the efficacy of chemotherapeutic drugs like cisplatin and doxorubicin that works on the dividing cells as DNA damaging agents<sup>66</sup>. Thus, efforts are being made to develop nanomedicine to activate and target the hypoxic condition of the tumor<sup>67,68</sup>. Moreover, the hypoxic condition in tumor also induces acidosis of tumor microenvironment thus benefiting the lower pH condition.

### 1.4.3 Overexpressed factors

Apart from cancer specific gene and intratumoral triggers there are some well reported molecules that are overexpressed in cancer cells and are being exploited for developing targeted cancer therapy. To name a few epidermal growth factor receptor (EGFR)<sup>70</sup>, CD44<sup>71</sup>, integrin  $\alpha v \beta 3$ <sup>72</sup> and SA<sup>73</sup> have been reported to be augmented in tumor microenvironment compared to normal tissues. Efforts are being made to target these overexpressed molecule as they are associated with most of the cancers regardless of the type and origin. EGFR is a well-studied overexpressed surface receptor in many cancers specially in lung cancer<sup>70</sup>. There have been many research to target EGFR in tumor microenvironment<sup>74</sup>. NPs have been developed with EGFR binding ligand such as peptides: GE11<sup>75,76</sup> or antibodies: cetuximab<sup>77</sup>. Such targeting have improved the treatment efficiency. Another factor CD44 that is overexpressed in cancer cells particularly in cancer stem cells (CSCs)<sup>78</sup> can be found on different cells including endothelial and parenchymal liver cells<sup>79</sup>. CD44 have been identified as an important molecule with significant influence in different types of cancers including head and neck, skin, lung, breast, prostate, pancreatic and liver cancer<sup>80,81,82</sup>. In our body CD44 can activate EGFR and ErbB-2 by binding with hyaluronan (HA) to induce cell adhesion<sup>83,84</sup>. Thus, there have been several studies to target CD44 using HA as a ligand on NPs surface<sup>85,86</sup>. Another family

of overexpressed cell surface receptors are integrins which are being exploited as a target for cancer therapy<sup>87</sup>. They are key player in cell-to-extracellular matrix (ECM) adhesion. They can also trigger cellular signal pathways leading to cell division and relocation. There are total 24 known subunits of integrins among them  $\alpha 5\beta 1$ ,  $\alpha v\beta 3$ ,  $\alpha v\beta 5$ ,  $\alpha v\beta 6$  and  $\alpha v\beta 8$  have been associated with malignant cancer<sup>72</sup>. These integrins can be targeted with Arg-Gly-Asp (RGD) peptide. Cyclic RGD have been conjugated to NPs surface to target integrins overexpressed in cancer cells<sup>88,89,90</sup>. Overexpression of cell surface SA in cancer, strategies to target SA and importance will be discussed separately in detail in the following sections.

## 1.5 Sialic acid as targeted epitope

Cells are coated with a layer of carbohydrates, *i.e.* glycans, composed of branched oligomer or polymer of monosaccharides. The glycan chain have been named the glycocalyx<sup>91</sup>. These glycans are responsible for encoding the glycome, which is the common language used by the cells to communicate<sup>92</sup>. There are various types of glycans comprising glycolipids, glycoproteins and proteoglycans. The family of glycan in the group that is of our interest is SA, the terminal group of the glycan chain<sup>93</sup>, which regulates a range of pathological processes. SA is negatively charged, hydrophilic molecule and they are involved in various cellular processes<sup>94</sup>. SA contributes in avoiding cell-cell interaction and filtering function of kidney. Altered glycosylation is a trademark of almost all type of cancers and minor alteration in glycan can trigger severe consequences in tumor biology<sup>95,96,97</sup>. The alteration is predominantly hyper activation of cancer related sialylated glycans<sup>98</sup>. Cancer cells of different origins overexpress sialoglycans including SLe<sup>X</sup>, SLe<sup>A</sup>, GM2 and STn on the surface of glycoproteins or glycolipids<sup>99</sup>. Anomalous and hyper expression of SA are unanimous feature of cancer cells of different type and origin<sup>96</sup>. Moreover, tumor prognosis and malignancy has been reported to be strongly related to the over expression of SA<sup>100</sup>.

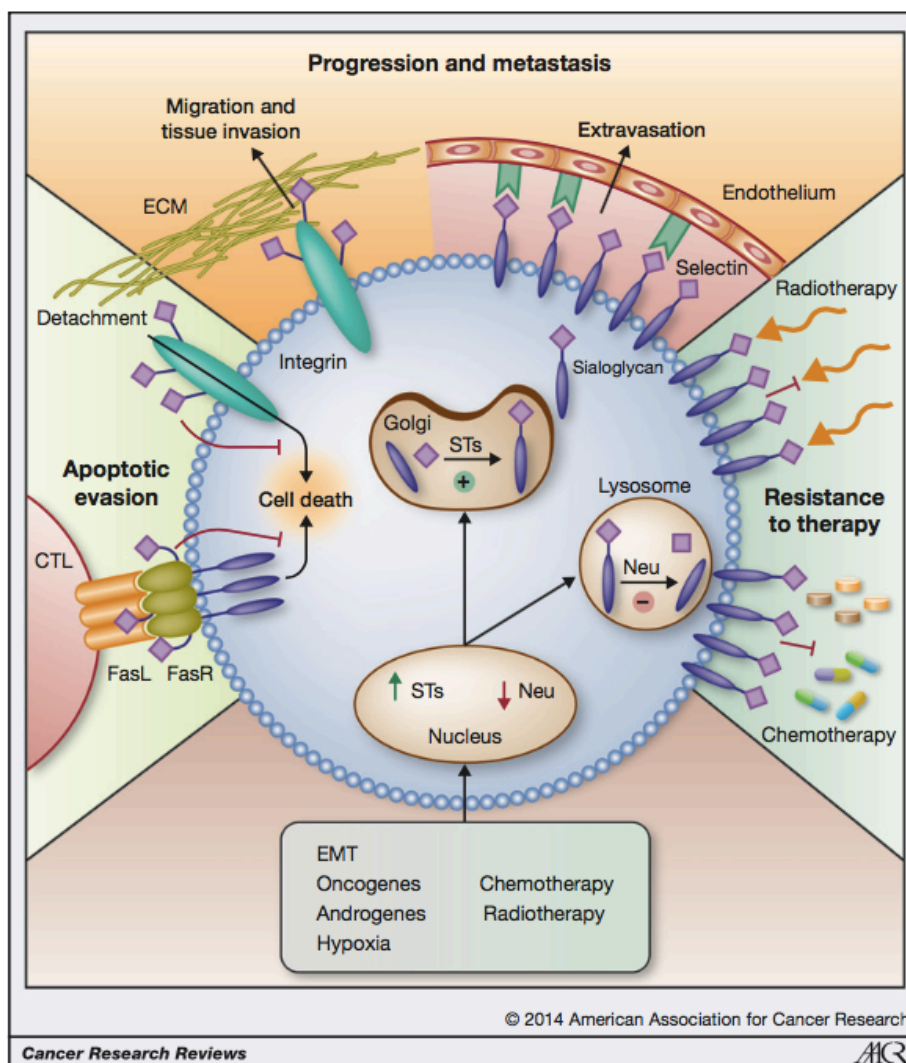


**Figure 4.** Effect of aberrant sialylation in cancer progression and metastasis<sup>101</sup>

The overexpression of SA on cancer cells have been described as their immune evasion mechanism from immune cells<sup>102</sup>. The ability of SA to modulate immune regulatory system is attributed as the cause for increased expression in cancer cells (**Fig. 4**)<sup>101</sup>. This overexpression of SA is reported to be more common than oncogene markers, such as HER2/ neu<sup>103</sup>, which makes SA as a universal targeting antigen for all type of tumors and recent advances in glycan study have prompted attention in developing strategies by targeting SA for cancer treatment<sup>104</sup>. Hypersialylation in cancer cells promotes features including increased migration and apoptosis resistance which is beneficial for tumor growth and affiliated with aggressiveness and prognosis for cancer patients<sup>105,106</sup>. Moreover, altered glycosylation of CSCs marker CD44v

and their expression have been linked with aggressiveness of cancer in clinical patients<sup>107</sup>. Therefore, targeting SA can yield an approach to eliminate both resistant CSCs and differentiated cancer cells. Hence, SA represents a broad marker for tumor targeting of therapeutic agents. Nevertheless, SA is also expressed in healthy tissues, thus, hindering the development of such targeting strategies. We will discuss benefits and shortcomings of various targeting ligand for SA in details in a separate section.

## 1.6 Cancer stem cells

Cancer stem cells (CSCs) also known as the cancer initiating cells (TICs) are deemed as one of the main reason of tumor relapse. Back in 1963 researchers reported cells with the ability of self-regeneration can form colonies in the spleen<sup>108</sup>. Such cell population were also reported in different type of cancers e.g. head and neck cancer<sup>109</sup>, liver cancer<sup>110</sup>, breast cancer<sup>111</sup>, brain cancer<sup>112</sup> and melanoma<sup>113</sup>. The name CSCs for this subpopulation of cells with self-renewal ability was first introduced in 2001<sup>114</sup>. Researchers have not yet been able to clearly uncover the origin of CSCs; but speculated the origin may be altered depending on the stage of cancer and possibly different inside the same tumor histology. The theories are that CSCs are the result of epithelial to mesenchymal transition (EMT) which allows differentiated and non-stem cells to develop characters like CSCs<sup>115</sup>; or alteration of non-malignant stem cells to CSCs due to oncogenic somatic mutation<sup>116</sup>. Till date one of the biggest challenge remnants are recognizing and isolating CSCs, as they consists only a tiny portion (usually less than 1%) of tumor which is made up of diverse cell population<sup>117</sup>. In recent years couple of markers of CSCs have been identified such as epithelial cell-adhesion molecule, CD44, CD133 and also an enzyme aldehyde dehydrogenase whose activity is upregulated in CSCs<sup>118</sup>. CD44 is a transmembrane glycoprotein with the ability to activate EGFR and ErbB-2 by binding to the extracellular matrix probably through HA mediated cell adhesion. Such activation have been linked to

increased cell differentiation and relocation<sup>83</sup>. CD44 can be found on leukocytes, mesenchymal cells, endothelial and parenchymal liver cells<sup>79</sup>. CD44 have been confirmed to be a major player in different types of cancers like head and neck, skin, lung, breast, prostate, pancreatic and liver cancer<sup>80,81,82</sup>. Thus, being hailed as a universal biomarker for CSCs. But the appearance of different isoform of CD44 (CD44v) is much more rare compared to standard CD44. Both the standard and variants of CD44 are reported to have altered N- and O- linked glycosylation. Such difference in the glycosylation is associated with their altered molecular weight<sup>119,120</sup>. Researchers have also reported the importance of five probable N-linked glycosylation locations on CD44 to initiate cell binding through HA<sup>121</sup>. Moreover, HA adhesion in ovarian cancer is also controlled by glycosylation of CD44<sup>122</sup>. Depending on the modification of glycosylation it can amplify or inhibit attachment of CD44 to HA. For example, improved binding have been reported via , O-linked glycans (N-deglycosylated), N-linked N-acetylglucosamine deposit and N-acetylgalactosamine recruitment in non-N-linked glycans on CD44. On the contrary,  $\alpha$  2, 3- linked SA on N-linked glycans have opposite effect and hinders such binding<sup>123</sup>. Furthermore, distorted glycosylation of CD44v and their expression have been linked with aggressiveness of cancer in clinical patients<sup>107</sup>. Therefore, the SA modification of CD44 and their expression in malignant tumor suggest the possibility of targeting such resistant cells via overexpressed SA.

## 1.7 Strategies for targeting sialic acid

Treatment strategies directing towards abnormal sialylation emerged as an appealing option<sup>124</sup> as their vital role in immune escape, cancer progression and metastasis have been well evidenced<sup>73</sup>. There have been reports on development of therapeutic and diagnostic approaches directed towards aberrant sialylation<sup>125</sup>. These tactics includes both targeting overexpressed SA in tumor to deliver therapeutic agents<sup>38,126,127,128</sup> and blocking SA by using glycomimetics<sup>129</sup>.

Furthermore, glycomimetic drugs such as Uproleselan (GMI 1271) and Rivipansel (GMI 1070), which are both selectin (SA binding molecule) inhibitors, are being tested in clinical trials for treating acute myeloid leukemia (NCT03616470)<sup>130,131</sup>. SA blockade approach may have proinflammatory effect and improve elimination of cancer cell by increasing amount and activation state of CD8<sup>+</sup> cells and reducing number of myeloid and regulatory T cells<sup>129</sup>. Polymer based imaging systems<sup>132,133,134</sup> and sensor based SA detection techniques<sup>135,136</sup> are also being developed to study cancer cells. Furthermore, researchers have also explored the idea of using phenylboronic acid (PBA) conjugated polymer as a mitogen to engage T cells and induce proliferation<sup>137,138</sup>. Such polymer system have been verified to induce proliferation of spleen lymphocytes collected from mice with elevated amount of IL-2 on the cell surface and demonstrated cytotoxic ability in combination with IL-2 treatment against YAC-1 cells. The reason for such proliferation phenomenon was probably due to the interaction between cell surface SA of lymphocyte and PBA molecule. Most of these systems are based on unique interaction of PBA and SA<sup>139</sup>. Targeting strategies with highly selective molecule for SA such as lectin<sup>140</sup> and antibodies<sup>141</sup> are challenging for systemic use due to their immunogenicity. Thus, development of ligands capable of recognizing tumor SA, while avoiding interaction with SA in healthy tissues, is still necessary for advancing SA targeted strategies. PBA can form ester bonds with diol-bearing molecules and shows selectivity to SA at intratumoral pH (pH 6.5). In fact, sugars, such as the common monosaccharides (*e.g.* glucose), contain diols, and as a consequence, boronic acids have proven to be helpful molecular ligands for binding and detection, working as synthetic lectins<sup>134</sup>. While the binding of boron to diol-containing molecules is commonly promoted at basic pH, the binding constant between these agents drops at neutral and acidic pH. On the other hand, the binding of boronic acids to SA opposes this trend, and the binding constant between boronic acid compound and SA increases at acidic pH<sup>142</sup>. For example, complexes between PBA and sugars were shown to be stable at pH higher



than their pKa, however, with pH lower than pKa only SA-PBA complexes were stable<sup>143</sup>. Such binding behavior of boronic acids could be exploited for selective recognition of SA at intratumoral pH conditions, which range between pH 6.5 to pH 7.2<sup>38</sup>. As the interaction between SA and PBA is low, we have concentrated on improving binding affinity of PBA to SA at intratumoral pH, which can further improve the tumor targeting ability. Recently, we have reported the superior affinity of 5-BPA for SA at intratumoral pH that is much higher compared to PBA<sup>142</sup>. The unique ability of 5-BPA to have specific and high binding to SA at reduced pH makes it an excellent targeting molecule directed towards hypersialylated cancer cells.

## 1.8 Nanomedicine design for sialic acid targeting

SA is can be recognized by selectins or SA-binding immunoglobulin-like lectins. Researchers have been trying to target SA by using lectin<sup>140</sup> and antibodies<sup>141</sup>. But they are yet to be used systematically due to their immunogenicity. Selectins are also present in endothelial cells, erythrocytes and leucocytes. So the binding of ligands at these sites are critical for targeting. Boronic acids are compounds which display the ability to forms reversible covalent interactions with diol molecules<sup>144</sup>. This ability has, in recent years, led to their use synthetic sugar receptive systems; sugars such as the common monosaccharides, fructose, glucose, mannose and galactose all contain such diol functional group, and as a consequence, boronic acids have provided to be a helpful molecular ligand for their binding and detection, and are sometimes consider to be synthetic lectins<sup>145,146</sup>. PBA have been reported to selectively recognize SA overexpressed on cancer cells to assess cancer metastasis<sup>136</sup>. In our laboratory, we have previously developed PBA installed polymeric micelles using PEG-*b*-PLGA block copolymer (**Fig. 5**)<sup>38</sup>. These PBA installed polymeric micelles were more selective to cancer cells than non-ligand micelles with similar circulating profile and no specific interaction with blood

component. This may be due to the binding of PBA with glucose while circulating as the concentration of glucose is much higher in blood stream. PBA can form ester bonds with diol-bearing molecules above physiological pH (pH 7.4), while at intratumoral pH (pH 6.5), it shows selectivity to SA. Complexes between PBA and sugars are stable at pH higher than their pKa, however with pH lower than pKa only SA-PBA complexes were found to be stable<sup>139</sup>. Therefore, polymeric micelles with PBA ligands on their surface can improve tumor targeting. These micelles achieved enhanced intracellular drug delivery in cancer cells at intratumoral pH after attaching to the SA on the cell surface<sup>38</sup>.

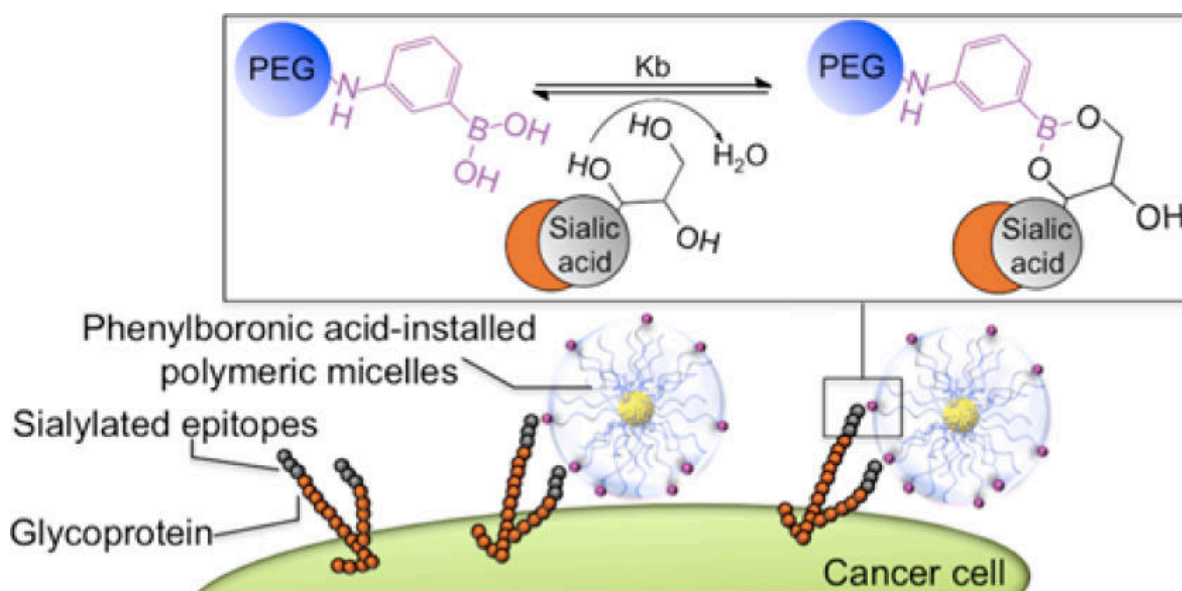


**Figure 5.** Recognition of SA by PBA-installed polymeric micelle<sup>38</sup>

However, the binding affinity of PBA for SA is relatively weak, and the installation of PBA derivatives with higher affinity for SA could provide enhanced targeting efficiency. Advantageously, we have recently identified the high affinity of 5-boronopicolinic acid (5-BPA) for SA at intratumoral pH<sup>142</sup>. After screening many boronic acid derivatives, 5-BPA a pyrimidine boronic acid was found to have higher binding affinity to SA compared to other sugars and it also demonstrated to be very specific to SA at reduced pH (**Fig. 6A**)<sup>142</sup>. Furthermore, binding with 5-BPA to other sugar like glucose is higher in neutral to alkaline condition but decreases in acidic condition. Such unique and pH depending reverse binding

affinity of 5-BPA to SA and glucose will allow the binding of ligand to shift from glucose in blood (pH 7.4) to SA in tumor microenvironment (pH 6.5-7.2). The binding affinity to SA was almost 30 fold higher compared to conventional PBA molecule at pH 6.5. Therefore, 5-BPA is an excellent choice of ligand for targeting intratumoral overexpressing SA.

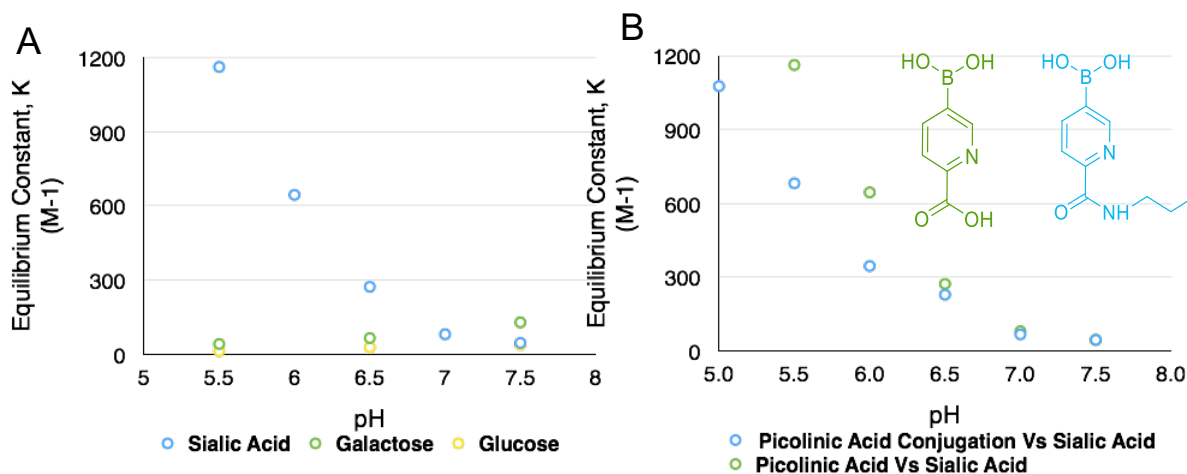


**Figure 6.** A) pH dependent binding constants of 5-BPA (picolinic acid) with sialic acid, galactose and glucose. B) pH dependent binding constants of 5-BPA (picolinic acid) and propyl amine conjugated 5-BPA (picolinic acid) with sialic acid<sup>142</sup>.

Advantageously, the 5-BPA molecule have a carboxylic acid group which can be easily conjugated with primary amine containing compounds using simple coupling reagents. To verify retention of binding constant of 5-BPA to SA researchers conjugated 5-BPA to propyl amine. They evaluated the binding constant of 5-BPA conjugate to SA and compared with values that of free 5-BPA. They confirmed after obtaining comparable binding constant values that 5-BPA still maintains its ability to bind with SA even after conjugation(**Fig. 6B**)<sup>142</sup>. Hence, proving rationale to use 5-BPA as a tumor targeting ligand on the surface of NPs. Besides, DACHPt loaded polymeric micelles (NC-4016) is undergoing phase I clinical trials for treating solid tumors and lymphoma (Study NCT01999491)<sup>6</sup> after demonstrating better performance in a xenograft model of gastric cancer<sup>147</sup>. We hypothesize by installing 5-BPA ligand on the

surface of DACHPt loaded micelle to specifically target cancer cells can further improve the treatment outcome.

## 1.9 Aim and outline of thesis

Overexpression of SA in cancer cells makes them an attractive target moiety. Our group has already been successful in targeting SA by installing PBA on micelle surface. Accordingly, we developed 5-BPA installed polymeric micelles loading a platinum drug, *i.e.* ((diaminocyclohexane)platinum(II) (DACHPt)) which is the active complex of clinically approved chemotherapeutic drug oxaliplatin. The ability of these micelles to specifically target SA in acidic pH was verified through improved *in vitro* cellular uptake and cytotoxicity. They were also effective in reducing highly malignant CSCs, which are involved in tumor aggressiveness and relapse, and have increased SA level. Thus, overall improving tumor growth suppression and survival in orthotopic human oral carcinoma (HSC2) bearing mice.

The thesis is composed of five chapters. **Chapter 1** and **Chapter 6** are general introduction and conclusion respectively.

In **Chapter 2**, quantification of sialic acid in different *in vitro* cultured cancer cell lines and tumor samples collected were reported. The concept of pH dependent binding of 5-BPA to cancer cell surface SA was verified. Retention of binding constant of 5-BPA after polymer conjugation was confirmed. Finally, superiority of 5-BPA over PBA was validated using Cy5 dye labeled 5-BPA-8-arm-PEG and PBA-8-arm-PEG through *in vitro* and *in vivo* assessment.

In **Chapter 3**, PEG-*b*-PLGA block copolymers were synthesized and characterized. PBA and 5-BPA was conjugated to the end terminus of PEG. Alexa 555 and 647 dye conjugated PEG<sub>10K</sub>-*b*-PLGA were prepared to construct fluorescent micelle. Existence of boron diol on 5-BPA and PBA conjugated block-copolymer was confirmed before micelle preparation.

Ultimately, DACHPt loaded polymeric micelles were constructed with 50% surface ligand (5-BPA or PBA) and characterized (size, PDI, drug loading and surface charge)

In **Chapter 4**, evaluation of biological activity of micelles are reported. Removal of sialic acid through sialidase treatment was confirmed before performing controlled *in vitro* studies. Effect of media pH on CSC population was studied. Evaluation of cellular uptake of the micelles by measuring internalized Pt and tracing fluorescent-labeled micelles using CLSM are reported. Cytotoxicity evaluation and effect of micelles on CSC population are stated. Subsequently, blood circulation and plasma clearance of the micelles was determined. Finally, *in vivo* studies using DACHPt loaded non-ligand and 5-BPA or PBA installed micelles including tumor accumulation, biodistribution, antitumor activity, survival and effect on CSC population are studied.

In **Chapter 5**, conjugation and *in vitro* proliferation assays of jurkat cell and mouse T cells after stimulation with 5-BPA and PBA conjugated 8-arm-PEGs are described. Effect of polymers on CD4 and CD8 positive cells collected from mice were studied.

In this dissertation the author tries to improve the targeting ability of drug carrier through ligand installation.

## 1.10 References

1. Hartshorn, C. M. *et al.* Nanotechnology Strategies To Advance Outcomes in Clinical Cancer Care. *ACS Nano* **12**, 24–43 (2018).
2. Björnalm, M., Thurecht, K. J., Michael, M., Scott, A. M. & Caruso, F. Bridging Bio–Nano Science and Cancer Nanomedicine. *ACS Nano* **11**, 9594–9613 (2017).
3. Richardson, J. J., Bjornmalm, M. & Caruso, F. Technology-driven layer-by-layer assembly of nanofilms. *Science (80-. )*. **348**, aaa2491–aaa2491 (2015).
4. Richardson, J. J. *et al.* Innovation in Layer-by-Layer Assembly. *Chem. Rev.* **116**, 14828–14867 (2016).
5. Cabral, H., Miyata, K., Osada, K. & Kataoka, K. Block Copolymer Micelles in

- Nanomedicine Applications. *Chem. Rev.* **118**, 6844–6892 (2018).
6. Varela-Moreira, A. *et al.* Clinical application of polymeric micelles for the treatment of cancer. *Mater. Chem. Front.* **1**, 1485–1501 (2017).
  7. Grimaldi, N. *et al.* Lipid-based nanovesicles for nanomedicine. *Chem. Soc. Rev.* **45**, 6520–6545 (2016).
  8. Fang, R. H., Jiang, Y., Fang, J. C. & Zhang, L. Cell membrane-derived nanomaterials for biomedical applications. *Biomaterials* **128**, 69–83 (2017).
  9. Hühn, J. *et al.* Selected Standard Protocols for the Synthesis, Phase Transfer, and Characterization of Inorganic Colloidal Nanoparticles. *Chem. Mater.* **29**, 399–461 (2017).
  10. Croissant, J. G., Fatieiev, Y. & Khashab, N. M. Degradability and Clearance of Silicon, Organosilica, Silsesquioxane, Silica Mixed Oxide, and Mesoporous Silica Nanoparticles. *Adv. Mater.* **29**, 1604634 (2017).
  11. Yang, X., Yang, M., Pang, B., Vara, M. & Xia, Y. Gold Nanomaterials at Work in Biomedicine. *Chem. Rev.* **115**, 10410–10488 (2015).
  12. Anselmo, A. C. & Mitragotri, S. Nanoparticles in the clinic: An update. *Bioeng. Transl. Med.* **4**, (2019).
  13. Shi, J., Kantoff, P. W., Wooster, R. & Farokhzad, O. C. Cancer nanomedicine: Progress, challenges and opportunities. *Nature Reviews Cancer* **17**, 20–37 (2017).
  14. Cabral, H. & Kataoka, K. Progress of drug-loaded polymeric micelles into clinical studies. *J. Control. Release* **190**, 465–476 (2014).
  15. Patra, J. K. *et al.* Nano based drug delivery systems: recent developments and future prospects. *J. Nanobiotechnology* **16**, 71 (2018).
  16. Salzano, G., Navarro, G., Trivedi, M. S., De Rosa, G. & Torchilin, V. P. Multifunctional Polymeric Micelles Co-loaded with Anti-Survivin siRNA and Paclitaxel Overcome Drug Resistance in an Animal Model of Ovarian Cancer. *Mol. Cancer Ther.* **14**, 1075 LP – 1084 (2015).
  17. Young, S. W. S., Stenzel, M. & Jia-Lin, Y. Nanoparticle-siRNA: A potential cancer therapy? *Crit. Rev. Oncol. Hematol.* **98**, 159–169 (2016).
  18. Yoo, J., Park, C., Yi, G., Lee, D. & Koo, H. Active Targeting Strategies Using Biological Ligands for Nanoparticle Drug Delivery Systems. *Cancers (Basel)*. **11**, 640 (2019).
  19. Matsumura, Y. & Maeda, H. A New Concept for Macromolecular Therapeutics in Cancer Chemotherapy: Mechanism of Tumoritropic Accumulation of Proteins and the

- Antitumor Agent Smancs. *Cancer Res.* **46**, 6387 LP – 6392 (1986).
20. Danson, S. *et al.* Phase I dose escalation and pharmacokinetic study of pluronic polymer-bound doxorubicin (SP1049C) in patients with advanced cancer. *Br. J. Cancer* **90**, 2085–2091 (2004).
  21. Hamaguchi, T. *et al.* A phase I and pharmacokinetic study of NK105, a paclitaxel-incorporating micellar nanoparticle formulation. *Br. J. Cancer* **97**, 170–176 (2007).
  22. Lee, K. S. *et al.* Multicenter phase II trial of Genexol-PM, a Cremophor-free, polymeric micelle formulation of paclitaxel, in patients with metastatic breast cancer. *Breast Cancer Res. Treat.* **108**, 241–250 (2008).
  23. Benahmed, A., Ranger, M. & Leroux, J. Novel Polymeric Micelles Based on the Amphiphilic Diblock Copolymer poly(N-vinyl-2-pyrrolidone)-block-poly(D,L-lactide). *Pharm. Res.* **18**, 323–328 (2001).
  24. Chung, J. ., Yokoyama, M., Aoyagi, T., Sakurai, Y. & Okano, T. Effect of molecular architecture of hydrophobically modified poly(N-isopropylacrylamide) on the formation of thermoresponsive core-shell micellar drug carriers. *J. Control. Release* **53**, 119–130 (1998).
  25. Cabral, H. & Kataoka, K. Multifunctional nanoassemblies of block copolymers for future cancer therapy. *Sci. Technol. Adv. Mater.* **11**, 014109 (2010).
  26. Kim, S., Shi, Y., Kim, J. Y., Park, K. & Cheng, J.-X. Overcoming the barriers in micellar drug delivery: loading efficiency, *in vivo* stability, and micelle–cell interaction. *Expert Opin. Drug Deliv.* **7**, 49–62 (2010).
  27. Mochida, Y. *et al.* Bundled assembly of helical nanostructures in polymeric micelles loaded with platinum drugs enhancing therapeutic efficiency against pancreatic tumor. *ACS Nano* **8**, 6724–6738 (2014).
  28. Nishiyama, N., Matsumura, Y. & Kataoka, K. Development of polymeric micelles for targeting intractable cancers. *Cancer Sci.* **107**, 867–874 (2016).
  29. Cabral, H. *et al.* Accumulation of sub-100 nm polymeric micelles in poorly permeable tumours depends on size. *Nat. Nanotechnol.* **6**, 815–823 (2011).
  30. Mi, P., Cabral, H. & Kataoka, K. Ligand-Installed Nanocarriers toward Precision Therapy. *Adv. Mater.* **1902604**, 1902604 (2019).
  31. Smith, B. *et al.* Hyperthermia-triggered intracellular delivery of anticancer agent to HER2+ cells by HER2-specific affibody (ZHER2-GS-Cys)-conjugated thermosensitive liposomes (HER2+ affisomes). *J. Control. Release* **153**, 187–194 (2011).

32. Chi, L. *et al.* Enhanced delivery of liposomes to lung tumor through targeting interleukin-4 receptor on both tumor cells and tumor endothelial cells. *J. Control. Release* **209**, 327–336 (2015).
33. Sugahara, K. N. *et al.* Coadministration of a Tumor-Penetrating Peptide Enhances the Efficacy of Cancer Drugs. *Science* (80-. ). **328**, 1031–1035 (2010).
34. Roncato, F. *et al.* Improvement and extension of anti-EGFR targeting in breast cancer therapy by integration with the Avidin-Nucleic-Acid-Nano-Assemblies. *Nat. Commun.* **9**, 4070 (2018).
35. Duo, Y. *et al.* CX-5461-loaded nucleolus-targeting nanoplatfrom for cancer therapy through induction of pro-death autophagy. *Acta Biomater.* **79**, 317–330 (2018).
36. He, X. *et al.* Sequentially Triggered Nanoparticles with Tumor Penetration and Intelligent Drug Release for Pancreatic Cancer Therapy. *Adv. Sci.* **5**, 1701070 (2018).
37. Lv, Y. *et al.* Ultrasound-Triggered Destruction of Folate-Functionalized Mesoporous Silica Nanoparticle-Loaded Microbubble for Targeted Tumor Therapy. *Adv. Healthc. Mater.* **6**, 1700354 (2017).
38. Deshayes, S. *et al.* Phenylboronic Acid-Installed Polymeric Micelles for Targeting Sialylated Epitopes in Solid Tumors. *J. Am. Chem. Soc.* **135**, 15501–15507 (2013).
39. Oh, D.-Y. & Bang, Y.-J. HER2-targeted therapies — a role beyond breast cancer. *Nat. Rev. Clin. Oncol.* **17**, 33–48 (2020).
40. Schmit, K. & Michiels, C. TMEM Proteins in Cancer: A Review. *Front. Pharmacol.* **9**, (2018).
41. Donehower, L. A. *et al.* Integrated Analysis of TP53 Gene and Pathway Alterations in The Cancer Genome Atlas. *Cell Rep.* **28**, 1370-1384.e5 (2019).
42. Nicolas, E., Bertucci, F., Sabatier, R. & Gonçalves, A. Targeting BRCA Deficiency in Breast Cancer: What are the Clinical Evidences and the Next Perspectives? *Cancers (Basel)*. **10**, 506 (2018).
43. Ryan, M. B. & Corcoran, R. B. Therapeutic strategies to target RAS-mutant cancers. *Nat. Rev. Clin. Oncol.* **15**, 709–720 (2018).
44. Vaught, D. B. *et al.* HER3 Is Required for HER2-Induced Preneoplastic Changes to the Breast Epithelium and Tumor Formation. *Cancer Res.* **72**, 2672–2682 (2012).
45. Turke, A. B. *et al.* MEK Inhibition Leads to PI3K/AKT Activation by Relieving a Negative Feedback on ERBB Receptors. *Cancer Res.* **72**, 3228–3237 (2012).
46. Chibon, F. *et al.* Prediction of HER2 gene status in Her2 2+ invasive breast cancer: a



- study of 108 cases comparing ASCO/CAP and FDA recommendations. *Mod. Pathol.* **22**, 403–409 (2009).
47. Ross, J. S. *et al.* The HER-2 Receptor and Breast Cancer: Ten Years of Targeted Anti-HER-2 Therapy and Personalized Medicine. *Oncologist* **14**, 320–368 (2009).
  48. Wang, J. & Xu, B. Targeted therapeutic options and future perspectives for HER2-positive breast cancer. *Signal Transduct. Target. Ther.* **4**, 34 (2019).
  49. Arteaga, C. L. *et al.* Treatment of HER2-positive breast cancer: current status and future perspectives. *Nat. Rev. Clin. Oncol.* **9**, 16–32 (2012).
  50. Foulkes, W. D. Germline BRCA1 Mutations and a Basal Epithelial Phenotype in Breast Cancer. *CancerSpectrum Knowl. Environ.* **95**, 1482–1485 (2003).
  51. Hartman, A.-R. *et al.* Prevalence of BRCA mutations in an unselected population of triple-negative breast cancer. *Cancer* **118**, 2787–2795 (2012).
  52. Couch, F. J. *et al.* Inherited Mutations in 17 Breast Cancer Susceptibility Genes Among a Large Triple-Negative Breast Cancer Cohort Unselected for Family History of Breast Cancer. *J. Clin. Oncol.* **33**, 304–311 (2015).
  53. Tang, H., Zhao, W., Yu, J., Li, Y. & Zhao, C. Recent Development of pH-Responsive Polymers for Cancer Nanomedicine. *Molecules* **24**, 4 (2018).
  54. Lou, Y. *et al.* Targeting Tumor Hypoxia: Suppression of Breast Tumor Growth and Metastasis by Novel Carbonic Anhydrase IX Inhibitors. *Cancer Res.* **71**, 3364–3376 (2011).
  55. Heiden, M. G. V., Cantley, L. C. & Thompson, C. B. Understanding the warburg effect: The metabolic requirements of cell proliferation. *Science* **324**, 1029–1033 (2009).
  56. Estrella, V. *et al.* Acidity generated by the tumor microenvironment drives local invasion. *Cancer Res.* **73**, 1524–1535 (2013).
  57. Swietach, P., Vaughan-Jones, R. D. & Harris, A. L. Regulation of tumor pH and the role of carbonic anhydrase 9. *Cancer Metastasis Rev.* **26**, 299–310 (2007).
  58. Lee, S.-H. *et al.* Carbonic anhydrase IX is a pH-stat that sets an acidic tumour extracellular pH in vivo. *Br. J. Cancer* **119**, 622–630 (2018).
  59. Anderson, M., Moshnikova, A., Engelman, D. M., Reshetnyak, Y. K. & Andreev, O. A. Probe for the measurement of cell surface pH in vivo and ex vivo. *Proc. Natl. Acad. Sci. U. S. A.* **113**, 8177–8181 (2016).
  60. Chiche, J., Brahimi-Horn, M. C. & Pouyssegur, J. Tumour hypoxia induces a metabolic shift causing acidosis: a common feature in cancer. *J. Cell. Mol. Med.* **14**, 771–794

- (2010).
61. Swietach, P. What is pH regulation, and why do cancer cells need it? *Cancer Metastasis Rev.* **38**, 5–15 (2019).
  62. Gilkes, D. M., Semenza, G. L. & Wirtz, D. Hypoxia and the extracellular matrix: drivers of tumour metastasis. *Nat. Rev. Cancer* **14**, 430–439 (2014).
  63. Kizaka-Kondoh, S. & Konse-Nagasawa, H. Significance of nitroimidazole compounds and hypoxia-inducible factor-1 for imaging tumor hypoxia. *Cancer Sci.* **100**, 1366–1373 (2009).
  64. Hockel, M. & Vaupel, P. Tumor Hypoxia: Definitions and Current Clinical, Biologic, and Molecular Aspects. *JNCI J. Natl. Cancer Inst.* **93**, 266–276 (2001).
  65. Kizaka-Kondoh, S., Inoue, M., Harada, H. & Hiraoka, M. *Tumor hypoxia: A target for selective cancer therapy.* *Cancer Sci* **94**, (2003).
  66. Song, X. *et al.* Hypoxia-induced resistance to cisplatin and doxorubicin in non-small cell lung cancer is inhibited by silencing of HIF-1 $\alpha$  gene. *Cancer Chemother. Pharmacol.* **58**, 776–784 (2006).
  67. Thambi, T. *et al.* Hypoxia-responsive polymeric nanoparticles for tumor-targeted drug delivery. *Biomaterials* **35**, 1735–1743 (2014).
  68. Xie, Z. *et al.* Targeting tumor hypoxia with stimulus-responsive nanocarriers in overcoming drug resistance and monitoring anticancer efficacy. *Acta Biomater.* **71**, 351–362 (2018).
  69. Chiche, J., Brahimi-Horn, M. C. & Pouyssegur, J. Tumour hypoxia induces a metabolic shift causing acidosis: A common feature in cancer. *J. Cell. Mol. Med.* **14**, 771–794 (2010).
  70. Sigismund, S., Avanzato, D. & Lanzetti, L. Emerging functions of the EGFR in cancer. *Mol. Oncol.* **12**, 3–20 (2018).
  71. Si, D., Yin, F., Peng, J. & Zhang, G. <p>High Expression of CD44 Predicts a Poor Prognosis in Glioblastomas</p>. *Cancer Manag. Res.* **Volume 12**, 769–775 (2020).
  72. Wu, P.-H., Opadele, A. E., Onodera, Y. & Nam, J.-M. Targeting Integrins in Cancer Nanomedicine: Applications in Cancer Diagnosis and Therapy. *Cancers (Basel).* **11**, 1783 (2019).
  73. Büll, C., Stoel, M. A., Den Brok, M. H. & Adema, G. J. Sialic acids sweeten a tumor's life. *Cancer Res.* **74**, 3199–3204 (2014).
  74. Xu, M. J., Johnson, D. E. & Grandis, J. R. EGFR-targeted therapies in the post-genomic

- era. *Cancer Metastasis Rev.* **36**, 463–473 (2017).
75. Li, C. *et al.* Development of EGFR-targeted evodiamine nanoparticles for the treatment of colorectal cancer. *Biomater. Sci.* **7**, 3627–3639 (2019).
  76. Jin, H. *et al.* EGFR-targeting PLGA-PEG nanoparticles as a curcumin delivery system for breast cancer therapy. *Nanoscale* **9**, 16365–16374 (2017).
  77. Ashton, J. R., Gottlin, E. B., Patz, E. F., West, J. L. & Badea, C. T. A comparative analysis of EGFR-targeting antibodies for gold nanoparticle CT imaging of lung cancer. *PLoS One* **13**, e0206950 (2018).
  78. Wang, L., Zuo, X., Xie, K. & Wei, D. The Role of CD44 and Cancer Stem Cells. in 31–42 (2018). doi:10.1007/978-1-4939-7401-6\_3
  79. Vermeulen, L. *et al.* Wnt activity defines colon cancer stem cells and is regulated by the microenvironment. *Nat. Cell Biol.* **12**, 468–476 (2010).
  80. Li, C. *et al.* Identification of Pancreatic Cancer Stem Cells. *Cancer Res.* **67**, 1030–1037 (2007).
  81. Prince, M. E. *et al.* Identification of a subpopulation of cells with cancer stem cell properties in head and neck squamous cell carcinoma. *Proc. Natl. Acad. Sci.* **104**, 973–978 (2007).
  82. Li, F., Tiede, B., Massagué, J. & Kang, Y. Beyond tumorigenesis: cancer stem cells in metastasis. *Cell Res.* **17**, 3–14 (2007).
  83. Misra, S., Toole, B. P. & Ghatak, S. Hyaluronan Constitutively Regulates Activation of Multiple Receptor Tyrosine Kinases in Epithelial and Carcinoma Cells. *J. Biol. Chem.* **281**, 34936–34941 (2006).
  84. Chen, C., Zhao, S., Karnad, A. & Freeman, J. W. The biology and role of CD44 in cancer progression: therapeutic implications. *J. Hematol. Oncol.* **11**, 64 (2018).
  85. Huang, W.-Y. *et al.* Nanoparticle Targeting CD44-Positive Cancer Cells for Site-Specific Drug Delivery in Prostate Cancer Therapy. *ACS Appl. Mater. Interfaces* **8**, 30722–30734 (2016).
  86. Gaio, E. *et al.* CD44 Targeting Mediated by Polymeric Nanoparticles and Combination of Chlorine TPCS2a-PDT and Docetaxel-Chemotherapy for Efficient Killing of Breast Differentiated and Stem Cancer Cells In Vitro. *Cancers (Basel)*. **12**, 278 (2020).
  87. Pazzagli, C. & Donnini, S. Targeting integrins in cancer. *For. Immunopathol. Dis. Therap.* **5**, 233–241 (2014).
  88. Miura, Y. *et al.* Cyclic RGD-linked polymeric micelles for targeted delivery of platinum

- anticancer drugs to glioblastoma through the blood-brain tumor barrier. *ACS Nano* **7**, 8583–8592 (2013).
89. Kagaya, H. *et al.* Impact of polyplex micelles installed with cyclic RGD peptide as ligand on gene delivery to vascular lesions. *Gene Ther.* **19**, 61–69 (2012).
90. Miyano, K. *et al.* cRGD peptide installation on cisplatin-loaded nanomedicines enhances efficacy against locally advanced head and neck squamous cell carcinoma bearing cancer stem-like cells. *J. Control. Release* **261**, 275–286 (2017).
91. Tarbell, J. M. & Cancel, L. M. The glycocalyx and its significance in human medicine. *J. Intern. Med.* **280**, 97–113 (2016).
92. Varki, A. Biological roles of glycans. *Glycobiology* **27**, 3–49 (2017).
93. Varki, A. Glycan-based interactions involving vertebrate sialic-acid-recognizing proteins. *Nature* **446**, 1023–1029 (2007).
94. Varki, N. M. & Varki, A. Diversity in cell surface sialic acid presentations: implications for biology and disease. *Lab. Invest.* **87**, 851–857 (2007).
95. Almaraz, R. T. *et al.* Metabolic Flux Increases Glycoprotein Sialylation: Implications for Cell Adhesion and Cancer Metastasis. *Mol. Cell. Proteomics* **11**, M112.017558 (2012).
96. Pinho, S. S. & Reis, C. A. Glycosylation in cancer: Mechanisms and clinical implications. *Nat. Rev. Cancer* **15**, 540–555 (2015).
97. Munkley, J. & Elliott, D. J. Hallmarks of glycosylation in cancer. *Oncotarget* **7**, (2016).
98. Munkley, J. The Role of Sialyl-Tn in Cancer. *Int. J. Mol. Sci.* **17**, 275 (2016).
99. Munkley, J. The glycosylation landscape of pancreatic cancer (Review). *Oncol. Lett.* (2019). doi:10.3892/ol.2019.9885
100. Miyagi, T., Takahashi, K., Hata, K., Shiozaki, K. & Yamaguchi, K. Sialidase significance for cancer progression. *Glycoconj. J.* **29**, 567–577 (2012).
101. Büll, C., Stoel, M. A., Den Brok, M. H. & Adema, G. J. Sialic acids sweeten a tumor's life. *Cancer Research* **74**, 3199–3204 (2014).
102. Büll, C., den Brok, M. H. & Adema, G. J. Sweet escape: Sialic acids in tumor immune evasion. *Biochim. Biophys. Acta - Rev. Cancer* **1846**, 238–246 (2014).
103. Picco, G. *et al.* Over-expression of ST3Gal-I promotes mammary tumorigenesis. *Glycobiology* **20**, 1241–1250 (2010).
104. Hudak, J. E. & Bertozzi, C. R. Glycotherapy: New Advances Inspire a Reemergence of Glycans in Medicine. *Chem. Biol.* **21**, 16–37 (2014).

105. Hanahan, D. & Weinberg, R. A. Hallmarks of cancer: the next generation. *Cell* **144**, 646–74 (2011).
106. Swindall, A. F. *et al.* ST6Gal-I Protein Expression Is Upregulated in Human Epithelial Tumors and Correlates with Stem Cell Markers in Normal Tissues and Colon Cancer Cell Lines. *Cancer Res.* **73**, 2368–2378 (2013).
107. Hakomori, S. Tumor Malignancy Defined by Aberrant Glycosylation and Sphingo(glyco)lipid Metabolism. *Cancer Res.* **56**, 5309 LP – 5318 (1996).
108. Becker, A. J., McCulloch, E. A. & Till, J. E. Spleen Colonies Derived From Transplanted Mouse Marrow Cells. *Nature* **197**, 452–454 (1963).
109. Yoshikawa, M. *et al.* XCT inhibition depletes CD44v-expressing tumor cells that are resistant to EGFR-targeted therapy in head and neck squamous cell carcinoma. *Cancer Res.* **73**, 1855–1866 (2013).
110. Tomuleasa, C. *et al.* Isolation and characterization of hepatic cancer cells with stem-like properties from hepatocellular carcinoma. *J. Gastrointest. Liver Dis.* **19**, 61–67 (2010).
111. Al-Hajj, M., Wicha, M. S., Benito-Hernandez, A., Morrison, S. J. & Clarke, M. F. Prospective identification of tumorigenic breast cancer cells. *Proc. Natl. Acad. Sci.* **100**, (2003).
112. Lenkiewicz, M., Li, N. & Singh, S. K. Culture and isolation of brain tumor initiating cells. *Curr. Protoc. Stem Cell Biol.* 1–10 (2009). doi:10.1002/9780470151808.sc0303s11
113. Nguyen, N., Luo, Y. & Fujita, M. Aldehyde dehydrogenase isozymes: Markers of cancer stem cells in human melanoma. *Expert Rev. Dermatol.* **8**, 111–113 (2013).
114. Lapidot, T. *et al.* Stem cells, cancer, and cancer stem cells. *Nature* **17**, 645–648
115. Espinoza, I. & Miele, L. Deadly crosstalk: Notch signaling at the intersection of EMT and cancer stem cells. *Cancer Letters* (2013). doi:10.1016/j.canlet.2013.08.027
116. Pattabiraman, D. R. & Weinberg, R. A. Tackling the cancer stem cells — what challenges do they pose? *Nat. Rev. Drug Discov.* **13**, 497–512 (2014).
117. Ishizawa, K. *et al.* Tumor-Initiating Cells Are Rare in Many Human Tumors. *Cell Stem Cell* **7**, 279–282 (2010).
118. Schulenburg, A. *et al.* Cancer stem cells in basic science and in translational oncology: can we translate into clinical application? *J. Hematol. Oncol.* **8**, 16 (2015).
119. Camp, R. L., Kraus, T. A. & Puré, E. Variations in the cytoskeletal interaction and posttranslational modification of the CD44 homing receptor in macrophages. *J. Cell Biol.*

- 115**, 1283–1292 (1991).
120. UNDERHILL, C. CD44: The hyaluronan receptor. *J. Cell Sci.* **103**, 293 LP – 298 (1992).
  121. Bartolazzi, A., Nocks, A., Aruffo, A., Spring, F. & Stamenkovic, I. Glycosylation of CD44 is implicated in CD44-mediated cell adhesion to hyaluronan. *J. Cell Biol.* **132**, 1199–1208 (1996).
  122. Catterall, J. B., Jones, L. M. H. & Turner, G. A. Membrane protein glycosylation and CD44 content in the adhesion of human ovarian cancer cells to hyaluronan. *Clin. Exp. Metastasis* **17**, 583–591 (1999).
  123. Skelton, T. P., Zeng, C., Nocks, A. & Stamenkovic, I. Glycosylation Provides Both Stimulatory and Inhibitory Effects on Cell Surface and Soluble CD44 Binding to Hyaluronan. *J. Cell Biol.* **140**, 431–446 (1998).
  124. Vajaria, B. N., Patel, K. R., Begum, R. & Patel, P. S. Sialylation: an Avenue to Target Cancer Cells. *Pathol. Oncol. Res.* **22**, 443–447 (2016).
  125. Munkley, J. & Scott, E. Targeting Aberrant Sialylation to Treat Cancer. *Medicines* **6**, 102 (2019).
  126. Zhao, D. *et al.* pH-Activated Targeting Drug Delivery System Based on the Selective Binding of Phenylboronic Acid. *ACS Appl. Mater. Interfaces* **8**, 14845–14854 (2016).
  127. Elgohary, M. M. *et al.* Targeting sialic acid residues on lung cancer cells by inhalable boronic acid-decorated albumin nanocomposites for combined chemo/herbal therapy. *J. Control. Release* (2018). doi:10.1016/j.jconrel.2018.07.014
  128. Ji, M. *et al.* Sialic Acid-Targeted Nanovectors with Phenylboronic Acid-Grafted Polyethylenimine Robustly Enhance siRNA-Based Cancer Therapy. *ACS Appl. Mater. Interfaces* **8**, 9565–9576 (2016).
  129. Büll, C. *et al.* Sialic acid blockade suppresses tumor growth by enhancing t-cell-mediated tumor immunity. *Cancer Res.* **78**, 3574–3588 (2018).
  130. Ernst, B. & Magnani, J. L. From carbohydrate leads to glycomimetic drugs. *Nat. Rev. Drug Discov.* **8**, 661–677 (2009).
  131. Mereiter, S., Balmaña, M., Campos, D., Gomes, J. & Reis, C. A. Glycosylation in the Era of Cancer-Targeted Therapy: Where Are We Heading? *Cancer Cell* **36**, 6–16 (2019).
  132. Dervisevic, M., Senel, M., Sagir, T. & Isik, S. Highly sensitive detection of cancer cells with an electrochemical cytosensor based on boronic acid functional polythiophene. *Biosens. Bioelectron.* **90**, 6–12 (2017).
  133. Liu, R. *et al.* Preparation of Sialic Acid-Imprinted Fluorescent Conjugated

- Nanoparticles and Their Application for Targeted Cancer Cell Imaging. *ACS Appl. Mater. Interfaces* **9**, 3006–3015 (2017).
134. Matsumoto, A., Kataoka, K. & Miyahara, Y. New directions in the design of phenylboronate-functionalized polymers for diagnostic and therapeutic applications. *Polym. J.* **46**, 483–491 (2014).
  135. Matsumoto, A., Sato, N., Kataoka, K. & Miyahara, Y. Noninvasive Sialic Acid Detection at Cell Membrane by Using Phenylboronic Acid Modified Self-Assembled Monolayer Gold Electrode. *J. Am. Chem. Soc.* **131**, 12022–12023 (2009).
  136. Matsumoto, A., Cabral, H., Sato, N., Kataoka, K. & Miyahara, Y. Assessment of Tumor Metastasis by the Direct Determination of Cell-Membrane Sialic Acid Expression. *Angew. Chemie Int. Ed.* **49**, 5494–5497 (2010).
  137. Uchimura, E., Otsuka, H., Okano, T., Sakurai, Y. & Kataoka, K. Totally synthetic polymer with lectin-like function: Induction of killer cells by the copolymer of 3-acrylamidophenylboronic acid with N,N-dimethylacrylamide. *Biotechnol. Bioeng.* **72**, 307–314 (2001).
  138. Otsuka, H., Ikeya, T., Okano, T. & Kataoka, K. Activation of lymphocyte proliferation by boronate-containing polymer immobilised on substrate: The effect of boron content on lymphocyte proliferation. *Eur. Cells Mater.* **12**, 36–42 (2006).
  139. Otsuka, H., Uchimura, E., Koshino, H., Okano, T. & Kataoka, K. Anomalous binding profile of phenylboronic acid with N-acetylneuraminic acid (Neu5Ac) in aqueous solution with varying pH. *J. Am. Chem. Soc.* **125**, 3493–3502 (2003).
  140. Sharon, N. Lectins: Carbohydrate-specific Reagents and Biological Recognition Molecules. *J. Biol. Chem.* **282**, 2753–2764 (2007).
  141. Koprowski, H., Herlyn, M., Steplewski, Z. & Sears, H. Specific antigen in serum of patients with colon carcinoma. *Science (80-. )*. **212**, 53–55 (1981).
  142. Matsumoto, A. *et al.* Heterocyclic boronic acids display sialic acid selective binding in a hypoxic tumor relevant acidic environment. *Chem. Sci.* **8**, 6165–6170 (2017).
  143. Otsuka, H., Uchimura, E., Koshino, H., Okano, T. & Kataoka, K. Anomalous binding profile of phenylboronic acid with N-acetylneuraminic acid (Neu5Ac) in aqueous solution with varying pH. *J. Am. Chem. Soc.* **125**, 3493–3502 (2003).
  144. Pappin, B., J., M. & A., T. Boron-Carbohydrate Interactions. in *Carbohydrates - Comprehensive Studies on Glycobiology and Glycotechnology* (InTech, 2012). doi:10.5772/50630

145. Bull, S. D. *et al.* Exploiting the reversible covalent bonding of boronic acids: Recognition, sensing, and assembly. *Acc. Chem. Res.* **46**, 312–326 (2013).
146. Brooks, W. L. A. & Sumerlin, B. S. Synthesis and Applications of Boronic Acid-Containing Polymers: From Materials to Medicine. *Chem. Rev.* **116**, 1375–1397 (2016).
147. Yamamoto, Y. *et al.* Effect of combined treatment with the epirubicin-incorporating micelles (NC-6300) and 1,2-diaminocyclohexane platinum (II)-incorporating micelles (NC-4016) on a human gastric cancer model. *Int. J. Cancer* **135**, 214–223 (2014).



# **Chapter 2**

## **Ligand Validation**

## Chapter 2: Ligand Validation

### Abstract

Prospect of 5-BPA to use as a ligand on nanoparticle for targeted cancer therapy was evaluated in this chapter. Quantification of sialic acid in different *in vitro* cultured murine and human cancer cell lines were reported. Relative expression of sialic acid in normal tissue and tumor samples collected from head and neck cancer patients was estimated. The concept of pH dependent binding of 5-BPA to cancer cell surface sialic acid was verified in *in vitro* using PANC 1 cell line as it appeared to have highest amount of sialic acid among all cell lines. Verification was done by two separate experiments. Firstly, lectin blocking ability of 5-BPA at pH 6.5 using sialic acid specific SNA lectin was assessed. Then, additional experiment was performed by using rhodamine conjugated 5-BPA and directly observing ability of 5-BPA-rhodamine to bind to cell surface sialic acid in sialidase treated and non-treated cells. Retention of binding constant of 5-BPA after polymer conjugation was confirmed through ARS (alizarin red s) assay using 5-BPA-PEG-acetal as model polymer. Finally, superiority of 5-BPA ligand over PBA was validated using Cy5 dye labeled 5-BPA-8-arm-PEG and PBA-8-arm-PEG through *in vitro* and *in vivo* assessment.

## Chapter 2: Ligand validation

### 2.1 Introduction

### 2.2 Experimental

#### 2.2.1 Materials

#### 2.2.2 Cell line

#### 2.2.3 *In vitro* expression of sialic acid

#### 2.2.4 Analysis of expression of sialic acid in patient sample

#### 2.2.5 *In vitro* evaluation of 5-BPA and sialic acid binding

#### 2.2.6 *In vitro* evaluation of 5-BPA-rhodamine

#### 2.2.7 Conjugation of 5-BPA to amine-PEG<sub>5.5K</sub>-acetal

#### 2.2.8 Binding constant of 5-BPA-PEG<sub>5.5K</sub>-acetal

#### 2.2.9 Conjugation of 5-BPA and PBA to 8-arm-PEG<sub>40K</sub>-amine

#### 2.2.10 *In vitro* cellular uptake of 8-arm-PEGs

#### 2.2.11 *In vivo* evaluation of 8-arm-PEGs

### 2.3 Results

#### 2.3.1 Quantification of sialic acid

#### 2.3.2 Sialic acid expression in patient sample

#### 2.3.3 *In vitro* binding of 5-BPA

##### 2.3.3.1 Lectin blocking assay

##### 2.3.3.2 5-BPA-rhodamine binding

#### 2.3.4 Polymer characterization of 5-BPA-PEG<sub>5.5K</sub>-acetal

#### 2.3.5 Binding constant of 5-BPA-PEG<sub>5.5K</sub>-acetal

#### 2.3.6 Polymer characterization of 8-arm-PEGs

#### 2.3.7 Cellular uptake of 8-arm-PEGs

### 2.3.8 *In vivo* tumor accumulation and biodistribution of 8-arm-PEGs

## 2.4 Discussion

## 2.5 Conclusion

## 2.6 References

## 2.1 Introduction

Altered glycosylation is a trademark of almost all type of cancers regardless of the origin and stage, and SA has been reported to be involved in immune modulation and support of cancer cells in immune evasion to create an immunosuppressive microenvironment<sup>1</sup>. For example, SA can bind to siglec (SA binding immunoglobulin type lectin) present on the surface of T cells and exert immunosuppressive signals<sup>2</sup>. The overexpression of SA has also been linked to cancer malignancy and metastasis<sup>3</sup>. Cancer cells of different origins show overexpression of SA on cell surface glycoproteins and glycolipids, which contributes to the overall higher amount of SA in tumor microenvironment. The ability of SA to modulate immune regulatory system is attributed as the cause for increased expression in tumor cells<sup>4</sup>. This overexpression of SA is reported to be more common than oncogene markers, such as HER2/ neu<sup>5</sup>, which makes SA as a universal targeting antigen for all type of tumors. Hypersialylation in cancer cells also promotes migration and apoptosis resistance, which are beneficial for tumor growth and correlated with aggressiveness and poor prognosis for cancer patients<sup>6</sup>. Thus, SA represents a broad marker for tumor targeting of therapeutic agents. Nevertheless, SA is also expressed in healthy tissues, thus, hindering the development of such targeted strategies. So, it is important to develop ligand strategies that can selectively recognize overexpressed SA in tumor while avoiding systemic interaction.

SA can be recognized by lectins<sup>7</sup> and antibodies<sup>8</sup>, though they are yet to be used

systematically due to their immunogenicity and lack of selectivity to tumor SA. Thus, the development of ligands capable of recognizing tumor SA, while avoiding interaction with SA in healthy tissues, is still necessary for advancing SA targeted strategies. Boronic acids can form reversible covalent interactions with diol-containing molecules<sup>9</sup>. In fact, sugars, such as the common monosaccharides (*e.g.* glucose), contain diols, and as a consequence, boronic acids have proven to be helpful molecular ligands for binding and detection, working as synthetic lectins<sup>10</sup>. While the binding of boron to diol-containing molecules is commonly promoted at basic pH, the binding constant between these agents drops at neutral and acidic pHs. On the other hand, the binding of boronic acids to SA opposes this trend, and the binding constant between boronic acid compound and SA increases at acidic pHs. For example, complexes between phenylboronic acid (PBA) and sugars were shown to be stable at pH higher than their pKa, however, with pH lower than pKa only SA-PBA complexes were stable<sup>9</sup>. Such binding behavior of boronic acids could be exploited for selective recognition of SA at intratumoral pH conditions, which range between pH 6.5 to pH 7.2.

PBA have been reported to selectively recognize SA overexpressed on cancer cells to improve the tumor targeting ability of polymeric micelles<sup>11</sup>. PBA molecules on the micelles can form ester bonds with diol-bearing molecules and shows selectivity to SA at intratumoral pH (pH 6.5). These micelles achieved enhanced intracellular drug delivery in cancer cells at intratumoral pH after attaching to the SA on the cell surfaces. As the interaction between SA and PBA is low, I have concentrated on finding PBA derivatives with higher binding affinity to SA at intratumoral pH, which can further improve the tumor targeting ability. Recently, we have reported the superior affinity of 5-boronopicolinic acid (5-BPA) for SA at intratumoral pH which is much higher compared to PBA<sup>12</sup>. While, 5-BPA glucose complexation is higher at at pH 7.4 but at pH 6.5 selectively binds to SA with more than 30-fold higher binding constant for SA than the standard PBA. Thus, providing excellent rationale for using 5-BPA as

a ligand for specific cancer targeting.

In this chapter, I have quantified amount of SA in different cancer cell line and human sample including normal tissue section and head & neck tumor section. Then I confirmed the superior binding ability of 5-BPA to SA *in vitro* using PANC 1 cancer cell line by two different assays. In first assay I evaluated lectin blocking capability 5-BPA at pH 7.4 & 6.5 and then by directly using rhodamine dye conjugated 5-BPA. Both experiment was performed using confocal laser scanning microscopy (CLSM). 5-BPA-PEG<sub>5.5K</sub>-acetal was used as a model polymer to verify retention of binding affinity of 5-BPA-SA after conjugation through ARS assay. Finally, I confirmed superiority of 5-BPA over PBA by conjugating to multi arm PEG and performing *in vitro* and *in vivo* experiments.

## 2.2 Experimental

### 2.2.1 Materials

Sialic Acid (NANA) Assay Kit was purchased from Abcam (Cambridge, United Kingdom). Neuraminidase (Sialidase) from *Clostridium perfringens* was purchased from Roche Diagnostics GmbH, (Mannheim, Germany). Head and neck cancer with normal tissue array (HN483a) was purchased from Biomax (Derwood, USA). Alexa Fluor 647-conjugated Wheat Germ Agglutinin (WGA) was purchased from Life Technologies (California, USA). Hoechst was purchased from ThermoFisher Scientific (Massachusetts, USA). Dulbecco's modified eagle's medium (DMEM) was obtained from Sigma-Aldrich Co. (ST. Louis, MO). Fetal bovine serum (FBS) was purchased from Dainippon Sumitomo Pharma Co., Ltd. (Osaka, Japan). Phosphate-buffered saline (PBS) was purchased from Wako Pure Chemical Industries Ltd. (Osaka, Japan). 5-Boronopicolinic acid (5-BPA) was obtained from Santa Cruze

Biotechnology, Inc (Texas, United States). Rhodamine B-5-BPA was received from Dr. Matsumoto. 3-aminophenylboronic acid (NH<sub>2</sub>-PBA), 4-(4,6-dimethoxy-1,3,5-triazin-2-yl)-4-methylmorpholinium chloride N-hydrate (DMT-MM), triethylamine (TEA, >99%), dimethyl sulfoxide (DMSO) (>99%) and alizarin red s (ARS) were obtained from Wako Pure Chemical Co., Inc. (Osaka, Japan).  $\alpha$ -acetal- $\omega$ -aminopropyl-poly(ethylene glycol) (acetal-PEG-amine; Mw = 5,500) was purchased from NOF Co., Inc. (Tokyo, Japan). Fluorescein labeled Sambucus Nigra Lectin (SNA, EBL) was purchased from Vector laboratories (California, USA). 8-arm-poly(ethylene glycol)-amine (8-arm-PEG; Mw = 40,000) was purchased from Sigma-Aldrich Co. (ST. Louis, MO). Cy5 NHS ester was obtained from Lumiprobe (Florida, USA).

### 2.2.2 Cell line and animals

Human pancreatic carcinoma (PANC1), murine melanoma cells (B16F10), mice mammary adenocarcinoma (4T1), human prostate cancer cell line (PC3), biopsy xenograft of pancreatic carcinoma line-3 (BxPC3), human colon adenocarcinoma cell line (HT 29), murine colon carcinoma (C26), human oral carcinoma (HSC2), human breast adenocarcinoma (MCF7) and (MDA MB 231) cells were purchased from Cell Bank, Riken BioResource Center (Tsukuba, Japan). All cells were cultured in Dulbecco's modified eagle's medium (DMEM) containing 10% of fetal bovine serum (FBS) and 1% of penicillin streptomycin in a humidified atmosphere containing 5% CO<sub>2</sub> at 37°C. BALB/c mice nu/nu (female; age 6 weeks;) were purchased from Charles River Japan (Kanagawa, Japan). All experiments were performed in accordance with the Guidelines for the Care and Use of Laboratory Animals as stated by the University of Tokyo.

### 2.2.3 Quantification of sialic acid on cancer cells

Quantification of expression of SA on different cancer cell lines was done using sialic acid assay kit<sup>13</sup>. Protocol provided by the manufacturer was followed for the quantification assay. For each cell line  $1 \times 10^6$  cells were collected after detachment of cells by trypsin treatment. Cells were washed with PBS and centrifuged before adding 100  $\mu$ l of PBS and heated to 95°C for 5 min. Then, incubated with sialidase for overnight to release all the SA from the cell surface. Supernatant was collected after centrifugation for quantification. Reaction mixture was prepared for fluorometric assay by adding reaction mixture and background reaction mixture provided in the assay kit. Series of standard SA dilution was also prepared for the generation of standard curve. Fluorescence measurement was taken (Ex/Em= 535/587 nm) after 30 min of mixing samples with reaction mixture using Tecan Microplate Reader (Tecan infinite 200).

### 2.2.4 Analysis of expression of sialic acid in patient sample

Recovery of antigens of head and neck cancer with normal tissue array (HN483a) was done by incubating slides in 100% Xylene, 100% Ethanol, 90% Ethanol, 70% Ethanol and two times in distilled water for 5 min each. Then the slide was heated at 95 °C in citric acid buffer (pH 6 ) for 30 min. Finally slide was incubated in PBS (pH 7.4) in room temperature for 20 min and 5 min under running water before starting staining of antibodies. Before staining process tissue sections were washed three times with PBS and incubated with tween in PBS for 30 min at room temperature. Then tissue sections were stained with alexa 647 labeled wheat germ agglutinin (WGA 1mg/20ml PBS) for two hours and washed three times. Finally, nuclei were stained with DAPI (0.03 mg/mL in PBS) for 5 min before mounting with cover glass. The slide was then imaged with Zeiss LSM 510 META nonlinear optics scan head attached to an



inverted Axiovert 200 M SP equipped with a  $63 \times 1.4$  numerical aperture Plan Apochromat oil immersion objective (Carl Zeiss). Fluorescence intensity was quantified using imageJ software and relative expression of SA was calculated.

### 2.2.5 *In-vitro* evaluation of 5-BPA and sialic acid binding

$2.5 \times 10^5$  PANC1 cells were plated on Iwaki 35mm glass base plate. Cells were incubated for 48 h at 37°C. Experiments were done in pH 7.4, physiological pH and pH 6.5, which is lowest pH found inside tumor. Cells were first stained with hoechst and then incubated for 20 minutes with 200µg/ml of PBA or 5-BPA at room temperature and finally stained with SA-specific *Sambucus Nigra* SNA-lectin (Fluorescein conjugated) 100µg/ml for 25 minutes at 4° C. Control samples were stained with only Hoechst and SNA-lectin. Finally, fluorescence imaging was done using CLSM and fluorescence intensity was calculated using imageJ software to estimate lectin blocking ability of PBA and 5-BPA.

### 2.2.6 *In vitro* evaluation of 5-BPA-rhodamine

$2 \times 10^4$  PANC1 cells were plated on Chambered # 1.0 Borosilicate Cover glass system (Lab Tek). After 48 h of incubation cells were incubated with hoechst for 5 min before washing two times with PBS. Cells were then incubated with rhodamine B conjugated 5-BPA solution having pH 7.4 and pH 6.5 at 4°C for 5 min. Any unbound Rhodamine B conjugated 5-BPA was removed by washing two times with PBS (pH 6.5 and pH 7.4). Control samples were incubated with sialidase enzyme for 40 min at 37°C to cleave SA from cell surface. Cells were then washed twice with PBS and stained with hoechst and rhodamine B-5-BPA described as above. Finally, fluorescence imaging was done using CLSM. Fluorescence intensity was quantified using imageJ software to directly estimate cell surface SA bound 5-BPA.

### 2.2.7 Conjugation of 5-BPA to acetal-PEG-amine

5-BPA (10 fold molar excess) was activated using DMT-MM in DMSO and added to a reaction mixture of 5 fold molar excess amine-PEG<sub>5.5K</sub>-acetal (Mw = 5,500) with TEA (**Fig. 1**). This reaction mixture was kept stirring for overnight. 5-BPA-PEG<sub>5.5K</sub>-acetal was obtained after purification by dialysis against deionized water and lyophilization.

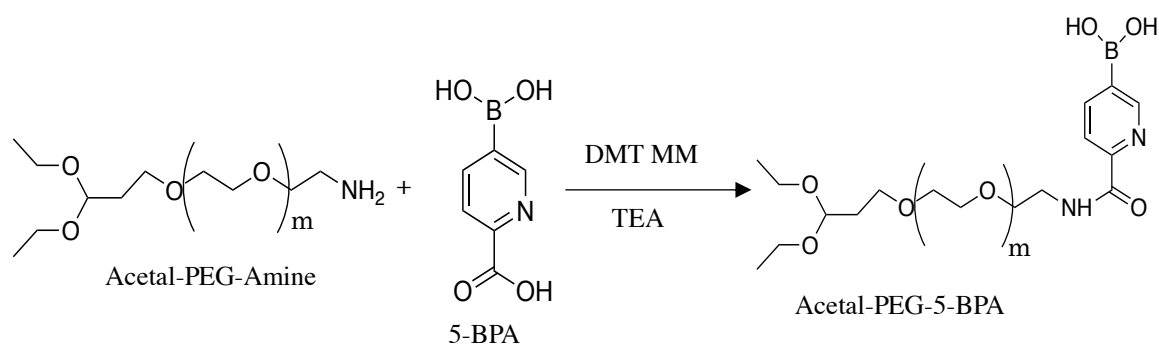


**Figure 1.** Synthesis scheme of 5-BPA conjugation to amine-PEG<sub>5.5K</sub>-acetal

### 2.2.8 Binding constant of 5-BPA-PEG<sub>5.5K</sub>-acetal

The interaction between boronic acids and diol complexation can be calculated by a three component assay reported by Springsteen and Wang<sup>14,15</sup> containing alizarin red s (ARS), boronic acid (BA) molecule and a diol containing compound e.g. glucose, fructose, mannose. In this experiment, the diol compound was SA and BA molecule was 5-BPA-PEG<sub>5.5K</sub>-acetal. ARS (**Fig 2. 6**) is very weakly fluorescent or non-fluorescent but the complex (**Fig 2. 7**) it forms with BA is fluorescent. On addition of a diol containing molecule (**Fig 2. 5**) ARS is replaced from the complex to generate new diol ester (**Fig 2. 8**) which is non-fluorescent. Thus, decreasing the amount of fluorescent ARS-BA (**Fig 2. 7**) complex. The assay was done in two steps. First, fluorescence of ARS-5-BPA-PEG<sub>5.5K</sub>-acetal was measured with varying concentration of 5-BPA-PEG<sub>5.5K</sub>-acetal and then BA molecule is replaced by addition of different concentration of SA. Fluorescence of ARS-5-BPA-PEG<sub>5.5K</sub>-acetal solution decreases

with increased concentration of SA as ARS molecule is replaced by SA to form non-fluorescent SA-5-BPA-PEG<sub>5.5K</sub>-acetal. Experimental details are given below.

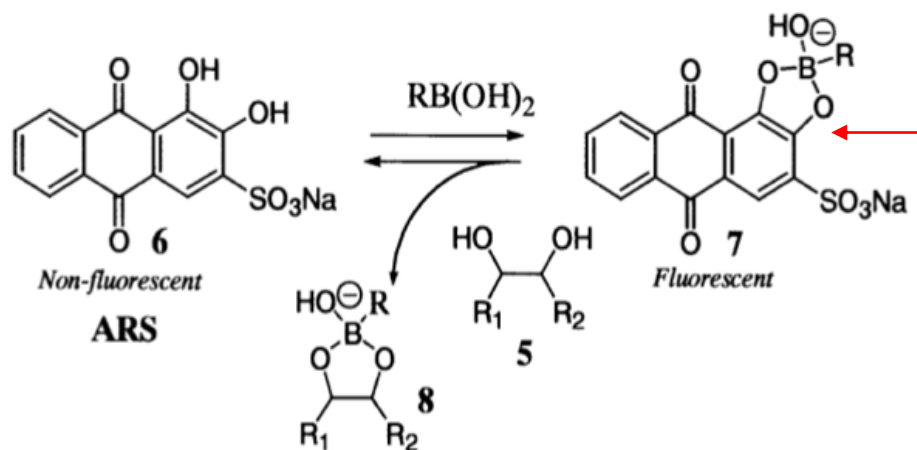


**Figure 2.** Mechanism of ARS assay<sup>15</sup>.

Step 1: Measurement of association constant between ARS and 5-BPA-PEG<sub>5.5K</sub>-acetal.

Solution A: 9 μM ARS was prepared and different experimental pH (6.5, 6.9 & 7.4) were adjusted accordingly. Solution B: The final concentration of ARS was 9 μM and 5-BPA-PEG<sub>5.5K</sub>-acetal was 2 mM (BA basis) and different experimental pH (6.5, 6.9 & 7.4) were adjusted accordingly. Solution A and B was serially mixed to prepare a solution with different final (0, 0.05, 0.1, 0.15, 0.2, 0.3, 0.4, 0.5, 0.75, 1, 1.5) concentration (mM) of 5-BPA-PEG<sub>5.5K</sub>-acetal in a 96 well plate. Fluorescence was measured at 468 nm using tecan Microplate Reader (Tecan infinite 200).

Step 2: Binding constant of 5-BPA-PEG<sub>5.5K</sub>-acetal and SA. Solution A: Solution A was prepared with 9 μM ARS and 2 mM 5-BPA-PEG<sub>5.5K</sub>-acetal and different experimental pH (6.5, 6.9 & 7.4) were adjusted accordingly. Solution B: The final concentration of ARS was 9 μM, 5-BPA-PEG<sub>5.5K</sub>-acetal was 2 mM (BA basis) and SA was 100 mM. Different experimental pH (6.5, 6.9 & 7.4) were adjusted accordingly. Titration of SA (Solution B) in to a solution of ARS-5-BPA-PEG<sub>5.5K</sub>-acetal (Solution A) complex was done by mixing them in various ratio to have

SA concentration as 0, 1, 2, 4, 6, 10, 12, 15, 20, 30, 50 (mM). Fluorescence was measured at 468 nm using tecan microplate reader. Calculation of binding constant between 5-BPA-PEG<sub>5.5K</sub>-acetal and SA was done by using Springsteen and Wang method<sup>15</sup>.

### 2.2.9 Conjugation of 5-BPA and PBA to 8-arm-PEG<sub>40K</sub>-amine

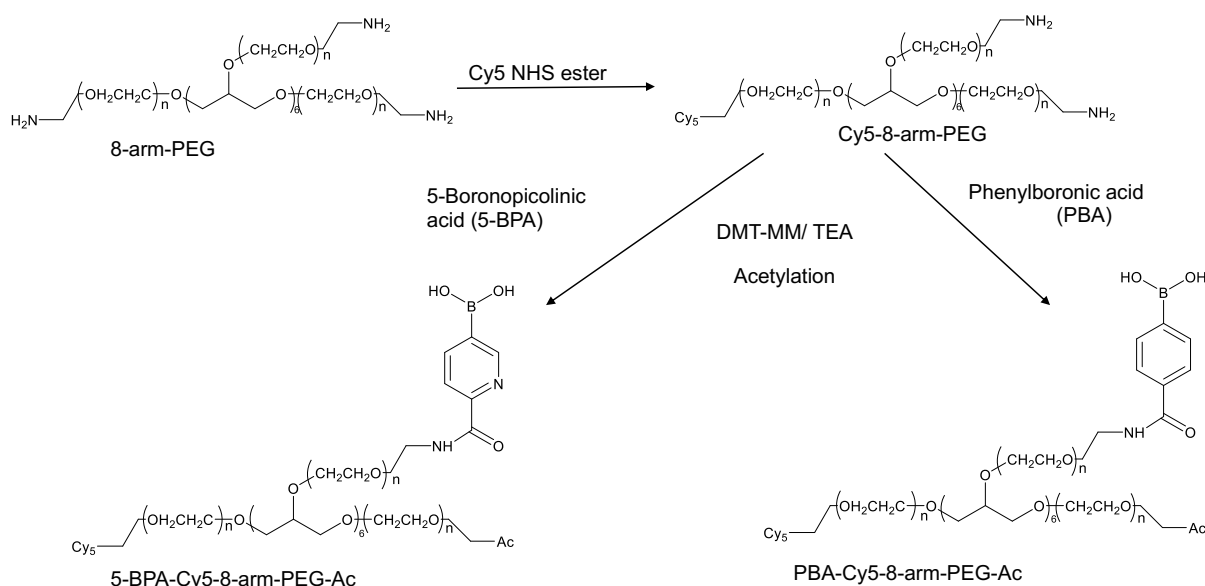


**Figure 3.** Synthesis scheme of 5-BPA and PBA conjugation to 8-arm-PEG

8-arm-PEG<sub>40K</sub>-amine was dissolved in buffer pH 8.4 and one equivalent of Cy5 NHS was dissolved in DMSO and added to the polymer (**Fig. 3**). Reaction was carried out overnight and then dialyzed against DMSO and then distilled water. Finally, the polymer was freeze dried. 10 fold molar excess of 5-BPA and PBA were activated using 10 fold molar excess of DMT-MM in DMSO and added to a reaction mixture of 8-arm-PEG<sub>40K</sub>-amine with TEA and reacted for 24 h (**Fig. 3**). Polymer was then purified by dialysis first against DMSO and then distilled water and freeze dried. Conjugation of 5-BPA and PBA was confirmed by <sup>1</sup>H-NMR measured in D<sub>2</sub>O at 25°C. Any free amine was capped using acetic anhydride and further dialyzed and lyophilized to obtain 5-BPA-Cy5-8-arm-PEG<sub>40K</sub>-Ac and PBA-Cy5-8-arm-PEG<sub>40K</sub>-Ac.

### 2.2.10 *In vitro* cellular uptake

C26 cells ( $2.5 \times 10^4$ ) were cultured on 8 Chambered # 1.0 Borosilicate Cover glass system (Lab Tek) and incubated for 48 h. Media was then replaced with fresh media of pH 7.4 and pH 6.5 containing 5-BPA or PBA conjugated Cy-5 labeled 8-arm-PEG<sub>40K</sub> and cellular uptake of polymers were evaluated after 1 h. Cell nucleus was stained with hoechst before checking fluorescence from the polymer using CLSM. Fluorescence intensity of the polymer was quantified using imageJ software to estimate cellular uptake of 5-BPA or PBA conjugated Cy-5 labeled 8-arm-PEG<sub>40K</sub>.

### 2.2.11 *In vivo* tumor accumulation and biodistribution

BALB/C mice with subcutaneous (SC) C-26 tumor model were prepared. Mice were then divided into two groups (per group n=4) and injected with 5-BPA and PBA conjugated 8-arm-PEG<sub>40K</sub> having Cy5 dye through tail vein injection. After 24 h we first imaged tumors *in vivo* and then mice were sacrificed and tumors and organs were collected and imaged immediately *ex vivo* using *in vivo* imaging system (IVIS) (excitation: 640 nm; emission: 720 nm). Blood circulation of both polymer conjugate was checked at 1, 6 and 24 h by collecting 10  $\mu$ l blood from the tail and imaged by IVIS. Finally fluorescence intensity of the images were quantified to estimate accumulation of polymers in tumors and organs.

## 2.3. Result

### 2.3.1 Quantification of Sialic acid

Overexpression of SA is a common trait of most type of cancers regardless of the origin and stage<sup>1</sup>. Researchers have previously reported almost thousand fold higher expression of

SA on the surface of murine melanoma cells<sup>11</sup> (~1.1 nmol/10<sup>6</sup> cells) compared to erythrocytes<sup>16</sup> (~20 nmol/10<sup>9</sup> cells). To verify if this value also holds true for other cancer cells we quantified expression of SA on multiple cancer cell lines. Quantification of expression of SA human and murine cancer cell lines was done using sialic acid assay kit following the method provided by the manufacturer<sup>13</sup>. A standard curve was generated from the measurement of standard SA provided in the assay kit and trendline equation was calculated based on the standard curve (**Fig. 4**). SA concentration per million cells for each cell line was then calculated from the following equation

$$\text{SA concentration} = \left(\frac{A}{B}\right) * D$$

Here,

A=Amount of SA in the sample well (concentration)

B= Sample volume added into the reaction well (μl)

D= Sample dilution factor

The value of A was calculated by extrapolating sample reading using following equation:

$$A = \left( \frac{\text{Corrected absorbance} - (y\text{-intercept})}{\text{Slope}} \right)$$

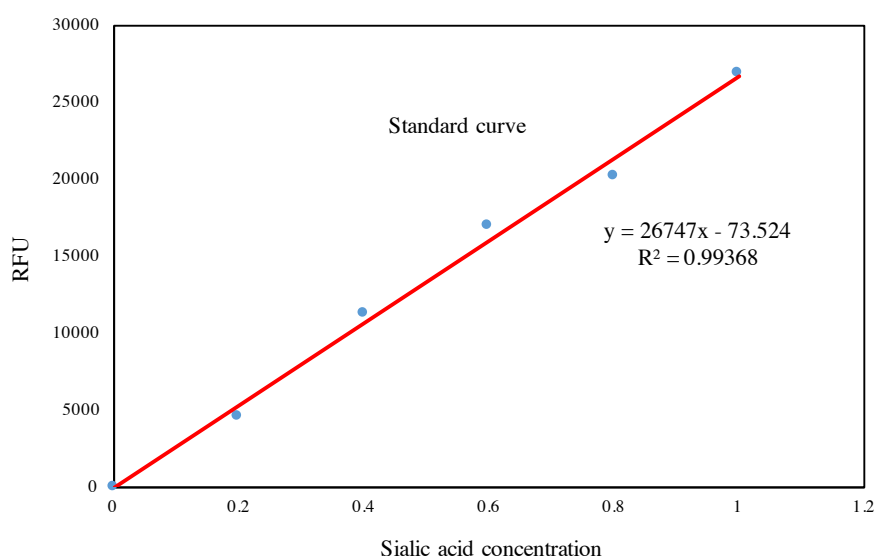


**Figure 4.** Standard curve generated from standard SA provided with assay kit

The amount of SA on *in vitro* cultured human and murine cancer cell line was determined through releasing surface SA using sialidase and generating a standard curve from pure SA provided with the assay kit. The SA amount was determined to be 1~4 nmol/  $10^6$  cells depending on the cell line (**Fig. 5**). This variation could be dependent on several factors like type of cell line, number of passing, origin and aggressiveness of the tumor. The amount of SA expression on murine melanoma cells was similar to previous reports<sup>11</sup>. The quantification values confirm overexpression of SA in all the cancer cell lines that were measured. Thus, confirming the rationality of using SA as universal targeting molecule for developing targeted cancer therapy. Among all the cell lines PANC1 demonstrated the highest expression of SA (**Fig. 5**). Hence, PANC1 was chosen to verify the targeting ability of 5-BPA molecule *in vitro*. All the quantified SA amount per million cells are represented in the graph below (**Fig. 5**).

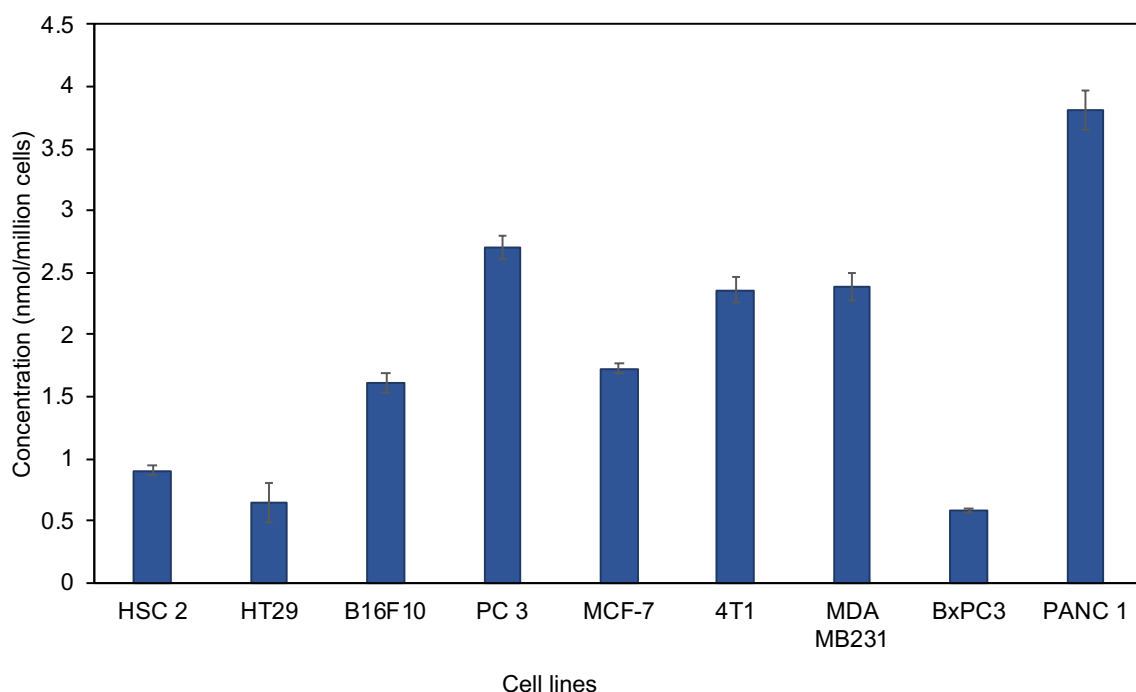


**Figure 5.** Amount of SA in different cancer cell lines (Data is represented as concentration per million cells)

### 2.3.2 Sialic acid expression in patient sample

In our previous experiment we verified the over expression of SA in *in vitro* cultured cancer cell lines. The minimum SA expression on cancer cell line was at least thousand fold higher compared to that of reported in erythrocyte<sup>16</sup>. As, SA is present in all cell surface we compared the expression in human tissue sample. To emulate the overexpression of *in vitro* cultured cancer cells in clinical condition an array of tissue samples from patient containing both cancerous (tumor) and non-cancerous (normal) tissues was purchased. The sections were then stained with SA specific lectin WGA (**Fig. 6A: green**) and nuclei was stained with DAPI (**Fig. 6A: blue**). The amount of SA expression was quantified by measuring relative fluorescence intensity in normal and tumor tissue. As expected, tumor tissue had relatively high expression of SA compared to normal tissue (**Fig. 6A&B**). Quantification of SA staining revealed relatively 6 fold higher expression of SA on cancerous tissues compared to non-cancerous tissues (**Fig. 6B**). This validates the approach of using a SA targeting system to specifically direct nanomedicine to cancer cells.

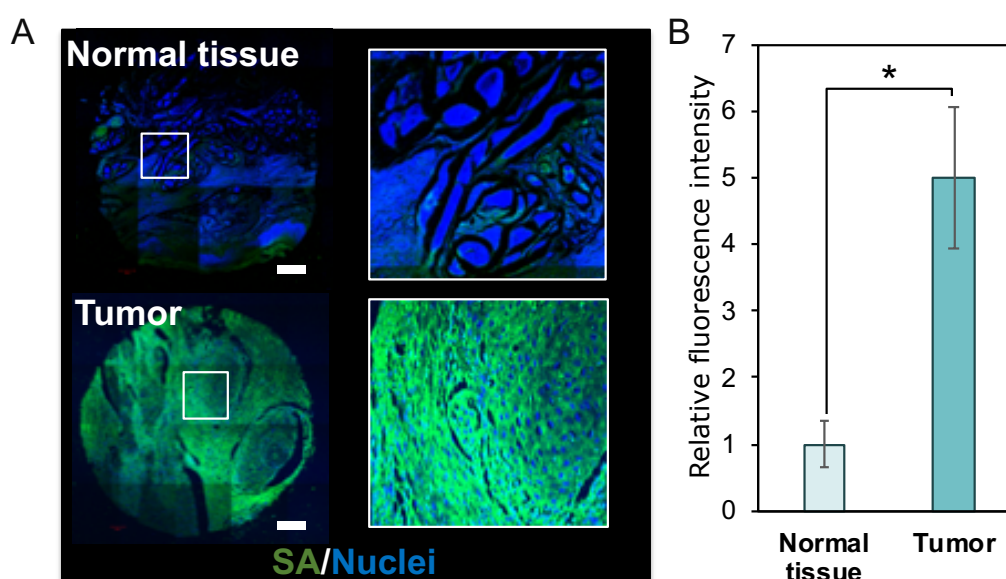


**Figure 6.** Staining of SA in human tissue array (normal tissue and tumor). **A)** Representative microscopic images of normal tissue (tongue; upper panel) and tumor (tongue; lower panel).



SA was stained with WGA (green) and nuclei with DAPI (blue). White square insets are the areas for magnification. Scale bars = 200  $\mu\text{m}$ . **B)** Quantification of the relative fluorescence intensity of SA in healthy tissue and tumor. Data are presented as average  $\pm$  standard deviation (S.D.) (n=3). \* $p < 0.001$  calculated by Student's t test.

### 2.3.3 *In-vitro* binding of 5-BPA

#### 2.3.3.1 *Lectin blocking assay*

In this experiment competitive binding affinity of 5-BPA was compared with conventional PBA. Both lectin and boronic acid have the ability to bind with the cell surface SA, which is the terminal sugar of the glycan chain. The experiment was conducted to observe if binding of boronic acid can inhibit the amount lectin binding thus working as an inhibitor for lectin. Our hypothesis is that higher binding affinity of boronic acid to SA will yield in more blocking ability to lectin binding as they will occupy the SA expressed on cancer cell surface. To verify our hypothesis we conducted controlled experiment in which cell surface SA were stained with SA-specific *Sambucus Nigra* (SNA) lectin (**Fig. 7 A: red**) and nuclei was stained with hoechst (**Fig. 7A: blue**). Then cells were exposed to PBA and 5-BPA at pH 7.4 and pH 6.5 before staining with SNA lectin. We observed reduced fluorescence intensity from SNA lectin upon prior incubation with PBA and 5-BPA (**Fig. 7 B,C**) due to binding of boronic acids with the cell surface SA. At pH 7.4 the SA-blocking effect of both PBA and 5-BPA were similar to that of control. On the contrary, when cells were incubated with 5-BPA at pH 6.5 SA-blocking effect was much higher compared to both control and PBA incubated samples (**Fig. 7 C**). Such improved blocking of lectin binding was probably due to increased binding of 5-BPA to SA at pH 6.5. So the better ability of 5-BPA to block lectin binding at pH 6.5 verifies increased interaction between SA and 5-BPA in acidic condition.

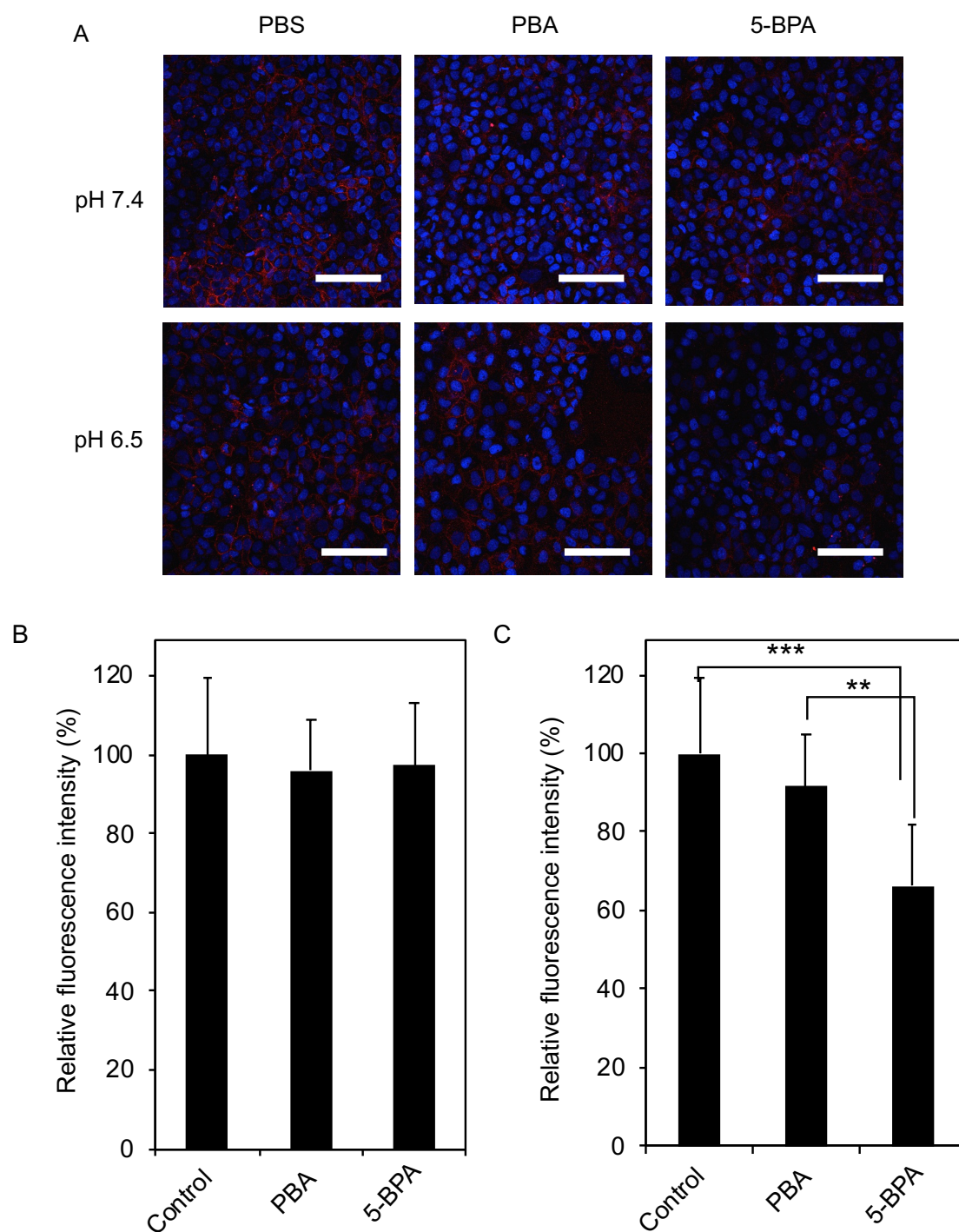


**Figure 7.** *In vitro* evaluation of the SA-binding ability of boronic acids by confocal laser scanning microscopy. **A)** Binding of *Sambucus Nigra* lectin (SNA; red) after incubating PANC 1 cells with PBS. Quantification of the SNA fluorescence intensity on PANC 1 cells at **B)** pH 7.4 and **C)** at pH 6.5 Data are presented as average  $\pm$  standard deviation (S.D.) (n=100 cells).

\*\* $p < 0.05$  and \*\*\* $p < 0.001$  calculated by Student's t test

### 2.3.3.2 Direct In-vitro evaluation of 5-BPA

In our previous lectin blocking experiment we found that 5-BPA has better ability to block binding of lectin to cell surface SA at acidic pH compared to PBA. To have more straightforward evidence of superior binding of 5-BPA to SA at intratumoral pH (pH 6.5) and verify if such binding was due to interaction between 5-BPA and SA, a dye (rhodamine B) was conjugated with 5-BPA. Binding of 5-BPA-rhodamine to cell surface SA was imaged using CLSM and fluorescence intensity was quantified. To verify the role of cell surface SA in binding with 5-BPA we cleaved SA from PANC1 cells using sialidase enzyme. If the binding was due to 5-BPA-SA interaction such removal of the SA binding site from the cell surface will decrease the uptake of 5-BPA-rhodamine. We conducted the experiment in both pH 7.4 and pH 6.5 to directly observe the binding of 5-BPA in different pH condition. Controlled experiment was performed by directly exposing cells to 5-BPA-rhodamine at pH 7.4 and pH 6.5 (**Fig. 8A & B; red**). We observed more binding of 5-BPA-rhodamine at pH 6.5 compared to pH 7.4 (**Fig. 8A & B**), which is in line with our lectin blocking assay and pH dependent binding affinity of 5-BPA-SA. Thus, proving the extraordinary binding ability of 5-BPA to SA at intratumoral pH condition (pH 6.5). To verify if such improved uptake was due to the interaction with cancer cell surface SA, terminal SA of carbohydrate chain was hydrolyzed using sialidase. Removal of SA completely diminishes the binding of 5-BPA-rhodamine at both pH 7.4 and pH 6.5 (**Fig. 8A & B**). The results of this experiment is in accordance with the previous experiment. Therefore, such improved binding of 5-BPA to SA at acidic pH allow us to conclude that 5-BPA have the potential to use as a ligand to selectively target intratumoral overexpressed SA. The ligand strategies using 5-BPA can be translated in to medical application by installing on polymer or NPs surface.

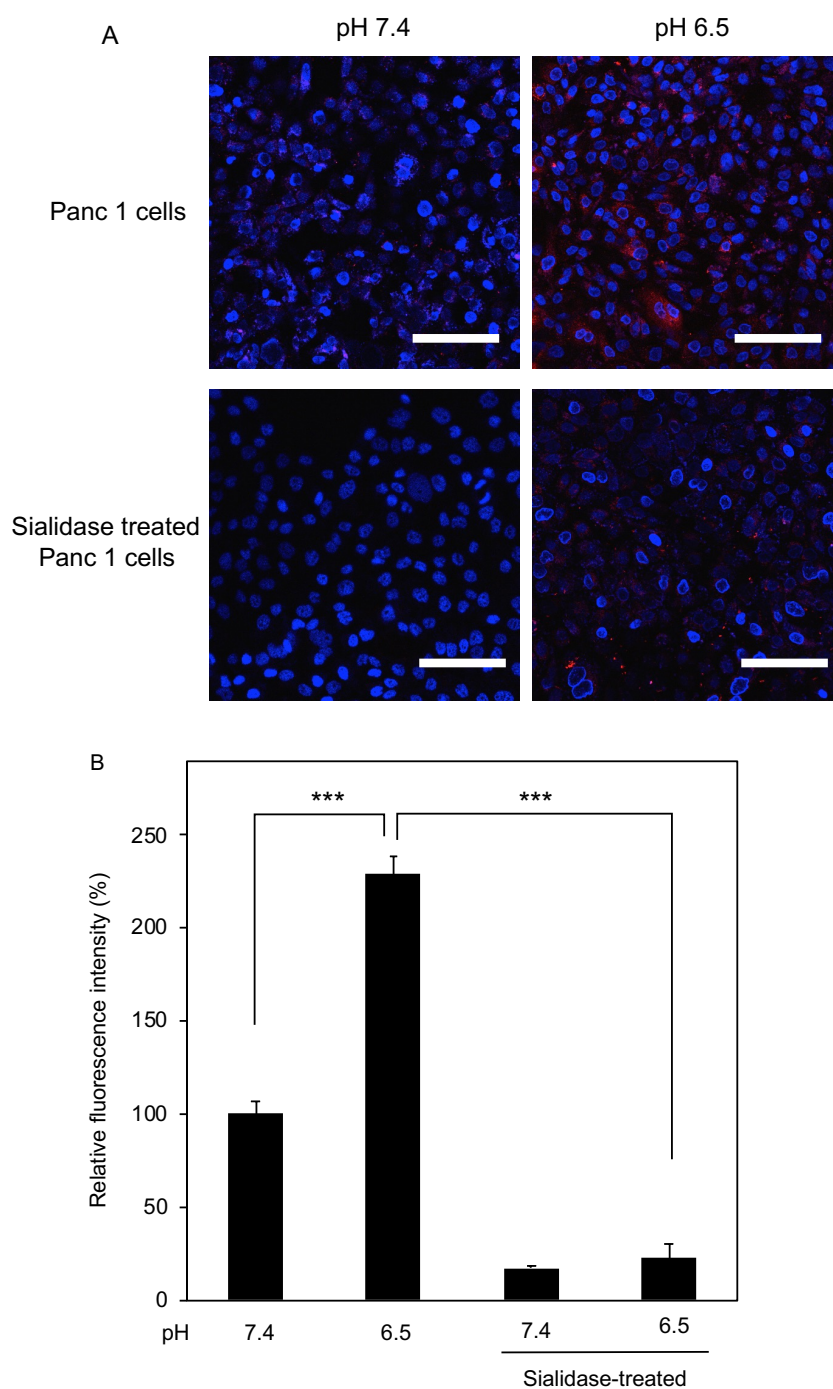


**Figure 8.** *In vitro* evaluation of the SA-binding ability of rhodamine-labeled 5-boronopicolinic acid by CLSM. **A)** Binding of rhodamine-labeled 5-BPA (red) after incubating PANC 1 cells with PBS for 5 min at pH 7.4 or pH 6.5, with and without sialidase treatment. Cell nuclei were stained with hoechst (blue). **B)** Quantification of the fluorescence intensity of rhodamine-labeled 5-boronopicolinic acid on PANC 1 cells at pH 7.4 and at pH 6.5, with and without

sialidase treatment. Data are presented as average  $\pm$  standard deviation (S.D.) (n=100 cells).

\*\*\* $p < 0.001$  calculated by Student's t test.

### 2.3.4 Polymer characterization of 5-BPA-PEG<sub>5.5K</sub>-acetal

To verify conservation of binding constant between 5-BPA and SA, 5-BPA-PEG<sub>5.5K</sub>-acetal was synthesized as a model polymer. Conjugation of 5-BPA was calculated to be 75% (**Fig. 9**) by comparing the proton units of ethylene units of PEG (-OCH<sub>2</sub>CH<sub>2</sub>:  $\delta = 3.7$  ppm) in PEG and H present in pyridine ring ( $\delta = 7.9$  ppm, 8.2 ppm, 8.8 ppm) of 5-BPA by <sup>1</sup>H-NMR spectroscopy (JEOL ECS-400; JEOL Inc., Tokyo, Japan); solvent: D<sub>2</sub>O, temperature: 25 °C.

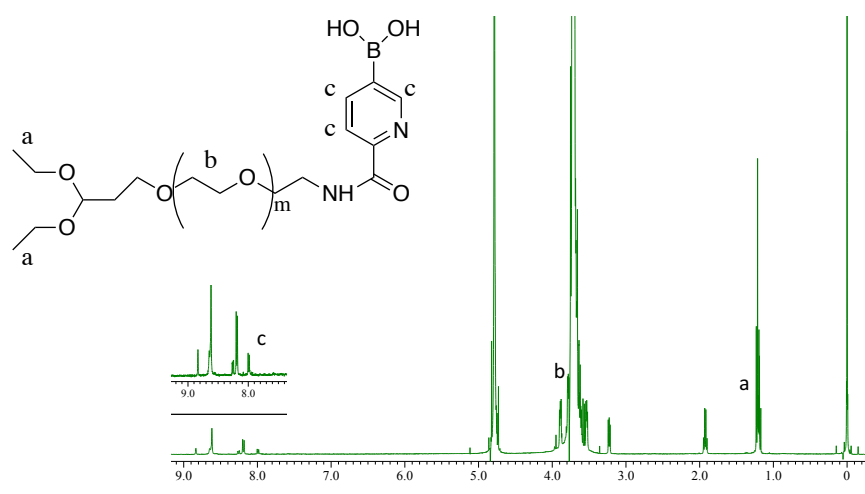


**Figure 9.** <sup>1</sup>H-NMR of 5-BPA-PEG-acetal (Mw 5500). <sup>1</sup>H-NMR measurement was done in D<sub>2</sub>O at 25°C.

### 2.3.5 Binding constant of 5-BPA-PEG<sub>5.5K</sub>-acetal

We have previously confirmed the upholding of binding constant of propylamine conjugate of 5-BPA<sup>17</sup>. To verify if the binding constant between 5-BPA conjugated polymer and SA is conserved, we used 5-BPA-PEG<sub>5.5K</sub>-acetal as a model polymer. The binding constant

between 5-BPA-PEG<sub>5.5K</sub>-acetal and SA was calculated by using a three component assay containing a fluorescent compound ARS reported by Springsteen and Wang<sup>14,15</sup>. The assay was done in two stages. First, fluorescence of ARS-5-BPA-PEG<sub>5.5K</sub>-acetal was measured with varying concentration of 5-BPA-PEG<sub>5.5K</sub>-acetal (**Fig. 10**) and then 5-BPA-PEG<sub>5.5K</sub>-acetal is replaced by addition of different concentration of SA (**Fig. 11**). Fluorescence of ARS-5-BPA-PEG<sub>5.5K</sub>-acetal solution decreases with increased concentration of SA as ARS molecule is replaced by SA to form non-fluorescent SA-5-BPA-PEG<sub>5.5K</sub>-acetal. All fluorescence measurements were done by using fluorometer (Tecan Microplate Reader: Tecan infinite 200). The experimental and analysis of data was done by following scheme described by Springsteen and Wang<sup>14</sup> (**Fig. 10-11**). The binding constant between SA and 5-BPA-PEG<sub>5.5K</sub>-acetal was found to be at pH 6.5  $K_{SA} = 243 \text{ M}^{-1}$ , at pH 6.9  $K_{SA} = 177 \text{ M}^{-1}$  and at pH 7.4  $K_{SA} = 52 \text{ M}^{-1}$ . The binding constant value that was calculated between 5-BPA-PEG<sub>5.5K</sub>-acetal and SA was similar to free 5-BPA and SA<sup>17</sup>. Thus, confirming preservation of binding constant between SA and 5-BPA after polymer conjugation. Such preservation of binding affinity of 5-BPA will allow researchers to install 5-BPA on NPs surface to use as a ligand to target overexpressed intratumoral SA.

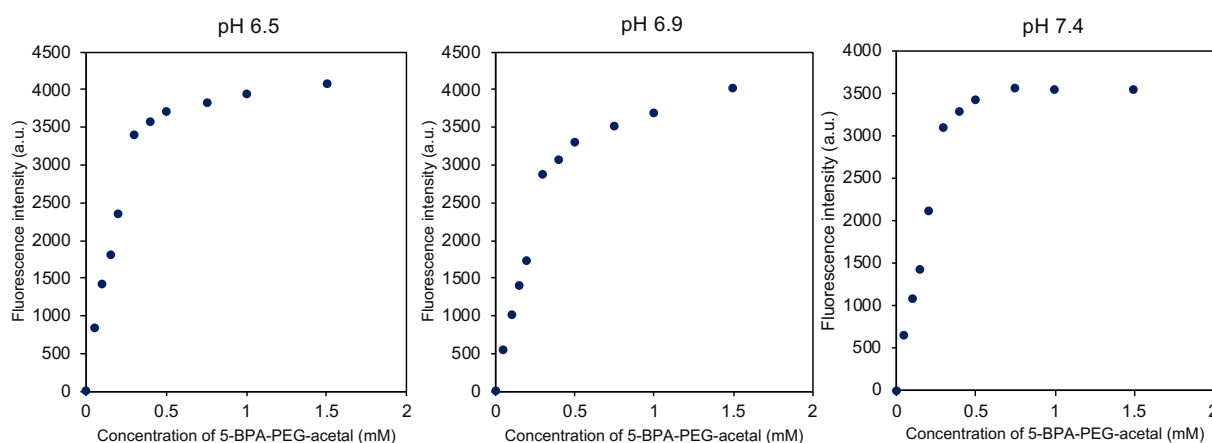


**Figure 10.** Increased fluorescence intensity (ex: 468 nm, em: 572 nm) of 9  $\mu\text{M}$  ARS solutions with increased concentration of 5-BPA-PEG<sub>5.5K</sub>-acetal in pH 6.5, pH 6.9 and pH 7.4. Data are

presented as average  $\pm$  standard deviation (S.D.), (n=3).

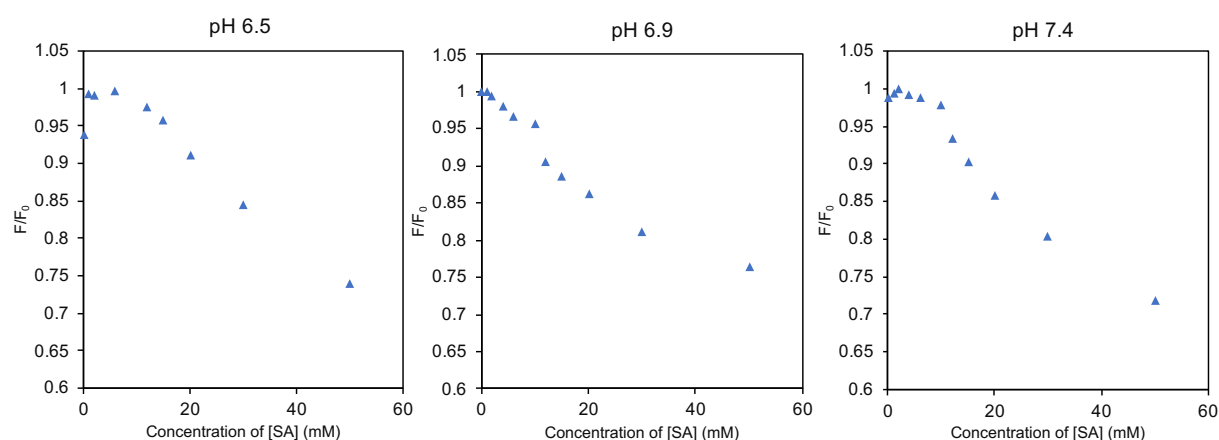


**Figure 11.** Decrease of florescent intensity (ex: 468 nm, em: 572 nm) of ARS-5-BPA-PEG<sub>5.5k</sub>-acetal complex by presence of SA at pH 6.5, pH 6.9 and pH 7.4. Data are presented as average  $\pm$  standard deviation (S.D.) (n=3). F<sub>0</sub>: Initial fluorescence intensity of solution. F: Fluorescence intensity of solution.

### 2.3.6 Polymer characterization of 8-arm-PEGs

After verifying retention of binding affinity of 5-BPA upon polymer conjugation next step was to validate superiority of 5-BPA compared to PBA as a ligand to target SA for anticancer therapy. For this purpose, a polymer with multiple conjugation site was chosen to replicate ligand density of polymeric micelle. 8-arm-PEG conjugating boronic acid derivatives provides the possibility for multivalent binding to glycoproteins of cells (**Fig. 12A**). We labeled the 8-arm-PEG with fluorescent Cy5 dye before boronic acid conjugation to observe *in vitro* cellular uptake using CLSM and perform *in vivo* evaluation using IVIS. Conjugation of 5-BPA and PBA was done using coupling reagent DMT-MM through formation of amide bond between the carboxylic acid group of boronic acids and amine group of 8-arm-PEGs. Any remaining amine group was capped though acetylation reaction and complete capping was

confirmed by checking fluorescence intensity by nanodrop using fluorescamine. The conjugation of 5-BPA and PBA was calculated by proton ratio of  $-\text{OCH}_2\text{CH}_2$  ( $\delta = 3.7$  ppm) in PEG and  $-\text{H}$  present in pyridine ring ( $\delta = 7.2$  ppm, 8.1 ppm, 8.8 ppm) of 5-BPA (**Fig. 12B**) and benzene ring ( $\delta = 7.5$  ppm, 7.8 ppm, 7.9 ppm, 8.1 ppm) of PBA (**Fig. 12C**) in the  $^1\text{H}$ -NMR spectra. Conjugation efficiency was 65% and 78% respectively.

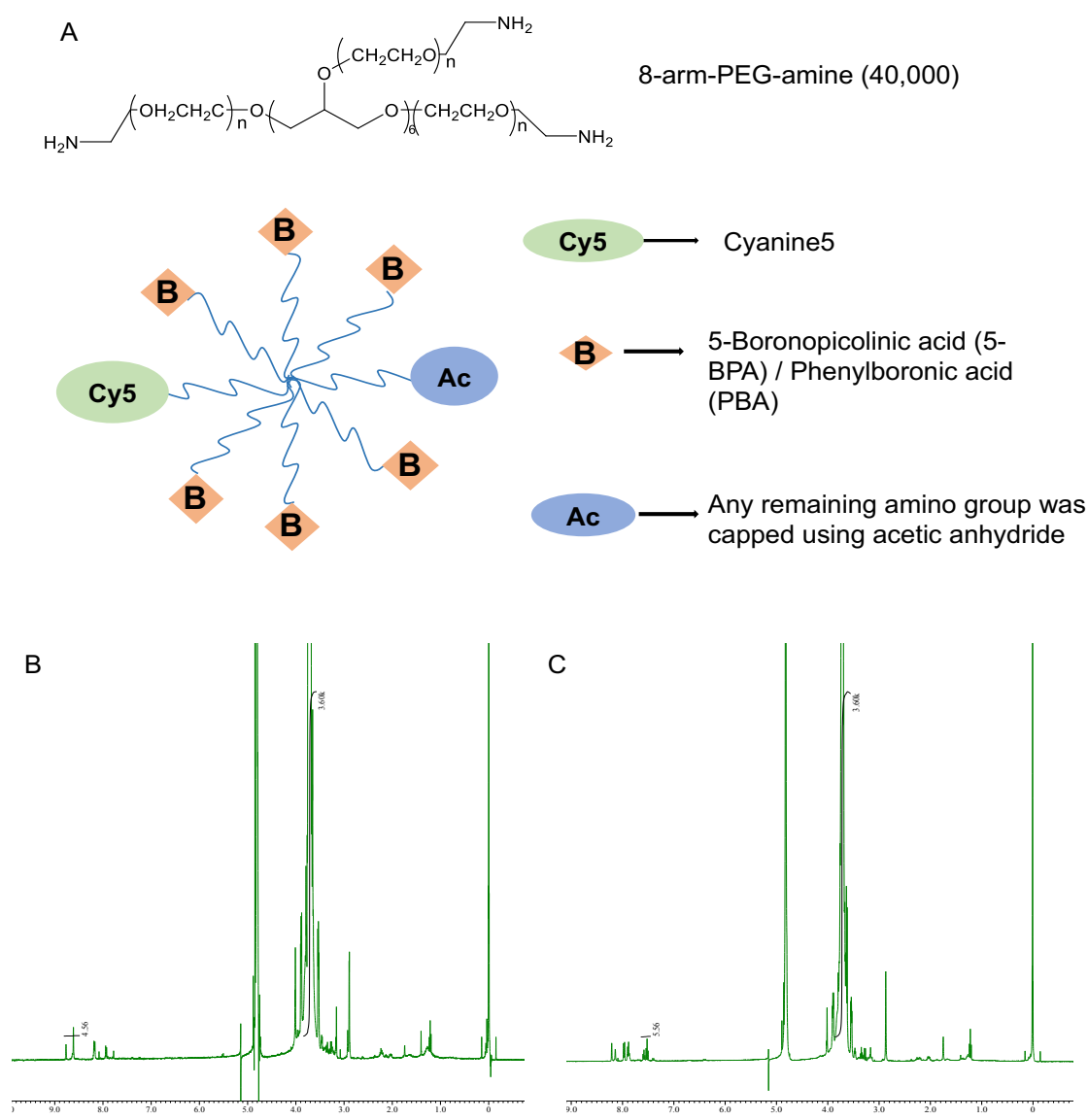
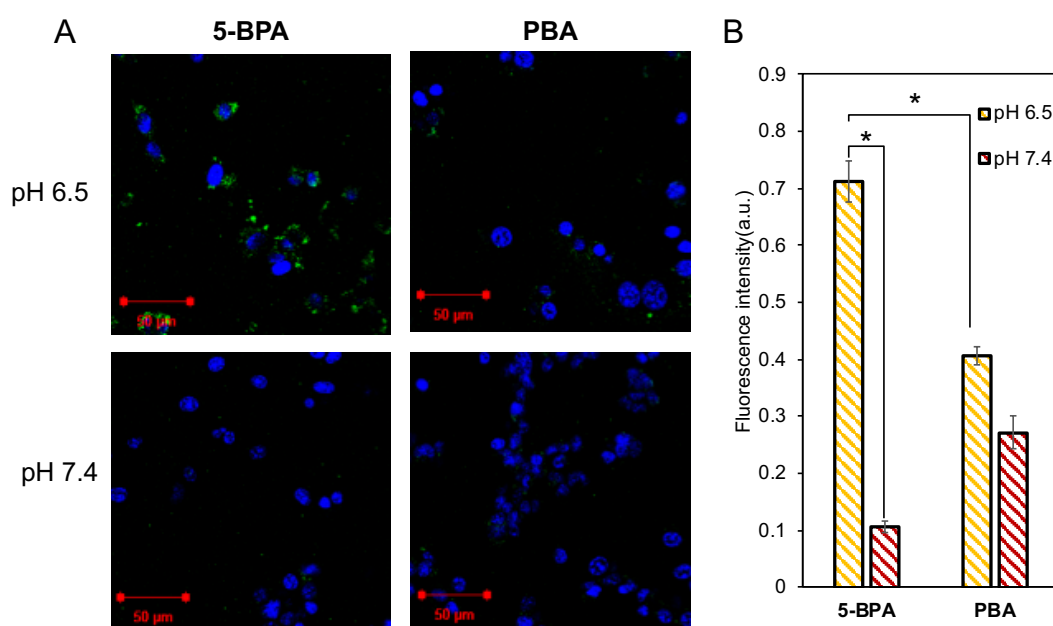


**Figure 12.** Strategy and characterization of 8-arm-PEG<sub>40K</sub> **A)** Design strategy of 8-arm PEG conjugating boronic acid derivatives.  $^1\text{H}$ -NMR spectra of **B)** 5-BPA-Cy5-8-arm-PEG<sub>40K</sub> and **C)** PBA-Cy5-8-arm-PEG<sub>40K</sub> measured in  $\text{D}_2\text{O}$  at  $25^\circ\text{C}$ .



### 2.3.7 Cellular uptake of 8-arm-PEGs

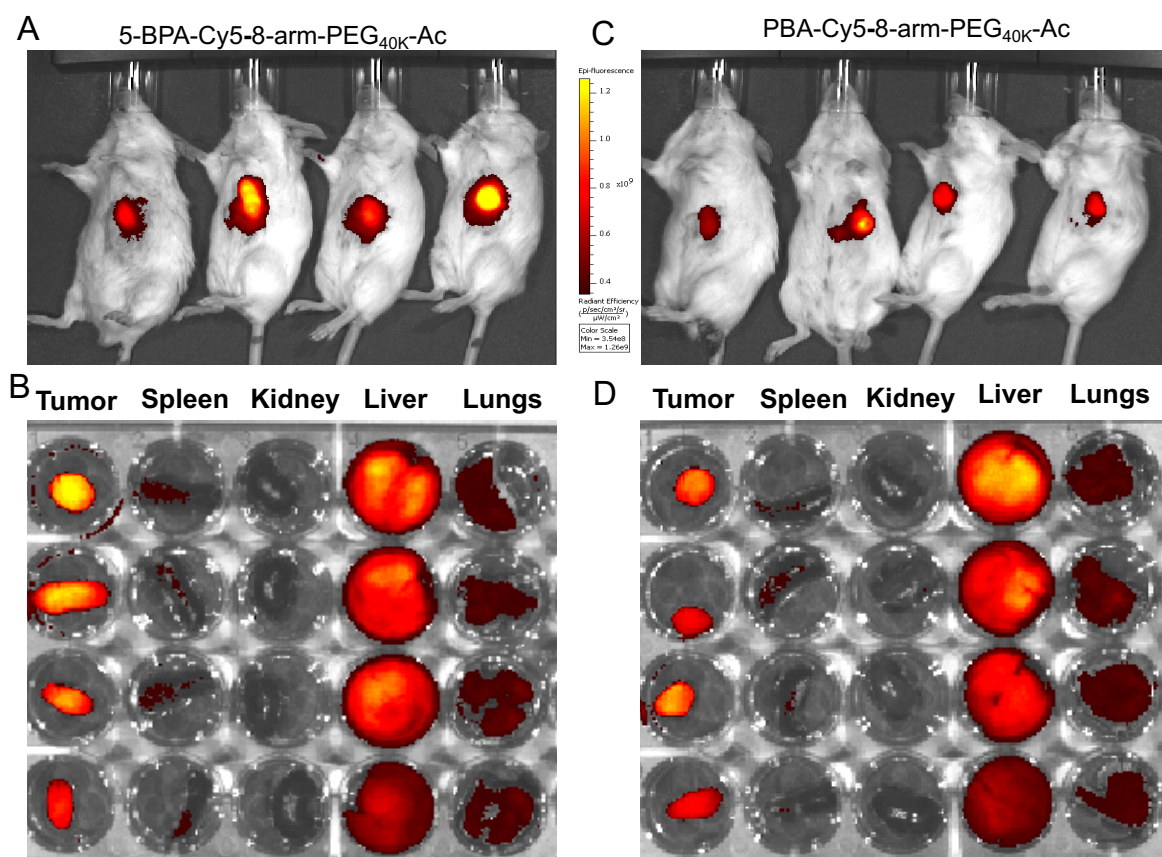
To evaluate superiority of 5-BPA ligand over PBA ligand we performed an *in vitro* cellular uptake of Cy5 labeled 5-BPA and PBA conjugated 8-arm-PEG<sub>40K</sub> (**Fig. 13A: green**) using confocal laser scanning microscopy (CLSM) in C26 cell line. Cell nuclei was stained with hoechst (**Fig. 13A: blue**). We incubated both polymers at pH 6.5 and pH 7.4 to assess the pH depending cellular uptake of the polymers due presence of different ligands. The result showed that both polymers had higher uptake at pH 6.5 compared to pH 7.4 but 5-BPA-Cy5-8-arm-PEG<sub>40K</sub>-Ac was taken up rapidly at pH 6.5 compared to pH 7.4 (**Fig. 13A & B**). Whereas, PBA-Cy5-8-arm-PEG<sub>40K</sub>-Ac showed higher uptake at pH 7.4.



**Figure 13.** Cellular uptake of Cy5 labeled 5-BPA or PBA conjugated polymer. **A)** Cellular uptake of 5-BPA-8-arm-PEG<sub>40K</sub>-Cy5 (5-BPA) and PBA-Cy5-8-arm-PEG<sub>40K</sub>-Ac (PBA) in C26 cells after 1-h at pH 6.5 and pH 7.4. Polymers are (green) and nuclei was stained with DAPI (blue). Scale bars =50 μm. **B)** Quantification of the uptake of fluorescent polymers at pH 6.5 (yellow stripe) and pH 7.4 (red stripe) into C26 cells. Data are expressed as averages ± S.D., n = 4, \**p* < 0.05. P value was calculated using Student's t test.

### 2.3.8 *In vivo* tumor accumulation and biodistribution of 8-arm-PEGs

Cy5 labeled 5-BPA or PBA conjugated 8-arm-PEG<sub>40K</sub> polymers were injected via intravenous route. 24 h after injection mice were anesthetized and tumor accumulation was imaged *in vivo* (**Fig. 14A & C**). Mice were then sacrificed and tumor, spleen, kidney, liver and lungs were collected and images were taken *ex vivo* (**Fig. 14B & D**). Clearance of the polymers was estimated by collecting blood from the tail vein and calculating percentage of remaining injected dosage. Both polymers demonstrated similar blood circulation profile (**Fig. 14E**). To quantify accumulation of polymers total radiance efficiency was calculated and normalized by the area. In the tumor, 5-BPA-Cy5-8-arm-PEG<sub>40K</sub>-Ac (5-BPA) accumulation was significantly higher compared to PBA-Cy5-8-arm-PEG<sub>40K</sub>-Ac (PBA) (**Fig. 14F**), this can be attributed to high specificity of 5-BPA to SA in acidic intratumoral pH. Accumulation in the spleen, kidney, liver, lungs for both polymers were comparable.



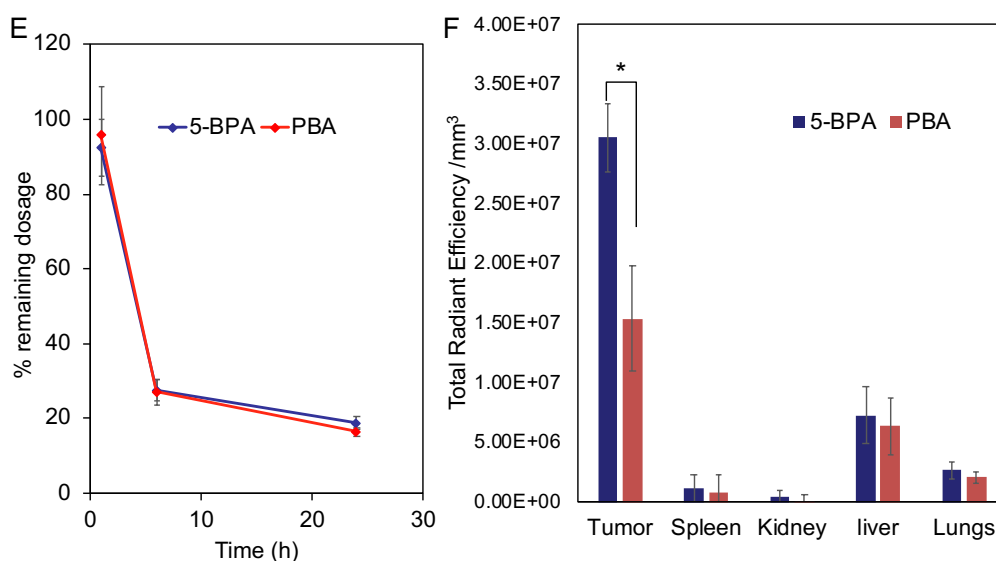


**Figure 14.** *In vivo* evaluation of 5-BPA-Cy5-8-arm-PEG<sub>40K</sub>-Ac (5-BPA) and PBA-Cy5-8-arm-PEG<sub>40K</sub>-Ac in (PBA) SC C26 tumor model. **A)** *In vivo* fluorescence absorbance of tumor accumulation **B)** *Ex vivo* fluorescence absorbance of tumor accumulation and biodistribution of 5-BPA-Cy5-8-arm-PEG<sub>40K</sub>-Ac. **C)** *In vivo* fluorescence absorbance of tumor accumulation **D)** *Ex vivo* fluorescence absorbance of tumor accumulation and biodistribution of PBA-Cy5-8-arm-PEG<sub>40K</sub>-Ac (PBA). **E)** Blood circulation of polymers after 24 h of injection. **F)** Quantification of the accumulation of fluorescent polymers in tumor and organs. Data are expressed as averages  $\pm$  S.D.,  $n = 4$ ,  $*p < 0.05$ . P value was calculated by Student's t test.

## 2.4 Discussion

High amount of SA on the cell surface was confirmed through quantification of SA in different *in vitro* cultured cancer cell lines. Further, relatively excessive amount of SA expression was also detected in human head and neck tumor tissues compared to normal tissues. We verified the ability of 5-BPA to bind to cell surface SA through SA-blocking assay using SNA lectin and directly quantifying rhodamine conjugated 5-BPA on PANC1 cell line. We have synthesized model 5-BPA-PEG<sub>5.5K</sub>-acetal polymer and confirmed conservation of binding

constant of 5-BPA conjugated with a polymer to SA. The data shows 5-BPA molecule does not lose its specific interaction to SA at reduced pH. Finally, we synthesized 5-BPA and PBA conjugated Cy5 labeled 8-arm-PEGs which can emulate multivalency presented in polymeric micelles for binding to glycoproteins of cells. Our *in vitro* cellular uptake data suggests 5-BPA-Cy5-8-arm-PEG<sub>40K</sub> have increased cellular uptake at intratumoral pH (pH 6.5) and better tumor accumulation *in vivo* compared to PBA-Cy5-8-arm-PEG<sub>40K</sub>. Contrary, comparable organ accumulation of both polymers and similar blood circulation points to the ability of 5-BPA to better target SA in acidic intratumoral pH microenvironment. Thus, resulting in greater tumor accumulation.

## 2.5 Conclusion

In this chapter, firstly we have confirmed increased expression of SA both in *in vitro* cultured human and murine cancer cell lines as well as tumor samples from patient. In patient sample SA expression was 6 fold higher in tumor tissue relative to normal tissue. We have demonstrated that the unique interaction of 5-BPA and SA can be translated biologically as 5-BPA can bind to cancer cell surface SA. Moreover, having a carboxylic moiety in the structure of 5-BPA makes it rather easy to conjugate with a primary amine bearing compound e.g. polymers by using conventional coupling mechanism. Furthermore, the ability of 5-BPA after polymer conjugation to maintain binding constant at reduced pH makes 5-BPA an excellent candidate to be used as a ligand on polymeric micelle surface to specifically target cancer cells at intratumoral pH. Superiority of 5-BPA ligand compared to PBA to improve the tumor accumulation while maintaining similar blood circulation profile and organ accumulation makes 5-BPA an excellent candidate for developing specific targeting strategies for cancer while avoiding interaction with normal tissue.

## 2.6 References

1. Hanahan, D. & Weinberg, R. A. Hallmarks of cancer: The next generation. *Cell* **144**, 646–674 (2011).
2. Bornhöfft, K. F., Goldammer, T., Rebl, A. & Galuska, S. P. Siglecs: A journey through the evolution of sialic acid-binding immunoglobulin-type lectins. *Developmental and Comparative Immunology* **86**, 219–231 (2018).
3. Schultz, M. J., Swindall, A. F. & Bellis, S. L. Regulation of the metastatic cell phenotype by sialylated glycans. *Cancer Metastasis Rev.* **31**, 501–518 (2012).
4. Büll, C., den Brok, M. H. & Adema, G. J. Sweet escape: Sialic acids in tumor immune evasion. *Biochim. Biophys. Acta - Rev. Cancer* **1846**, 238–246 (2014).
5. Picco, G. *et al.* Over-expression of ST3Gal-I promotes mammary tumorigenesis. *Glycobiology* **20**, 1241–1250 (2010).
6. Julien, S. *et al.* Selectin Ligand Sialyl-Lewis x Antigen Drives Metastasis of Hormone-Dependent Breast Cancers. *Cancer Res.* **71**, 7683–7693 (2011).
7. Tatsuta, T., Satoh, T., Sugawara, S., Hara, A. & Hosono, M. Sialic acid-binding lectin from bullfrog eggs inhibits human malignant mesothelioma cell growth in vitro and in vivo. *PLoS One* **13**, e0190653 (2018).
8. Loureiro, L. R. *et al.* Novel monoclonal antibody L2A5 specifically targeting sialyl-Tn and short glycans terminated by alpha-2–6 sialic acids. *Sci. Rep.* **8**, 12196 (2018).
9. Otsuka, H., Uchimura, E., Koshino, H., Okano, T. & Kataoka, K. Anomalous binding profile of phenylboronic acid with N-acetylneuraminic acid (Neu5Ac) in aqueous solution with varying pH. *J. Am. Chem. Soc.* **125**, 3493–3502 (2003).
10. Matsumoto, A., Kataoka, K. & Miyahara, Y. New directions in the design of phenylboronate-functionalized polymers for diagnostic and therapeutic applications. *Polymer Journal* **46**, 483–491 (2014).
11. Deshayes, S. *et al.* Phenylboronic Acid-Installed Polymeric Micelles for Targeting Sialylated Epitopes in Solid Tumors. *J. Am. Chem. Soc.* **135**, 15501–15507 (2013).
12. Matsumoto, A. *et al.* Heterocyclic boronic acids display sialic acid selective binding in a hypoxic tumor relevant acidic environment. *Chem. Sci.* **8**, 6165–6170 (2017).
13. Mudd, A. T. *et al.* Porcine Milk Oligosaccharides and Sialic Acid Concentrations Vary Throughout Lactation. *Front. Nutr.* **3**, (2016).
14. Springsteen, G. & Wang, B. Alizarin Red S. as a general optical reporter for studying

- the binding of boronic acids with carbohydrates. *Chem. Commun.* 1608–1609 (2001). doi:10.1039/b104895n
15. Springsteen, G. & Wang, B. A detailed examination of boronic acid-diol complexation. *Tetrahedron* **58**, 5291–5300 (2002).
  16. Miller, A., Sullivan, J. F. & Katz, J. H. Sialic Acid Content of the Erythrocyte and of an Ascites Tumor Cell of the Mouse. *Cancer Res.* **23**, 485–490 (1963).
  17. Matsumoto, A. *et al.* Heterocyclic boronic acids display sialic acid selective binding in a hypoxic tumor relevant acidic environment. *Chem. Sci.* **8**, 6165–6170 (2017).

## **Chapter 3**

### **Preparation of DACHPt loaded 5-BPA installed polymeric micelle**

## Chapter 3: Preparation of DACHPt loaded 5-BPA installed polymeric micelle

### Abstract

Polymers and micelles were prepared and characterized. PEG-*b*-PLGA block copolymers were synthesized and characterized. PBA and 5-BPA was conjugated to the end terminus of PEG. Alexa 555 & 647 dye conjugated PEG<sub>10K</sub>-*b*-PLGA were prepared to construct fluorescent micelles to observe cellular uptake *in vitro* and blood circulation *in vivo* by imaging technique. Existence of boron diol on 5-BPA and PBA conjugated block-copolymer was confirmed before micelle preparation through ARS assay. Ultimately, DACHPt loaded polymeric micelles were constructed with 50% surface ligand 5-BPA or PBA in water through polymer metal complexation. Size, PDI, drug loading and surface charge of all the micelles were measured. All the micelles size was around 30 nm with narrow size distribution. The drug loading was calculated to be 30% (pt/polymer wt/wt).



## Chapter 3: Preparation of DACHPt loaded 5-BPA installed polymeric micelle

### 3.1 Introduction

### 3.2 Experimental

#### 3.2.1 Materials

#### 3.2.2 Synthesis of block co-polymer

##### 3.2.2.1 Synthesis of MeO-PEG<sub>12K</sub>-b-PLGA and acetal-PEG<sub>12K</sub>-b-PLGA

##### 3.2.2.2 Synthesis of Azide-PEG<sub>11K</sub>-b-PLGA-Ac

##### 3.2.2.3 Synthesis of MeO-PEG<sub>10K</sub>-b-PLGA

#### 3.2.3 Conjugation of 5-BPA

#### 3.2.4 Conjugation of PBA

#### 3.2.5 Confirmation of presence of boron diol on conjugated block-copolymer

#### 3.2.6 Conjugation of Alexa 647 and alexa 555

#### 3.2.7 Preparation of DACHPt-loaded micelles

### 3.3 Results

#### 3.3.1 Characterization of polymers

##### 3.3.1.1 Characterization of MeO-PEG<sub>12K</sub>-b-PBLG and acetal-PEG<sub>12K</sub>-b-PBLG

##### 3.3.1.2 Characterization of Azide-PEG<sub>11K</sub>-b-PBLG

##### 3.3.1.3 Characterization of MeO-PEG<sub>10K</sub>-b-PLGA

#### 3.3.2 Conjugation of 5-BPA

#### 3.3.3 Conjugation of PBA

#### 3.3.4 Confirmation of presence of boron diol on conjugated block-copolymer

#### 3.3.5 Characterization of micelles

### 3.4 Discussion

### 3.5 Conclusion

### 3.6 References

### 3.1. Introduction

Polymeric micelles have received remarkable attention due to their size and stability profile<sup>1,2</sup>. Polymeric micelles constructed with synthetic biodegradable polymers have been being used to solve issues related to formulation of drug like low solubility in aqueous solution<sup>3</sup>. Moreover, these NPs are also improving the pharmacokinetics of the formulation including prolong blood circulation, avoid detection by reticuloendothelial system (RES), fast clearance and unexpected protein absorption. Due to their small size and stability in the blood circulation polymeric micelles can accumulate in solid tumors by the enhanced permeability and retention (EPR) effect<sup>4</sup>. Tailor ability of micelles also enables us to change size and characteristics of the polymeric micelles<sup>5</sup>. High hydrophobic drug loading capacity also makes micelles a unique delivery system<sup>6</sup>.

Our group has been pioneer in developing polymeric micelle constructed from block copolymers<sup>7,6</sup>. In our polymer design we are using PEG-*b*-poly(amino acid) block copolymers and incorporating platinum drugs in the micelle core. Micelle is formed spontaneously in the water through polymer metal complexation. PEG can form hydrogen bond with the water molecule and form a hydrophilic shell around the hydrophobic core. The hydrophilic shell gives micelle stealth properties and protects the core from recognition by reticuloendothelial system. This technique of pegylation has been extensively used for designing drug delivery systems<sup>2</sup>. The release of drug can be tuned to stimuli responsive for example intratumoral pH, thus causing selective release of drug at target site<sup>8</sup>. Moreover, we can modify the PEG end terminus and conjugate ligand to selectively target tumors<sup>9,10,11</sup>. Such ligand installed targeted nanoparticles have the potential to improve tumor accumulation of loaded anticancer drugs and increase efficacy.

Recently, researchers are exploiting SA as a target site for cancer cells due to their overexpression in tumor<sup>12</sup>. Treatment strategies directing towards abnormal sialylation emerged as an appealing option<sup>13</sup> as their vital role in immune escape, cancer progression and metastasis have been well evidenced<sup>12</sup>. There have been reports on development of therapeutic and diagnostic approaches directed towards aberrant sialylation<sup>14</sup>. These tactics includes both targeting overexpressed SA in tumor to deliver therapeutic agents<sup>10,15, 16, 17</sup> and blocking SA by using glycomimetics<sup>18</sup>. Polymer based imaging systems<sup>19,20,21</sup> and sensor based SA detection techniques<sup>22,23</sup> are also being developed to study cancer cells. Most of these systems are based on unique interaction of PBA and SA<sup>24</sup>. PBA can form ester bonds with diol-bearing molecules and shows selectivity to SA at intratumoral pH (pH 6.5). As targeting strategies with highly selective molecule for SA such as lectin<sup>25</sup> and antibodies<sup>26</sup> are challenging for systemic use due to their immunogenicity. Thus, the development of ligands capable of recognizing tumor SA, while avoiding interaction with SA in healthy tissues, is still necessary for advancing SA targeted strategies. Boronic acids can form reversible covalent interactions with diol-containing molecules. In fact, sugars, such as the common monosaccharides (*e.g.* glucose), contain diols, and as a consequence, boronic acids have proven to be helpful molecular ligands for binding and detection, working as synthetic lectins<sup>21</sup>. Complexes between PBA and sugars were shown to be stable at pH higher than their pKa, however, with pH lower than pKa only SA-PBA complexes were stable<sup>27</sup>. We have already taken advantage of such binding behavior of boronic acids and demonstrated that PBA installed DACHPt loaded polymeric micelles enhanced selectivity against the SA-rich B16F10 melanoma cells<sup>10</sup>. Moreover, DACHPt loaded polymeric micelles (NC-4016) is undergoing phase I clinical trials for treating solid tumors and lymphoma (Study NCT01999491)<sup>28</sup> after demonstrating better performance in a xenograft model of gastric cancer<sup>29</sup>. I aim to further improve treatment outcome by installing boronic acid derivative ligand on the surface of DACHPt loaded micelle to specifically target

cancer cells. Recently, we have reported the superior affinity of 5-boronopicolinic acid (5-BPA) for SA at intratumoral pH which is much higher compared to PBA<sup>30</sup>. We have also conjugated an amine bearing small molecule propylamine and demonstrated preservation of binding constant of 5-BPA conjugate to SA after modification<sup>31</sup>. So herein, I focused on developing drug delivery systems using 5-BPA for increased binding to intratumoral SA. We developed polymeric micelles loading platinum drugs aimed at eliminating highly malignant cancer stem cells (CSCs), which have increased SA. We have already verified our recent findings about specific interaction between 5-BPA and SA in reduced pH *in vitro*. As the 5-BPA has a functional carboxylic group it can be attached to any primary amine by forming amide bond. We have also conjugated 5-BPA with PEG polymer and demonstrated retention of binding affinity to SA in acidic pH. We have also found 5-BPA conjugated 8-arm-PEG with multivalency have higher tumor accumulation compared to PBA conjugated 8-arm-PEG.

In this chapter, I have reported synthesis and characterization of poly(ethylene glycol-poly(L-glutamic acid) block copolymers: *MeO-PEG<sub>12K</sub>-b-PLGA*, *acetal-PEG<sub>12K</sub>-b-PLGA* and azide-PEG<sub>11K</sub>-b-PLGA-Ac. PBA and 5-BPA were conjugated at the end terminus of *acetal-PEG<sub>12K</sub>-b-PLGA* and azide-PEG<sub>11K</sub>-b-PLGA-Ac respectively. Confirmation of presence of boron diol on conjugated block-copolymers was done before moving to construction of polymeric micelles. A short PEG length block copolymer MeO-PEG<sub>10K</sub>-b-PLGA was also synthesized and characterized to mix with ligand polymers and prepare 50% ligand density on micelle surface. MeO-PEG<sub>10K</sub>-b-PLGA was labeled with alexa 555 and alexa 647 fluorescent dye to prepare fluorescent micelle and trace under confocal laser scanning microscope (CLSM). DACHPt containing block copolymer micelles were prepared in distilled water through polymer metal complex formation between DACHPt and PLGA segment of block copolymer. Finally, size, surface charge and drug loading of the prepared micelles was measured.

## 3.2 Experimental

### 3.2.1 Materials

$\alpha$ -Methoxy- $\omega$ -aminopropyl-poly(ethylene glycol) (MeO-PEG-NH<sub>2</sub>; Mw = 12,000 & 10,000) and  $\alpha$ -acetal- $\omega$ -aminopropyl-poly(ethylene glycol) (Acetal-PEG-NH<sub>2</sub>; Mw = 12,000) were purchased from NOF Co., Inc. (Tokyo, Japan).  $\alpha$ -azide- $\omega$ -aminopropyl-poly(ethylene glycol) (N<sub>3</sub>-PEG-OH; Mw = 12,000) received from (Dr. Miura).  $\gamma$ - Benzyl-L-glutamate N-carboxyanhydride (BLG-NCA) was purchased from Chuo Kaseihin Co., Inc. (Tokyo, Japan). DBCO-PEG<sub>2k</sub>-amine was purchased from Nanocs (New York, USA). Triethylamine (TEA, >99%), 4-(4,6-dimethoxy-1,3,5-triazin-2-yl)-4-methylmorpholinium chloride n-hydrate (DMT-MM), methanesulfonyl chloride (MsCl, >99%), N,N-dimethylformamide (DMF), dimethyl sulfoxide (DMSO) (>99%), 3-aminophenylboronic acid (PBA), acetic anhydride (>97%) and sodium hydroxide (96%) was purchased from, Wako Pure Chemical Industries Ltd., (Osaka, Japan). Silver nitrate (AgNO<sub>3</sub>, 99.999%) was purchased from Aldrich Chemical Co., (Milwaukee, WI). 5-Boronopicolinic acid were obtained from Santa Cruze Biotechnology, Inc (Texas United States). Sodium cyanoborohydride (NaBH<sub>3</sub>CN) was purchased from Tokyo Chemical Industry Co., Inc. Alexa 647- succinimidyl ester and Alexa Fluor 555 succinimidyl ester were purchased from Life Technologies Corporation (Tokyo, Japan). Dichloro (1,2-diaminocyclohexane) platinum (II) (DACHPtCl<sub>2</sub>) and alizarin red s (ARS) was obtained from Sigma-Aldrich Co. (ST. Louis, U.S.A).

### 3.2.2 Synthesis of block co-polymers

#### 3.2.2.1 Synthesis of MeO-PEG<sub>12K</sub>-b-PLGA and acetal-PEG<sub>12K</sub>-b-PLGA

Methoxy-poly(ethylene glycol)-b-poly( $\gamma$ -benzyl-L-glutamate) (MeO-PEG<sub>12K</sub>-b-

PBLG) (molecular weight of PEG ( $M_{n,PEG}$ ) = 12,000, degree of polymerization of PBLG ( $DP_{PBLG}$ ) = 40) and acetal-poly(ethylene glycol)-*b*-poly( $\gamma$ -benzyl-L-glutamate) (acetal-PEG<sub>12K</sub>-*b*-PBLG) (molecular weight of PEG ( $M_{n,PEG}$ ) = 12,000, degree of polymerization of PBLG ( $DP_{PBLG}$ ) = 40) were synthesized through previously reported method<sup>10</sup>. MeO-PEG<sub>12K</sub>-NH<sub>2</sub> and acetal-PEG<sub>12K</sub>-NH<sub>2</sub> were dried by benzene freeze drying technique for overnight to remove any water. The N-carboxyanhydride of  $\gamma$ -benzyl-L-glutamate (BLG-NCA) polymerization was initiated by using corresponding amine initiator: MeO-PEG<sub>12K</sub>-NH<sub>2</sub> and acetal-PEG<sub>12K</sub>-NH<sub>2</sub> in dry DMF. Polymerization reaction was continued for 3 days at 37°C. MeO-PEG<sub>12K</sub>-*b*-PBLG and acetal-PEG<sub>12K</sub>-*b*-PBLG were collected by ether precipitation using ice and dried under vacuum. Ether precipitation was conducted twice to remove any impurities from the polymers. The molecular weight distribution of MeO-PEG<sub>12K</sub>-*b*-PBLG and acetal-PEG<sub>12K</sub>-*b*-PBLG were measured by gel permeation chromatography (GPC) (column: TSK-gel G3000<sub>HHR</sub>, G4000<sub>HHR</sub>) (Tosoh Co., Inc., Yamaguchi, Japan); eluent: DMF having 10 mM LiCl; flow rate 0.8 ml/min; detector: refractive index (RI); temperature: 25°C. Degree of polymerization of  $\gamma$ -benzyl-L-glutamate unit of ( $DP_{PBLG}$ ) of MeO-PEG<sub>12K</sub>-*b*-PBLG and acetal-PEG<sub>12K</sub>-*b*-PBLG were calculated by comparing the proton units of ethylene units of PEG (-OCH<sub>2</sub> CH<sub>2</sub>-:  $\delta$  = 3.7 ppm) with the phenyl groups of PBLG (-C<sub>6</sub>H<sub>5</sub>-:  $\delta$  = 7 ppm) by <sup>1</sup>H-NMR spectroscopy (JEOL ECS-400; JEOL Inc., Tokyo, Japan); solvent: DMSO-*d*<sub>6</sub>, temperature: 80°C. Methoxy-poly(ethylene glycol)-*b*-poly(L-glutamic acid) (MeO-PEG<sub>12K</sub>-*b*-PLGA) and acetal-poly(ethylene glycol)-*b*-poly(L-glutamic acid) (acetal-PEG<sub>12K</sub>-*b*-PLGA) were obtained by cleaving benzyl group of side chain of MeO-PEG<sub>12K</sub>-*b*-PBLG and acetal-PEG<sub>12K</sub>-*b*-PBLG in 0.5 N NaOH at room temperature overnight. On addition of NaOH polymers appear turbid but as the reaction proceeds and benzyl group from the side chain is removed both polymers start to dissolve in the solution. Polymers were purified to remove cleaved group and alkali by dialysis against distilled water and freeze dried to finally prepare MeO-PEG<sub>12K</sub>-*b*-PLGA and

acetal-PEG<sub>12K</sub>-*b*-PLGA. Deprotection of the benzyl ester group was confirmed by <sup>1</sup>H-NMR (solvent: D<sub>2</sub>O; temperature: 25°C).

### 3.2.2.2 Synthesis of azide-PEG<sub>11K</sub>-*b*-PLGA-Ac

$\alpha$ -azide- $\omega$ -aminopropyl-poly(ethylene glycol) (azide-PEG-NH<sub>2</sub>; Mw = 11,000) was synthesized following previously reported method<sup>9</sup>. Azide-poly(ethylene glycol)-*b*-poly( $\gamma$  - benzyl-L-glutamate) (azide-PEG<sub>11K</sub>-*b*-PBLG) (molecular weight of PEG (M<sub>n,PEG</sub>) = 11,000, degree of polymerization of PBLG (DP<sub>PBLG</sub>) = 40) was synthesized through previously reported method<sup>9</sup>. Azide-PEG<sub>11K</sub>-NH<sub>2</sub> were dried by benzene freeze drying technique for overnight to remove any water. The N-carboxyanhydride of BLG-NCA polymerization was initiated by using azide-PEG<sub>11K</sub>-NH<sub>2</sub> in dry DMF. Polymerization reaction was continued for 3 days at 37°C. Azide-PEG<sub>11K</sub>-*b*-PBLG were collected by ether precipitation and dried under vacuum (**Fig.1**). The molecular weight distribution of azide-PEG<sub>11K</sub>-*b*-PBLG was measured by GPC (column: TSK-gel G3000<sub>HHR</sub>, G4000<sub>HHR</sub>) (Tosoh Co., Inc., Yamaguchi, Japan); eluent: DMF having 10 mM LiCl; flow rate 0.8 ml/min; detector: RI; temperature: 25°C. Degree of polymerization of  $\gamma$ -benzyl-L-glutamate unit of (DP<sub>PBLG</sub>) of azide-PEG<sub>11K</sub>-*b*-PBLG was calculated by comparing the proton units of ethylene units of PEG (-OCH<sub>2</sub> CH<sub>2</sub>-.  $\delta$  = 3.7 ppm) with the phenyl groups of PBLG (-C<sub>6</sub>H<sub>5</sub>-.  $\delta$  = 7 ppm) by <sup>1</sup>H-NMR spectroscopy (JEOL ECS-400; JEOL Inc., Tokyo, Japan); solvent: DMSO-*d*<sub>6</sub>, temperature: 80°C. Acetylation of  $\omega$ -amino group of azide-PEG<sub>11K</sub>-*b*-PBLG was done using acetic anhydride in dry DMF for 12 h at 37°C. To observe complete primary amine capping reaction was followed by measuring fluorescence intensity of reaction mixture and fluorescamine solution at 495 nm using nanodrop. Reaction was ceased when fluorescence intensity value was recorded almost zero. Finally, azide-PEG<sub>11K</sub>-*b*-PBLG-Ac was recovered by ether precipitation and dried under

vacuum. Azide-PEG<sub>11K</sub>-*b*-PBLG-Ac was stirred in 0.5 N NaOH overnight to remove the benzyl ester group from the side chain. Azide-PEG<sub>11K</sub>-*b*-poly(L-glutamic acid)-Ac (azide-PEG<sub>11K</sub>-*b*-PLGA-Ac) was obtained after purification and freeze drying. Deprotection of the benzyl ester group was confirmed by <sup>1</sup>H-NMR (solvent: D<sub>2</sub>O; temperature: 25°C).

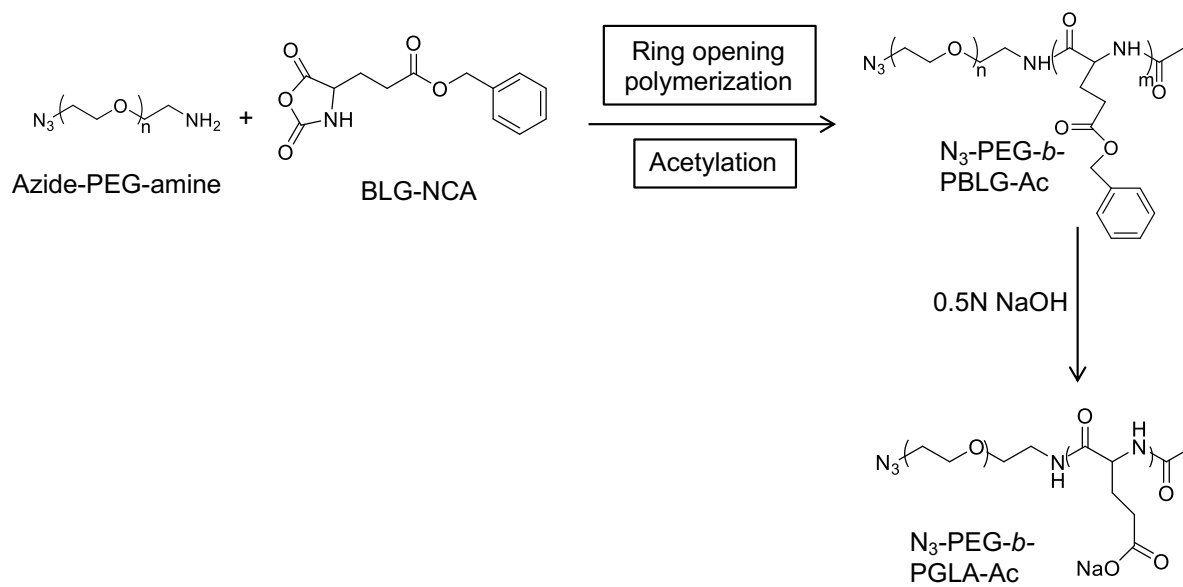


**Figure 1.** Synthesis scheme of azide-PEG<sub>11K</sub>-*b*-PLGA-Ac

### 3.2.2.3 Synthesis of MeO-PEG<sub>10K</sub>-*b*-PLGA

Methoxy-poly(ethylene glycol)-*b*-poly( $\gamma$ -benzyl-L-glutamate) (MeO-PEG<sub>10K</sub>-*b*-PBLG) (molecular weight of PEG ( $M_{n,PEG}$ ) = 10,000, degree of polymerization of PBLG ( $DP_{PBLG}$ ) = 40) was synthesized through previously reported method<sup>10</sup>. MeO-PEG<sub>10K</sub>-NH<sub>2</sub> was dried by benzene freeze drying technique for overnight to remove any water. The N-carboxyanhydride of BLG-NCA polymerization was initiated by using corresponding amine initiator: MeO-PEG<sub>10K</sub>-NH<sub>2</sub> in dry DMF. Polymerization reaction was continued for 3 days at 37°C. MeO-PEG<sub>10K</sub>-*b*-PBLG was collected by ether precipitation and dried under vacuum. The molecular weight distribution of MeO-PEG<sub>10K</sub>-*b*-PBLG was measured by GPC (column: TSK-gel G3000<sub>HHR</sub>, G4000<sub>HHR</sub>) (Tosoh Co., Inc., Yamaguchi, Japan); eluent: DMF having 10 mM



LiCl; flow rate 0.8 ml/min; detector: RI; temperature: 25°C. Degree of polymerization of  $\gamma$ -benzyl-L-glutamate unit of (DP<sub>PBLG</sub>) of MeO-PEG<sub>10K</sub>-*b*-PBLG was calculated by comparing the proton units of ethylene units of PEG (-OCH<sub>2</sub> CH<sub>2</sub>-.:  $\delta$  = 3.7 ppm) with the phenyl groups of PBLG (-C<sub>6</sub>H<sub>5</sub>-.:  $\delta$  = 7 ppm) by <sup>1</sup>H-NMR spectroscopy (JEOL ECS-400; JEOL Inc., Tokyo, Japan); solvent: DMSO-*d*<sub>6</sub>, temperature: 80°C. Methoxy-poly(ethylene glycol)-*b*-poly(L-glutamic acid) (MeO-PEG<sub>10K</sub>-*b*-PLGA) was obtained by cleaving benzyl group of side chain of MeO-PEG<sub>10K</sub>-*b*-PBLG in 0.5 N NaOH at room temperature overnight. MeO-PEG<sub>10K</sub>-*b*-PLGA was obtained by purification through dialysis against distilled water and lyophilization. Deprotection of the benzyl ester group was confirmed by <sup>1</sup>H-NMR (solvent: D<sub>2</sub>O; temperature: 25°C).

### 3.2.3 Conjugation of 5-BPA

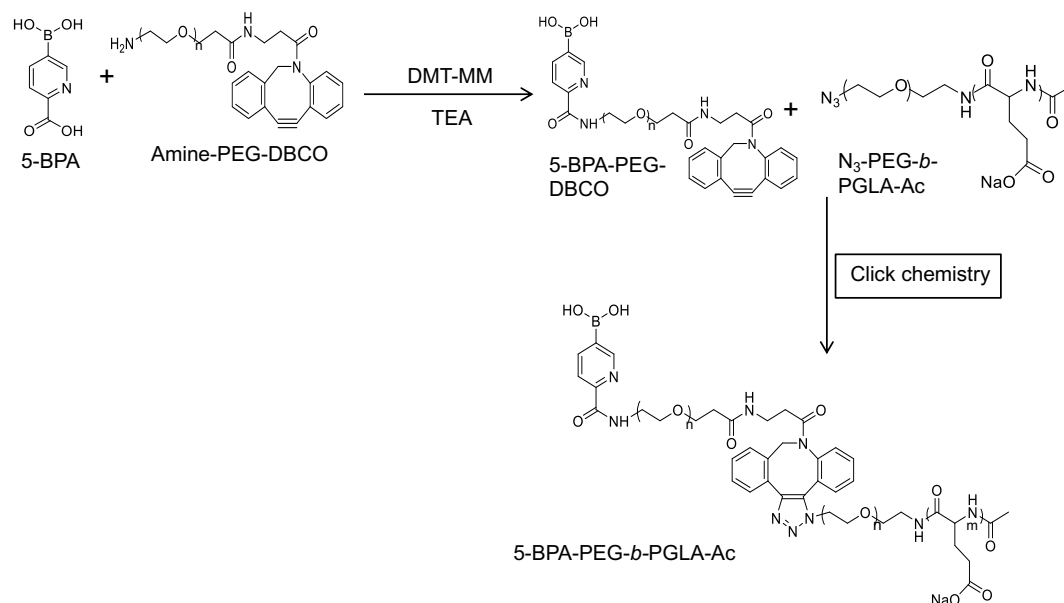


**Figure 2.** Conjugation scheme of 5-BPA-PEG-DBCO-PEG-*b*-PLGA-Ac

10 fold molar excess of 5-BPA were activated using DMT-MM in DMSO and added to a reaction mixture of 5 fold molar excess of DBCO-PEG<sub>2K</sub>-NH<sub>2</sub> with TEA (**Fig. 2**). This

reaction mixture was kept stirring for overnight and added to azide-PEG<sub>11K</sub>-*b*-PLGA-Ac. The mixture was further stirred for 24 h. Then, the mixture was incubated at -20 °C further for 24 h. Finally, reaction mixture was defrosted, purified by dialysis against deionized water and freeze dried to obtain 5-BPA-PEG<sub>11K+2K</sub>-*b*-PLGA-Ac. Conjugation of 5-BPA was confirmed by <sup>1</sup>H-NMR (solvent: D<sub>2</sub>O; temperature: 25°C).

### 3.2.4 Conjugation of PBA

The conjugation of PBA to acetal-PEG<sub>12K</sub>-*b*-PLGA was done by following a previous strategy with minor modification<sup>10</sup>. First, the acetal group of acetal-PEG<sub>12K</sub>-*b*-PLGA was deprotected and converted to aldehyde using 0.1 M HCl having 10 fold molar excess of PBA. The solution was then stirred for 2 h and then neutralized to pH 7.0 using 0.1 M NaOH. After neutralization reaction mixture was stirred for another hour. The aldehyde group reacts with the amine of PBA present in the solution which formed Schiff base. The formed Schiff base was converted to secondary amine by adding 10 fold molar excess of NaBH<sub>3</sub>CN and this mixture was further stirred for 3 days. PBA-PEG<sub>12K</sub>-*b*-PLGA was purified using deionized water and lyophilized. Conjugation of PBA was confirmed by <sup>1</sup>H-NMR (solvent: D<sub>2</sub>O; temperature: 25°C).

### 3.2.5 Confirmation of boron diol presence on conjugated polymer

Here, we confirmed presence diols of boronic acid using ARS. Fluorescence intensity increases with increased amount of polymer due to binding of 5-BPA and PBA of conjugated polymer with ARS. Free ARS is non-fluorescent to weakly fluorescent. The fluorescence of ARS increases upon formation of boronate ester with boronic acid. MeO-PEG<sub>12K</sub>-*b*-PLGA, 5-BPA-PEG<sub>11K+2K</sub>-*b*-PLGA-Ac and PBA-PEG<sub>12K</sub>-*b*-PLGA block-copolymers were mixed with

ARS (9 $\mu$ M) at 0.5 mg/ml and 2.5 mg/ml concentration. Florescent intensity (ex: 468 nm, em: 572 nm) of ARS-boronic acid complex was measured using Tecan Microplate Reader.

### 3.2.6 Conjugation of Alexa 647 and alexa 555 to MeO-PEG<sub>10K</sub>-b-PLGA

MeO-PEG<sub>10K</sub>-b-PLGA was labeled with fluorescent dye alexa fluor 647 carboxylic acid succinimidyl ester and alexa fluor 555 carboxylic acid succinimidyl ester at the  $\omega$ -amino group of the polymer in sodium bicarbonate buffer at pH 8. The reaction was done for six hours in dark at room temperature. Any free dye was removed using PD-10 column and purified polymer powder was obtained by lyophilization.

### 3.2.7 Preparation of DACHPt loaded micelles

Aqueous complex DACHPtClNO<sub>3</sub> was prepared by precipitating Cl from DACHPtCl<sub>2</sub> using silver nitrate (AgNO<sub>3</sub>). Same molar ratio of DACHPtCl<sub>2</sub> and AgNO<sub>3</sub> were mixed in water and stirred overnight. The solution was then centrifuged at 14°C, 3000 rpm for 10 min and allowed to sediment for 12 h to remove AgCl precipitate. Supernatant solution was filtrated through a 0.22  $\mu$ m filter three times and freeze-dried to obtain DACHPtClNO<sub>3</sub> powder. DACHPt-loaded polymeric micelles (DACHPt/m) were prepared by following a previously reported method<sup>32</sup>. DACHPtClNO<sub>3</sub> (5 mM) was dissolved in distilled water by heating at 70°C and mixed with MeO-PEG<sub>12K</sub>-b-PLGA, PBA-PEG<sub>12K</sub>-b-PLGA and 5-BPA-PEG<sub>11K+2K</sub>-b-PLGA-Ac (PLGA=5mM, [DACHPt]/[PLGA]=1.0 ) to prepare DACHPt/m, PBA-DACHPt/m and 5-BPA-DACHPt/m respectively. In preparation of 50% PBA-installed DACHPt/m (PBA-DACHPt/m), PBA-PEG<sub>12K</sub>-b-PLGA was mixed with MeO-PEG<sub>10K</sub>-b-PLGA to maintain 5mM carboxylate concentration. Then, the polymer solution was mixed with 5 mM DACHPt and incubated for 120 h at 37°C to obtain PBA-DACHPt/m (**Fig.3**). For preparing 50 % 5-BPA-

installed DACHPt/m (5-BPA-DACHPt/m), 5-BPA-PEG<sub>2K+11K</sub>-*b*-PLGA-Ac and MeO-PEG<sub>10K</sub>-*b*-PLGA were mixed while maintaining 5-BPA ligand at 50% and keeping the 5 mM carboxylate concentration, which was incubated with DACHPt (5 mM) for 120 h at 37°C. All solutions were filtered through a 0.22 µm filter before mixing.

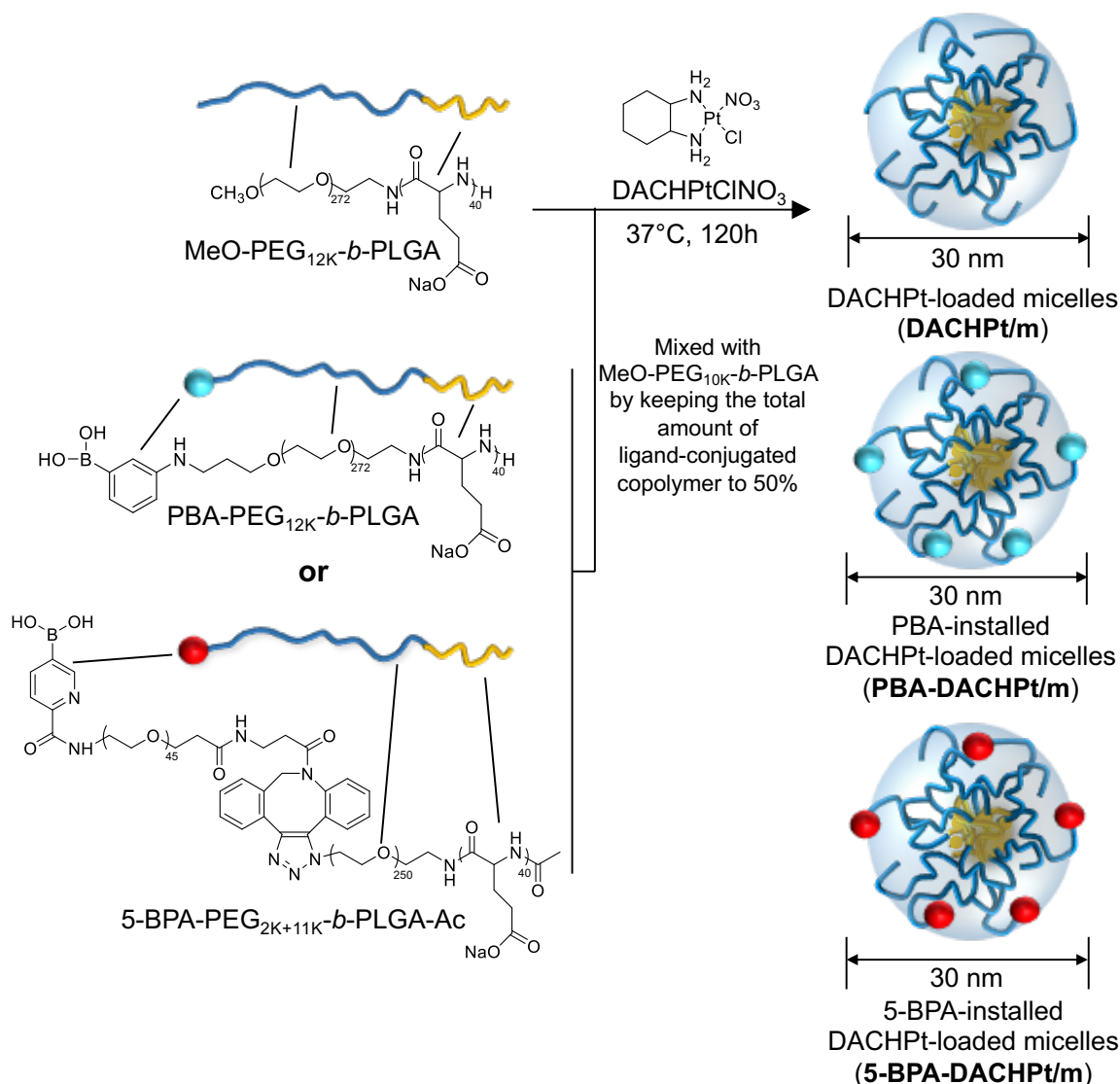


**Figure 3.** Preparation of DACHPt-loaded micelles (DACHPt/m). All the micelles were constructed in water through self-assembly. between DACHPt and poly(ethylene glycol)-*b*-poly(L-glutamic acid) block copolymers (PEG-*b*-PLGA) formed polymer-metal complexation. Ligands (PBA and 5-BPA) were kept at 50% of the micelle surface by mixing with shorter PEG length PEG<sub>10K</sub>-*b*-PLGA .

Micelles are formed spontaneously in the water through polymer metal complexation. PEG can form hydrogen bond with the water molecule and form a hydrophilic shell around the hydrophobic core. DACHPt is loaded in the core of the micelle. Prepared micelles were purified by dialysis (Spectra Pro 6 membrane; molecular weight cut off size MWCO: 6,000-8,000) against distilled water and ultrafiltration (MWCO: 30,000) in water. Fluorescent labeled micelles were also constructed in following similar process. The amount of PBA and 5-BPA on the surface of micelle was fixed at 50% of the total PEG chain for fare comparison of the boronic acid functionalized micelles. Zeta ( $\zeta$ ) potential of the micelles were measured in phosphate buffer (PB) at pH 7.4 and pH 6.5. The size distribution of the prepared micelles were checked using dynamic light scattering (DLS) at 25 °C using a Zetasizer Nano-ZS instrument (Malvern Instruments, Malvern, UK) equipped with a He-Ne ion laser (at wave length 532 nm) with detection angle equal to 90° at 37°C. The Pt content of micelles was measured using inductively coupled plasma mass spectrometry (ICP-MS) [7700 X ICP-MS (Agilent Technologies, California, USA); RF power: 1200 W; peripump:0.16 rps; montoring mass: m/z 195 (Pt); integrating interval; 0.1 sec; sampling period:0.3 sec].

### 3.3 Result

#### 3.3.1. Characterization of polymers

##### 3.3.1.1 Characterization of MeO-PEG<sub>12K</sub>-b-PBLG and acetal-PEG<sub>12K</sub>-b-PBLG

Both methoxy and acetal end functionalized block copolymers were synthesized by NCA polymerization using respective amine bearing initiator. The target degree of block side chain was 40, as at this DP the micelles demonstrated to have best stability and drug loading according to previous research. DP<sub>PBLG</sub> of MeO-PEG<sub>12K</sub>-b-PBLG (**Fig. 4A**) and acetal-PEG<sub>12K</sub>-b-PBLG (**Fig. 5A**) were calculated to be 40 by comparing the proton units of ethylene

units of PEG ( $-\text{OCH}_2\text{CH}_2-$ :  $\delta = 3.7$  ppm) with the phenyl groups of PBLG ( $-\text{C}_6\text{H}_5-$ :  $\delta = 7$  ppm) by  $^1\text{H}$ -NMR spectroscopy in  $\text{DMSO}-d_6$ , at  $80^\circ\text{C}$ . The molecular weight distribution of both MeO-PEG<sub>12K</sub>-*b*-PBLG (**Fig. 4B**) and acetal-PEG<sub>12K</sub>-*b*-PBLG (**Fig. 5B**) was 1.03, measured by GPC.

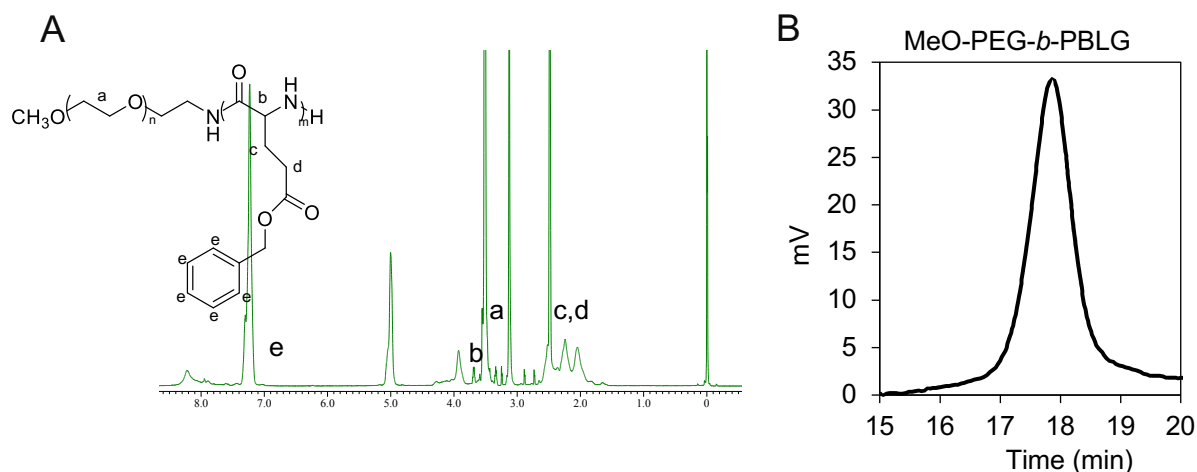


**Figure 4.** A)  $^1\text{H}$ -NMR Spectra and B) GPC chromatogram of MeO-PEG<sub>12K</sub>-*b*-PBLG 12-40 block copolymer.  $^1\text{H}$ -NMR measurement were done in  $\text{DMSO}-d_6$  at  $80^\circ\text{C}$  and GPC chromatogram was done in DMF containing 10 mM LiCl at 0.8ml/min (Detector: RI)

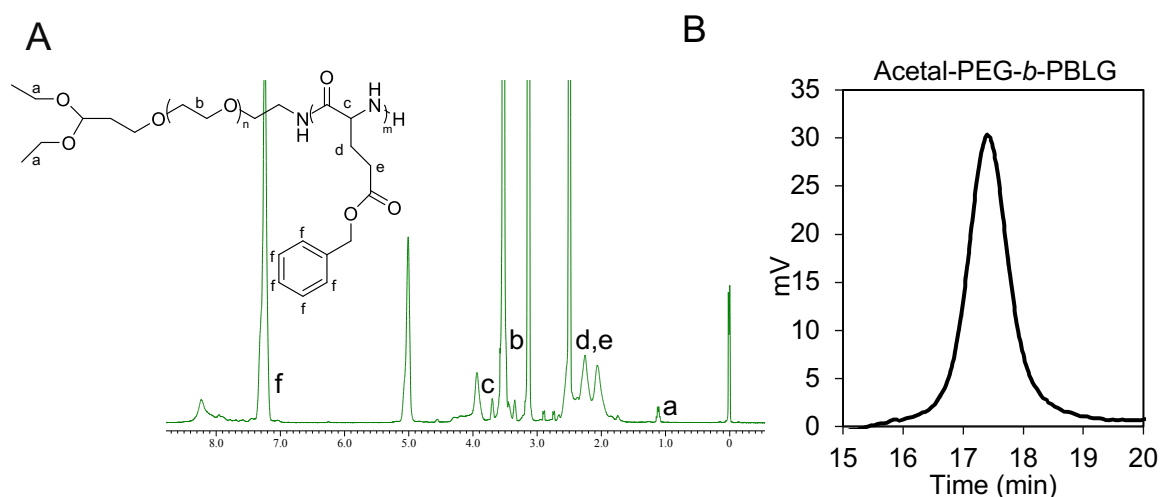


**Figure 5.** A)  $^1\text{H}$ -NMR Spectra and B) GPC chromatogram of acetal-PEG<sub>12K</sub>-*b*-PBLG 12-40 block copolymer.  $^1\text{H}$ -NMR measurement were done in  $\text{DMSO}-d_6$  at  $80^\circ\text{C}$ . GPC chromatogram was done in DMF containing 10 mM LiCl at 0.8ml/min (Detector: RI)

### 3.3.1.2 Characterization of Azide-PEG<sub>11K</sub>-b-PBLG

Azide end functionalized polymer was synthesized to perform click reaction using a shorter PEG-DBCO to conjugate 5-BPA. 5-BPA will be first conjugated to shorter PEG having an amine and DBCO end group. This will allow the 5-BPA ligand on the surface of polymeric micelle to have spacer effect and flexibility after construction in water through polymer metal complexation. The degree of polymerization of azide-PEG<sub>11K</sub>-b-PBLG block co-polymers were calculated by comparing the proton units of ethylene units of PEG (-OCH<sub>2</sub>CH<sub>2</sub>-,  $\delta = 3.7$  ppm) with the phenyl groups of PBLG (-C<sub>6</sub>H<sub>5</sub>-,  $\delta = 7$  ppm) (**Fig. 6A**) by <sup>1</sup>H-NMR in DMSO-*d*<sub>6</sub>, at 80 °C. Azide-PEG<sub>11K</sub>-b-PBLG block co-polymers was measured to be 1.02 using GPC (**Fig. 6B**). The polymer had a narrow weight distribution according to the measurement. The ω-amino group of azide-PEG<sub>11K</sub>-b-PBLG was acetylated before deprotection of benzyl side chain to avoid any unwanted reaction with the carboxylic acid group of glutamic acid in later stage of the conjugation reaction.

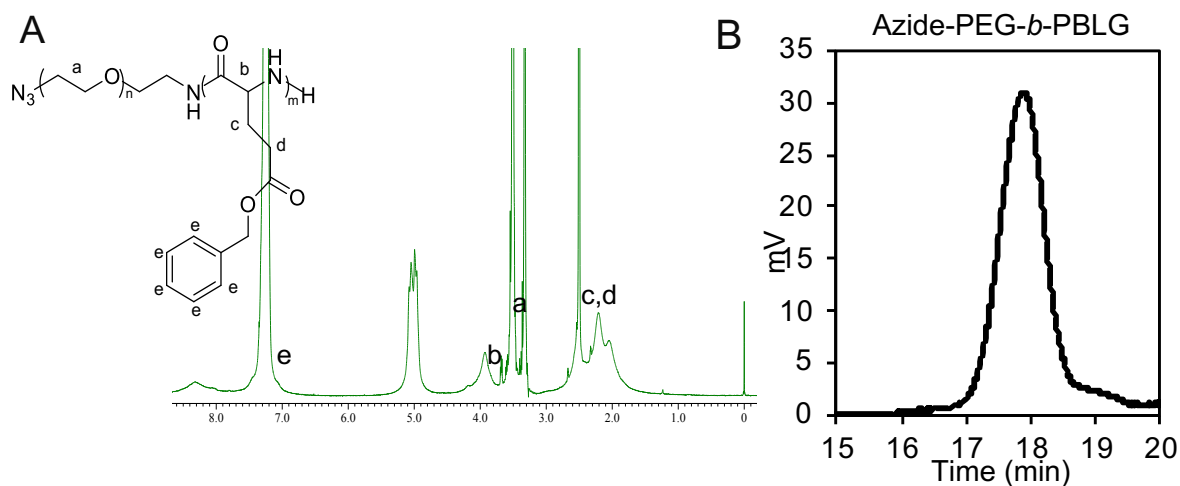


**Figure 6.** A) <sup>1</sup>H-NMR Spectra and B) GPC chromatogram of azide-PEG<sub>11K</sub>-b-PBLG 11-40 block copolymer. <sup>1</sup>H-NMR measurement were done in DMSO-*d*<sub>6</sub> at 80°C and GPC chromatogram was done in DMF containing 10 mM LiCl at 0.8ml/min (Detector: RI).

### 3.3.1.3 Characterization of MeO-PEG<sub>10K</sub>-b-PLGA

MeO-PEG<sub>10K</sub>-b-PLGA with shorter PEG (MW 10,000) was synthesized to mix with ligand polymers to prepare micelles with different amount of surface ligand. Shorter PEG was used to hinder any hiding of ligand on surface upon micelle preparation. The polymer was also labeled with fluorescent dye to construct fluorescence micelle to conduct CLSM studies. The molecular weight distribution of MeO-PEG<sub>10K</sub>-b-PBLG were measured to be 1.02 using GPC (**Fig. 7A**). The polymer had a narrow weight distribution. Methoxy-poly(ethylene glycol)-b-poly(L-glutamic acid) (MeO-PEG<sub>10K</sub>-b-PLGA) was obtained by deprotecting MeO-PEG<sub>10K</sub>-b-PBLG in 0.5 N NaOH at room temperature overnight. Deprotection of the benzyl ester group was confirmed by <sup>1</sup>H-NMR (solvent: D<sub>2</sub>O; temperature: 25°C) (**Fig. 7B**).

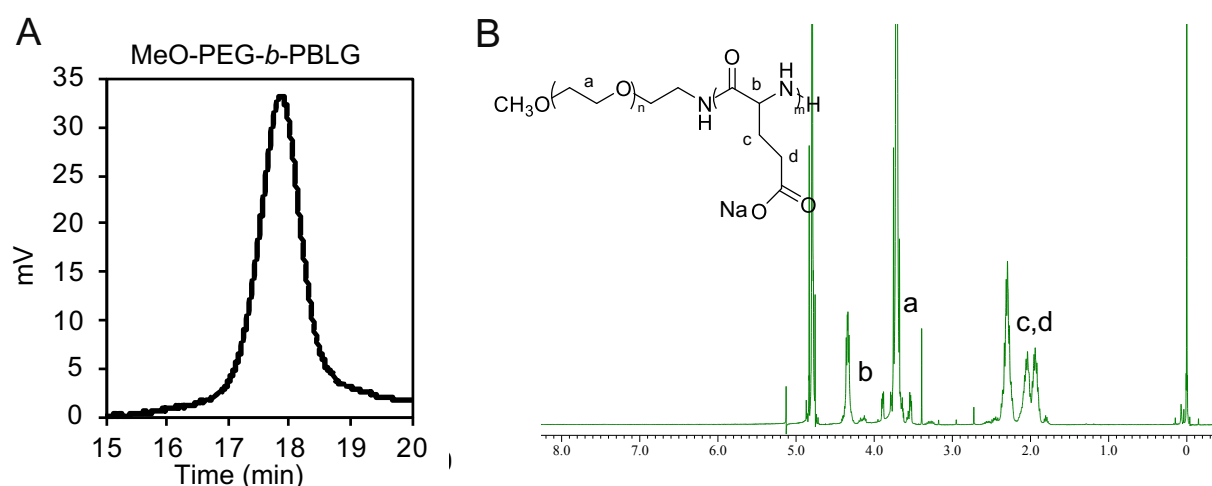


**Figure 7.** A) GPC chromatograms of MeO-PEG<sub>10K</sub>-b-PBLG and B) <sup>1</sup>H-NMR Spectra of MeO-PEG<sub>10K</sub>-b-PLGA. GPC was done in DMF containing 10 mM LiCl at 0.8 ml/min (detector: refractive index). <sup>1</sup>H-NMR measurement was done in D<sub>2</sub>O at 25°C.

### 3.3.2 Quantification of 5-BPA conjugation

Conjugation of 5-BPA was confirmed through <sup>1</sup>H-NMR measurement done in D<sub>2</sub>O after



clicking 5-BPA-PEG-DBCO to azide-PEG<sub>11K</sub>-b-PLGA. The conjugation rate was calculated to be 70% by comparing proton ratio of  $-\text{OCH}_2\text{CH}_2$  ( $\delta = 3.7$  ppm) in PEG and H present in pyridine ring ( $\delta = 7.9$  ppm, 8.2 ppm, 8.8 ppm) of 5-BPA (**Fig. 8**). The absence of any peak at 7 ppm also confirms complete removal of benzyl side chain after reaction with NaOH.

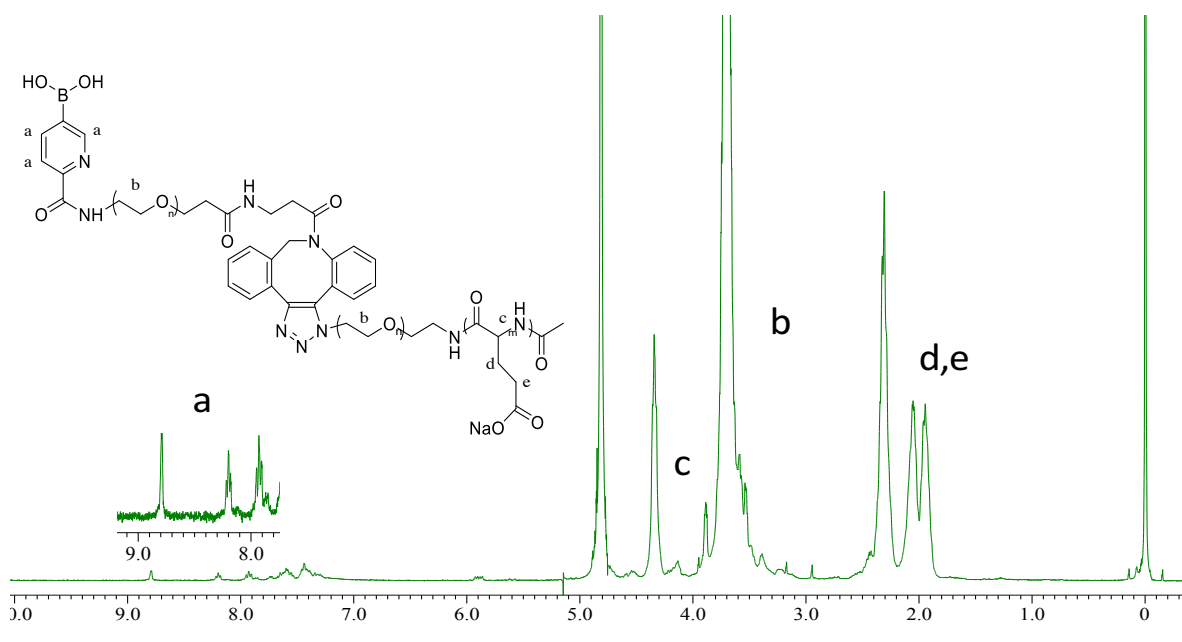


**Figure 8.**  $^1\text{H}$ -NMR Spectra of 5-BPA-PEG<sub>11K+2K</sub>-b-PLGA-Ac polymer.  $^1\text{H}$ -NMR measurement were done in  $\text{D}_2\text{O}$  at  $25^\circ\text{C}$ .

### 3.3.3 Quantification of PBA conjugation

Conjugation of 5-BPA was confirmed through  $^1\text{H}$ -NMR measurement done in  $\text{D}_2\text{O}$  after conjugating PBA with the acetal group of block copolymer. The PBA conjugation was confirmed to be 75% by comparing proton ratio of  $-\text{OCH}_2\text{CH}_2$  ( $\delta = 3.7$  ppm) in PEG  $^1\text{H}$ -NMR (Solvent:  $\text{D}_2\text{O}$ ; Temperature:  $25^\circ\text{C}$ ) and protons from the benzene ring of PBA ( $\delta = 7.0$  ppm, 7.02 ppm and 7.4 ppm) (**Fig. 9**). The absence of any peak at 7 ppm also confirms complete removal of benzyl side chain after reaction with NaOH.

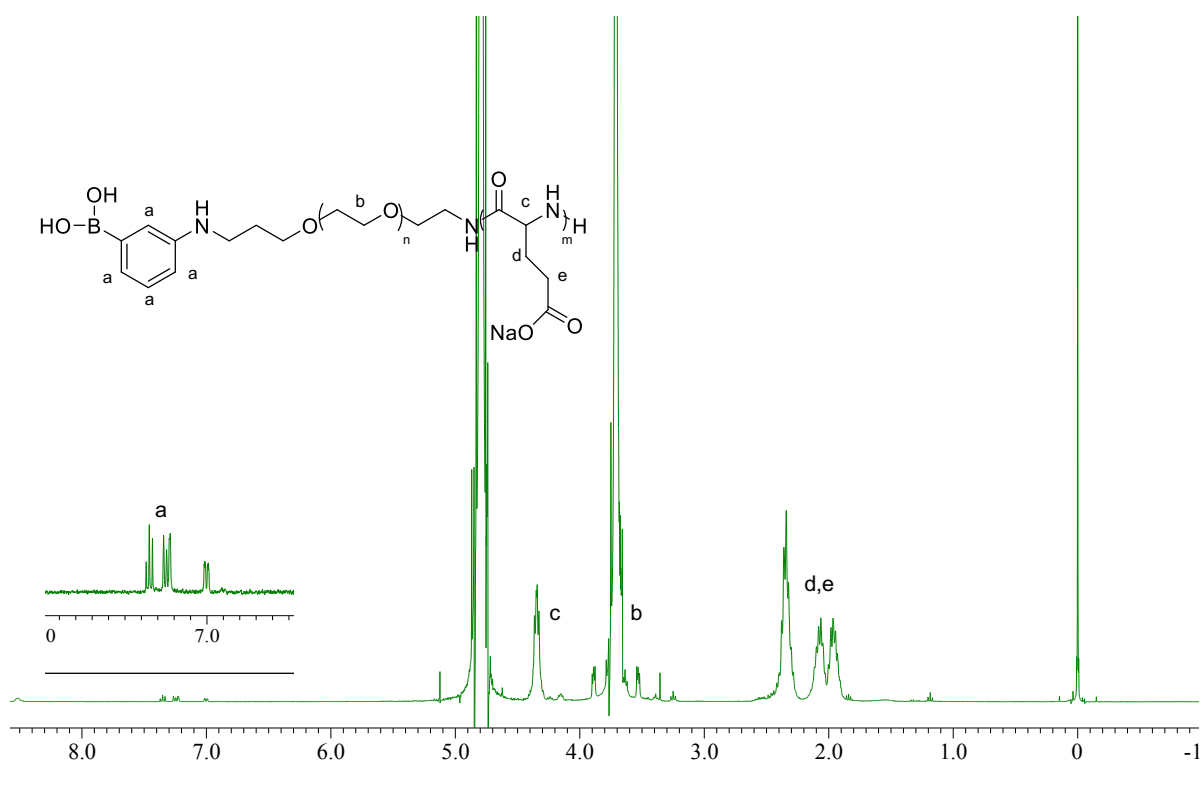


**Figure 9.**  $^1\text{H}$ -NMR Spectra of PBA-PEG<sub>12K</sub>-*b*-PLGA polymer.  $^1\text{H}$ -NMR measurement were done in  $\text{D}_2\text{O}$  at  $25^\circ\text{C}$ .

### 3.3.4 Confirmation of presence of boron diol on conjugated block-copolymer

To confirm the presence of boron diols on polymer surface after conjugation we performed a simple fluorescence assay using ARS. The interaction between boronic acids (BA) and diol complexation can be calculated by a three component assay containing fluorescent compound ARS, BA and a diol containing<sup>33</sup>. Herein, we confirmed presence of diols of boronic acid by detecting elevated fluorescence intensity with increased amount of polymer due to binding of 5-BPA and PBA of conjugated polymer with ARS. Free ARS is non-fluorescent to weakly fluorescent. The fluorescence of ARS increases upon formation of boronate ester with BA (**Fig. 10A**). Increase of fluorescence upon addition of 5-BPA and PBA conjugated polymer

verifies the presence of boron diols on conjugated block-copolymer (**Fig. 10B**).

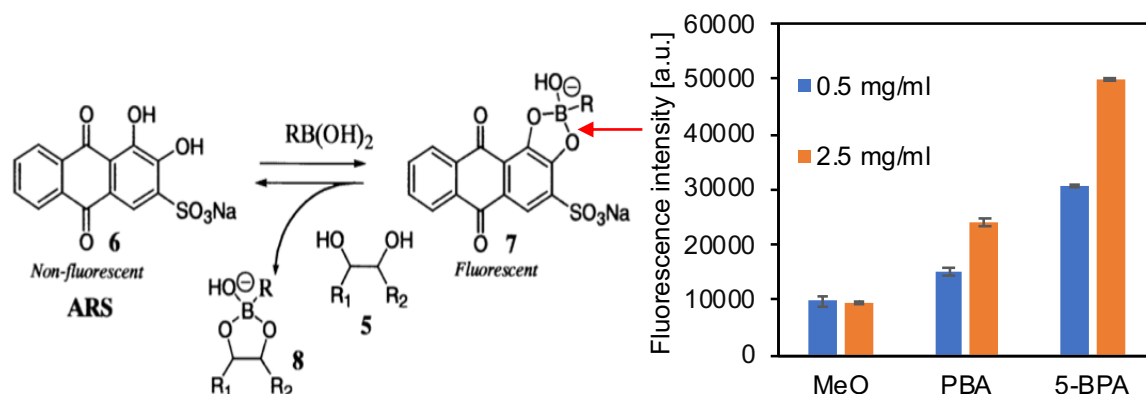


**Figure 10.** A) Mechanism of fluorescence absorbance of ARS-boronic acid molecule. B) Fluorescence intensity of ARS-block-copolymer complex.

### 3.3.5 Micelle Characterization

All micelles were constructed by self-assembly owing to polymer metal complexation of carboxylic group of PLGA and platinum of DACHPt through a previously reported method<sup>34</sup>. DACHPt/m, PBA-DACHPt/m and 5-BPA-DACHPt micelles demonstrated similar characteristics (**Table 1**). DLS measurements confirmed the size of the micelles were around ~30 nm with narrow size distribution. This size range is crucial for deep infiltration of micelles inside the tumor nest according to our previous study<sup>35</sup>.  $\zeta$  potential of the prepared micelles were slightly negative to neutral measured at pH 7.4 and pH 6.5. Efficient loading of Pt was confirmed through ICP-MS which was in lined with our previous report<sup>10</sup>. The size distribution of the prepared micelles were checked using DLS at 25 °C. The loading of Pt in micelles was calculated to be around 30% (Pt/polymer wt/wt) where Pt was measured by ICP-MS. As the micelles demonstrated similar properties they can be evaluated and compared in further biological studies.

**Table 1.** Characterization of micelles

Micelle	Size <sup>a</sup> (nm)	PDI <sup>a</sup>	Pt/polymer (wt/wt%) <sup>b</sup>	Zeta potential (mV) <sup>c</sup>	
				pH 7.4	pH 6.5
DACHPt/m	28	0.12	30	-5.37	-5.47
PBA-DACHPt/m	35	0.15	31	-2.62	-4.58
5-BPA-DACHPt/m	32	0.09	29	0.062	-2.25

<sup>a</sup>Measured by DLS, <sup>b</sup>Determined by ICP MS, <sup>c</sup>Determined in PB buffer

### 3.4. Discussion

Structure, stability and biological activity of polymeric micelles have been studied comprehensively<sup>34,36</sup>. In this study we chose the PEG length and length of the block chain depending on previous observations. We used PEG of molecular weight between 10,000 to 12,000 to construct block copolymers, as previous studies showed that polymeric micelle prepared with short PEG length were unsuccessful to attain long blood circulation. The poly(L-glutamic acid) block was set to be 40 for the best stability and drug loading capacity. The PEG length of MeO-PEG<sub>10K</sub>-*b*-PLGA was shorter to allow the ligand to avoid covering of PBA or 5-BPA ligands on the micelle surface from PEG shelling as this polymer was mixed with ligand conjugated block copolymer to construct micelles having 50% ligands on surface<sup>37</sup>. All the micelles size was maintained around 30 nm as previous study demonstrated micelles with larger diameter fails to achieve deep penetration inside the tumor<sup>35</sup>.

In this chapter, methoxy-PEG-*b*-PLGA, acetal-PEG-*b*-PLGA and azide-PEG-*b*-PLGA-Ac polymers were synthesized. All the polymers were characterized by <sup>1</sup>H-NMR and GPC. All of the block-copolymers had narrow molecular weight distribution and the degree of polymerization was calculated from <sup>1</sup>H-NMR spectra. Alexa 555 and alexa 647 dye was

conjugated with shorter methoxy-PEG<sub>10K</sub>-*b*-PLGA to prepare fluorescent micelles. PBA was conjugated to end terminus of acetal-PEG-*b*-PLGA and 5-BPA was clicked with azide-PEG-*b*-PLGA using 5-BPA-PEG-DBCO for spacer effect. Confirmation of presence of boron diol molecule on both PBA and 5-BPA block-copolymers were done before micelle construction. Finally, DACHPt-loaded polymeric micelles with 50% surface ligand were prepared from the synthesized polymer in water through polymer metal complexation. All the micelles demonstrated similar size, drug loading and surface charge thus allowing us to compare their biological activity for the ligand efficiency.

### 3.5 Conclusion

Prepared polymeric micelles with DACHPt in the core and PEG had a size of 30 nm, which is ideal for avoiding the RES and penetrating inadequately permeable tumors. The amount of surface ligand for 5-BPA and PBA installed micelles were kept at 50% for unbiased comparison. The ligand decorated and non-ligand micelles demonstrated similar slightly negative to neutral surface charge at both pH 7.4 and pH 6.5. Drug loading efficiency of the prepared micelles were also comparable. Therefore, it can be concluded that installation of 5-BPA and PBA ligands on polymeric micelle surface do not have any significant effect on their physical properties. Consequently, it will be reasonable to compare these micelles for their biological activity allowing us to clearly demonstrate any difference in efficacy due to ligand installation.

### 3.6 References

1. Kataoka, K., Harada, A., Yu., N. & Kataoka K., Harada A., Nagasaki Yu. Block copolymer micelles for drug delivery: design, characterization and biological significance. *Adv. Drug Deliv. Rev.* **47**, 113 (2001).
2. Cabral, H. & Kataoka, K. Progress of drug-loaded polymeric micelles into clinical

- studies. *J. Control. Release* **190**, 465–476 (2014).
3. Varela-Moreira, A. *et al.* Clinical application of polymeric micelles for the treatment of cancer. *Materials Chemistry Frontiers* **1**, 1485–1501 (2017).
  4. Matsumura, Y. & Maeda, H. A. A new concept for macromolecular therapeutics in cancer-chemotherapy - mechanism of tumoritropic accumulation of proteins and the antitumor agent Smancs. *Cancer Res* **46**, 6387-6392. (1986).
  5. Cabral, H. *et al.* Accumulation of sub-100 nm polymeric micelles in poorly permeable tumours depends on size. *Nat. Nanotechnol.* **6**, 815–823 (2011).
  6. Kwon, G. S. *et al.* Block copolymer micelles as vehicles for hydrophobic drugs. *Colloids Surfaces B Biointerfaces* **2**, 429–434 (1994).
  7. Kazunori, K., Glenn S., K., Masayuki, Y., Teruo, O. & Yasuhisa, S. Block copolymer micelles as vehicles for drug delivery. *J. Control. Release* **24**, 119–132 (1993).
  8. Mi, P. *et al.* A pH-activatable nanoparticle with signal-amplification capabilities for non-invasive imaging of tumour malignancy. *Nat. Nanotechnol.* **11**, 724–730 (2016).
  9. Miura, Y. *et al.* Cyclic RGD-linked polymeric micelles for targeted delivery of platinum anticancer drugs to glioblastoma through the blood-brain tumor barrier. *ACS Nano* **7**, 8583–8592 (2013).
  10. Deshayes, S. *et al.* Phenylboronic Acid-Installed Polymeric Micelles for Targeting Sialylated Epitopes in Solid Tumors. *J. Am. Chem. Soc.* **135**, 15501–15507 (2013).
  11. Mi, P., Cabral, H. & Kataoka, K. Ligand-Installed Nanocarriers toward Precision Therapy. *Adv. Mater.* 1902604 (2019). doi:10.1002/adma.201902604
  12. Büll, C., Stoel, M. A., Den Brok, M. H. & Adema, G. J. Sialic acids sweeten a tumor's life. *Cancer Res.* **74**, 3199–3204 (2014).
  13. Vajaria, B. N., Patel, K. R., Begum, R. & Patel, P. S. Sialylation: an Avenue to Target Cancer Cells. *Pathol. Oncol. Res.* **22**, 443–447 (2016).
  14. Munkley, J. & Scott, E. Targeting Aberrant Sialylation to Treat Cancer. *Medicines* **6**, 102 (2019).
  15. Zhao, D. *et al.* pH-Activated Targeting Drug Delivery System Based on the Selective Binding of Phenylboronic Acid. *ACS Appl. Mater. Interfaces* **8**, 14845–14854 (2016).
  16. Elgohary, M. M. *et al.* Targeting sialic acid residues on lung cancer cells by inhalable boronic acid-decorated albumin nanocomposites for combined chemo/herbal therapy. *J. Control. Release* (2018). doi:10.1016/j.jconrel.2018.07.014
  17. Ji, M. *et al.* Sialic Acid-Targeted Nanovectors with Phenylboronic Acid-Grafted

- Polyethylenimine Robustly Enhance siRNA-Based Cancer Therapy. *ACS Appl. Mater. Interfaces* **8**, 9565–9576 (2016).
18. Büll, C. *et al.* Sialic acid blockade suppresses tumor growth by enhancing t-cell-mediated tumor immunity. *Cancer Res.* **78**, 3574–3588 (2018).
  19. Dervisevic, M., Senel, M., Sagir, T. & Isik, S. Highly sensitive detection of cancer cells with an electrochemical cytosensor based on boronic acid functional polythiophene. *Biosens. Bioelectron.* **90**, 6–12 (2017).
  20. Liu, R. *et al.* Preparation of Sialic Acid-Imprinted Fluorescent Conjugated Nanoparticles and Their Application for Targeted Cancer Cell Imaging. *ACS Appl. Mater. Interfaces* **9**, 3006–3015 (2017).
  21. Matsumoto, A., Kataoka, K. & Miyahara, Y. New directions in the design of phenylboronate-functionalized polymers for diagnostic and therapeutic applications. *Polym. J.* **46**, 483–491 (2014).
  22. Matsumoto, A., Sato, N., Kataoka, K. & Miyahara, Y. Noninvasive Sialic Acid Detection at Cell Membrane by Using Phenylboronic Acid Modified Self-Assembled Monolayer Gold Electrode. *J. Am. Chem. Soc.* **131**, 12022–12023 (2009).
  23. Matsumoto, A., Cabral, H., Sato, N., Kataoka, K. & Miyahara, Y. Assessment of Tumor Metastasis by the Direct Determination of Cell-Membrane Sialic Acid Expression. *Angew. Chemie Int. Ed.* **49**, 5494–5497 (2010).
  24. Otsuka, H., Uchimura, E., Koshino, H., Okano, T. & Kataoka, K. Anomalous binding profile of phenylboronic acid with N-acetylneuraminic acid (Neu5Ac) in aqueous solution with varying pH. *J. Am. Chem. Soc.* **125**, 3493–3502 (2003).
  25. Sharon, N. Lectins: Carbohydrate-specific Reagents and Biological Recognition Molecules. *J. Biol. Chem.* **282**, 2753–2764 (2007).
  26. Koprowski, H., Herlyn, M., Stepkowski, Z. & Sears, H. Specific antigen in serum of patients with colon carcinoma. *Science (80-. )*. **212**, 53–55 (1981).
  27. Otsuka, H., Uchimura, E., Koshino, H., Okano, T. & Kataoka, K. Anomalous binding profile of phenylboronic acid with N-acetylneuraminic acid (Neu5Ac) in aqueous solution with varying pH. *J. Am. Chem. Soc.* **125**, 3493–3502 (2003).
  28. Varela-Moreira, A. *et al.* Clinical application of polymeric micelles for the treatment of cancer. *Mater. Chem. Front.* **1**, 1485–1501 (2017).
  29. Yamamoto, Y. *et al.* Effect of combined treatment with the epirubicin-incorporating micelles (NC-6300) and 1,2-diaminocyclohexane platinum (II)-incorporating micelles

- (NC-4016) on a human gastric cancer model. *Int. J. Cancer* **135**, 214–223 (2014).
30. Matsumoto, A. *et al.* Heterocyclic boronic acids display sialic acid selective binding in a hypoxic tumor relevant acidic environment. *Chem. Sci.* **8**, 6165–6170 (2017).
  31. Matsumoto, A. *et al.* Heterocyclic boronic acids display sialic acid selective binding in a hypoxic tumor relevant acidic environment. *Chem. Sci.* **8**, 6165–6170 (2017).
  32. Cabral, H., Nishiyama, N., Okazaki, S., Koyama, H. & Kataoka, K. Preparation and biological properties of dichloro(1,2-diaminocyclohexane)platinum(II) (DACHPt)-loaded polymeric micelles. *J. Control. Release* **101**, 223–232 (2005).
  33. Springsteen, G. & Wang, B. A detailed examination of boronic acid-diol complexation. *Tetrahedron* **58**, 5291–5300 (2002).
  34. Cabral, H., Nishiyama, N. & Kataoka, K. Optimization of (1,2-diaminocyclohexane)platinum(II)-loaded polymeric micelles directed to improved tumor targeting and enhanced antitumor activity. *J. Control. Release* **121**, 146–155 (2007).
  35. Cabral, H. *et al.* Accumulation of sub-100 nm polymeric micelles in poorly permeable tumours depends on size. *Nat. Nanotechnol.* **6**, 815–823 (2011).
  36. Cabral, H., Miyata, K., Osada, K. & Kataoka, K. Block Copolymer Micelles in Nanomedicine Applications. *Chem. Rev.* **118**, 6844–6892 (2018).
  37. Ishii, T. *et al.* Enhanced target recognition of nanoparticles by cocktail PEGylation with chains of varying lengths. *Chem. Commun.* **52**, 1517–1519 (2016).



## **Chapter 4**

### **Biological activity of 5-BPA installed polymeric micelle**

## Chapter 4: Biological activity of 5-BPA installed polymeric micelle

### Abstract

Biological activities of 5-BPA installed DACHPt loaded micelles (5-BPA-DACHPt/m) were assessed in cancer stem cell (CSC) rich head and neck cancer cell line and compared with other micelles. Before evaluating role of sialic acid (SA) through controlled *in vitro* studies, removal of SA by sialidase treatment was confirmed. Cellular uptake of the micelles was evaluated first by measuring internalized Pt in HSC2 cells using ICP MS and then tracing fluorescent-labeled 5-BPA and PBA installed micelles in sialidase treated and non-treated cells using CLSM at various time point at pH 7.4 and pH 6.5. Quantification of internalized Pt in HSC2 cells revealed higher cellular uptake of 5-BPA-DACHPt/m compared to other micelles at pH 6.5. The improved cellular uptake at pH 6.5 was also analogous in CLSM study and confirmed such enhanced uptake was due to the interaction of 5-BPA with cell surface SA. Relatively lower  $IC_{50}$  value demonstrated by 5-BPA-DACHPt/m compared to DACHPt/m confirms effectiveness of ligand installation. Treatment with 5-BPA-DACHPt/m effectively reduced SA rich CSC population in cellular study. Subsequently, blood circulation and plasma clearance of all the micelles were comparable with long circulation profile. 5-BPA-DACHPt/m showed significantly higher tumor accumulation and retention after 48 h compared to other micelles in subcutaneous HSC2 tumor model. Finally, antitumor study against orthotopic head and neck tumor model revealed the extraordinary ability of 5-BPA-DACHPt/m to suppress tumor growth and improved survival compared to both PBA-DACHPt/m and DACHPt/m treated groups. Assessment of CSC population in tumor after treatment revealed significantly lower fraction of CSCs in 5-BPA-DACHPt/m treated animals, probably leading to better tumor suppressing ability and treatment outcome.

## Chapter 4: Biological activity of 5-BPA installed polymeric micelle

### 4.1 Introduction

### 4.2 Experimental

#### 4.2.1 Materials

#### 4.2.2 Cell line and animals

#### 4.2.3 Confirmation of sialic acid cleaving

#### 4.2.4 *In vitro* cellular uptake

##### 4.2.4.1 Platinum internalization

##### 4.2.4.2 CLSM study

#### 4.2.5 Cytotoxicity of micelles

#### 4.2.6 *In vitro* effect of micelle in CSCs

#### 4.2.7 *In vivo* blood circulation

#### 4.2.8 *In vivo* tumor accumulation and biodistribution

#### 4.2.9 Antitumor activity and survival study

#### 4.2.10 Evaluation of CSCs after treatment

### 4.3 Result

#### 4.3.1 Verification of removal of sialic acid

#### 4.3.2 Intracellular platinum accumulation

#### 4.3.3 Cellular uptake of fluorescent micelles

#### 4.3.4 *In vitro* growth inhibitory activity

#### 4.3.5 Treatment effect on CSCs

#### 4.3.6 Blood circulation and plasma clearance

#### 4.3.7 Tumor accumulation and biodistribution

4.3.8 Antitumor activity against orthotopic HSC2 tumor model

4.3.9 *In vivo* assessment of CSCs after treatment

**4.4 Discussion**

**4.5 Conclusion**

**4.6 References**

## 4.1 Introduction

Complex surgery procedure and sensitive locations of tumors makes head and neck squamous cell carcinoma (HNSCC) very hard to treat. Even though modern medicine have been progressing in treating such challenging type of cancer, still improvement in overall survival have been nominal<sup>1</sup>. Failure of treatment, metastasis and tumor relapse are major setback in clinical settings. The key reason for these problems have been stated as cancer stem cells (CSCs). These CSCs are harder to eliminate due to their resistance nature to chemo and radio therapy compared other cell populations in the tumor microenvironment<sup>2</sup>. Previous study have verified such resistance of CD44 positive cells in HNSCC<sup>3</sup>. HNSCC have been reported to express CD44 variant (CD44v) positive subpopulation along with other cell population<sup>4</sup>. Since CD44 expressing cells demonstrated CSCs characteristics it might be necessary to develop treatment strategies to target and eliminate these type of cells for treating patients with HNSCC. Researchers have been able to avoid activation of detoxification mechanism by CD44v9 positive cells via loading chemotherapeutic drug cisplatin inside polymeric nanoparticles<sup>5</sup>. Such system improved intratumoral localization of the drug and somewhat overcame the resistance otherwise posed by such CD44v9 expressing CSCs. As per reports such CD44v usually have high expression of SA which regulates their HA mediated cell adhesion<sup>6</sup>. Thus, it is possible to develop a ligand strategy specifically target SA in intratumoral acidic pH and

effectively target not only sensitive non-stem like cells but also resistant stem like cells. Such system could further enhance the ability of platinum loaded polymeric micelles in overcoming CSC resistance.

To highlight the importance of SA targeted cancer therapy it is worth mentioning that glycomimetics, blocking SA metabolism are being tested for their antitumor efficacy in animal model<sup>7,8</sup>. In addition, ligands to target overexpressed SA such as lectins<sup>9</sup> and antibodies<sup>10</sup> are being developed. However, the expression of SA in healthy tissues, such as erythrocytes<sup>11</sup> and endothelial cells<sup>12,13,14</sup> makes it difficult to develop such SA targeting strategies. Due to the immunogenicity or toxicity of such systems confine these tactics to *in vitro* studies or intratumoral administration only<sup>15</sup>. To solve this issue, we hypothesize development of smart ligand that will be only activated in intratumoral conditions such as acidic pH, consequently could enhance selective targeting of SA in tumors<sup>16</sup> while avoiding systemic interaction with SA expressed in healthy tissues. The concept of such smart ligand system was demonstrated using phenylboronic acid (PBA) as a ligand on polymeric micelle surface with exclusive selectivity to SA at intratumoral pH (pH 7.2-6.5)<sup>17,18,19</sup>. PBA can make stable esters with carbohydrates at pHs higher than its pKa, but only SA-PBA esters are stable at pH lower than the pKa of PBA<sup>20</sup>. PBA decorated nanomedicines highlighted the capability of such smart ligand system for enhancing delivery of loaded cytotoxic drugs in tumor tissues and improving the antitumor efficacy *in vivo*<sup>19</sup>. These micelles achieved enhanced intracellular drug delivery in cancer cells at intratumoral pH after attaching to the SA on the cell surface. As the selectivity and binding affinity of PBA-based ligands to SA at intratumoral pH could be tuned through chemical design, the strategy has the potential for further engineering systems with enhance tumor targeting capability. However, the binding affinity of PBA for SA is relatively weak, and the installation of PBA derivatives with higher affinity for SA could provide enhanced targeting

efficiency. As mentioned before, we have recently identified the high affinity of 5-boronopicolinic acid (5-BPA) for SA at intratumoral pH<sup>21</sup>. The unique ability of 5-BPA to have very specific and high binding to SA at reduced pH makes them an excellent targeting molecule to install on polymeric micelle surface to target overexpressed SA in tumor.

In this chapter, evaluation of biological activity of micelles are reported. Removal of SA through sialidase treatment was confirmed before performing controlled *in vitro* studies. Effect of media pH on CD44v9 positive CSCs was assessed. Evaluation of cellular uptake of the micelles by measuring internalized Pt and tracing fluorescent-labeled micelles using CLSM are reported. *In vitro* cytotoxicity evaluation and effect of micelles on CSC population are stated. Subsequently, blood circulation and plasma clearance of the micelles was determined. Finally, *in vivo* studies using DACHPt loaded non-ligand and 5-BPA or PBA installed micelles including tumor accumulation, biodistribution, antitumor activity, survival and effect on CSC population are studied.

## 4.2 Experimental

### 4.2.1 Materials

Neuraminidase (Sialidase) from *Clostridium perfringens* were purchased from Roche Diagnostics GmbH. (Mannheim, Germany). Dichloro (1,2-diaminocyclohexane) platinum (II) (DACHPtCl<sub>2</sub>) and dulbecco's modified eagle's medium (DMEM) was obtained from Sigma-Aldrich Co. (ST. Louis, U.S.A). Fetal bovine serum (FBS) was purchased from Dainippon Sumitomo Pharma Co., Ltd. (Osaka, Japan). Phosphate-buffered saline (PBS) and oxaliplatin was purchased from Wako Pure Chemical Industries Ltd. (Osaka, Japan). Cell Counting Kit-8 was purchased from Dojindo Laboratories (Kumamoto, Japan). Isoflurane was purchased from Pfizer Inc. (New York, USA). Matrigel Matrix was purchased from CORNING (New York,

USA). Head and neck cancer with normal tissue array (HN483a) was purchased from Biomax (Derwood, USA). Blocking One solution was purchased from Nacalai Tesque Inc (Kyoto, Japan). Alexa Fluor 488 goat anti-mouse IgG (H + L), Alexa Fluor 594 donkey anti-rat IgG (H + L) and Alexa Fluor 488 conjugated lectin HPA From *Helix pomatia* (edible snail) was purchased from ThermoFisher Scientific (Massachusetts, USA). Alexa Fluor 488- and Alexa Fluor 647-conjugated Wheat Germ Agglutinin was purchased from Life Technologies (California, USA). CD44v9 antibody (anti-human, rat; clone number: RV3) was purchased from CosmoBio (Tokyo, Japan). Involucrin antibody (anti-human, mouse monoclonal; clone number: SY5) was purchased from Abcam (Cambridge, United Kingdom).

#### **4.2.2 Cell line and animals**

Human oral carcinoma (HSC2) cells were purchased from Cell Bank, Riken BioResource Center (Tsukuba, Japan). HSC2 cells were maintained in Dulbecc's modified Eagles medium (DMEM) containing 10% of fetal bovine serum (FBS) and 1% of penicillin and streptomycin in a humidified atmosphere containing 5% CO<sub>2</sub> at 37°C. BALB/c mice (female; age 6 weeks;) were purchased from Charles River Japan (Kanagawa, Japan). All experiments were performed in accordance with the Guidelines for the Care and Use of Laboratory Animals as stated by The University of Tokyo.

#### **4.2.3 Confirmation of SA cleavage from cell surface by sialidase treatment**

5-BPA and PBA installed micelles are expected to improve intracellular delivery of drugs by binding to cell surface SA thus it is important to conduct controlled studies by removing SA from the surface of cells through enzymatic hydrolysis. To verify removal of SA from HSC2 cells through enzymatic hydrolysis using sialidase, N-acetylgalactosamine

(GalNAc), the sugar next to SA, was stained. GalNAc becomes uncovered after removal of SA. *Helix pomatia* agglutinin (HPA) is a lectin specific to GalNAc<sup>22</sup>.  $2 \times 10^4$  HSC2 cells /200  $\mu$ l were plated on 8 Chambered # 1.0 Borosilicate Cover glass system (Lab Tek). After 48 h incubation, medium was replaced with pH 5 acetate buffer with and without sialidase for 2 h. Then cells were washed twice with PBS and incubated with Alexa Fluor 488-labeled HPA (1mg/ 20ml) for 5 min on ice. Finally, the cells were stained with DAPI and imaged using Leica DMi8 inverted microscope. Image analysis was done using ImageJ software.

#### 4.2.4 Analysis of stemness in different pH

To understand the effect of pH on CSC population *in vitro* after 48 h of plating HSC2 cell, media was replaced with pH 6.5 media. After further incubation for 24 h cells were collected using trypsin and washed with 2% FBS containing PBS. Unspecific binding was blocked by using Blocking One solution (Nacalai Tesque, Kyoto, Japan) for 25 min. Then, the cells were washed and incubated with anti-CD44v9 antibody clone RV3 (anti-human, rat; Cosmobio) in PBS for 45 min on ice. After 2 times washing with PBS, the cells were resuspended in 50  $\mu$ l Alexa Fluor 488-conjugated secondary antibody and incubated for 30 min in dark on ice. Finally, the cells were stained with DAPI (0.03 mg/ml), washed and suspended in 1 ml PBS (containing 2% FBS). The cells were then analyzed using Flow cytometry (Becton Dickinson, Franklin Lakes, NJ, USA) and FlowJo software.

#### 4.2.5 *In vitro* cellular uptake

##### 4.2.5.1 Platinum internalization

HSC2 cells ( $1.5 \times 10^5$  /well) were plated in 12 well plates. After 36 h of incubation medium was replaced with fresh medium (1ml) containing 20  $\mu$ M (DACHPt basis) DACHPt/m,



PBA-DACHPt/m, 5-BPA-DACHPt/m and oxaliplatin. Cells were then incubated for 1,6 and 9h. Cells were washed three times with PBS before collection using trypsin. Cell counting was done to ensure presence of consistent cell numbers in each well. Finally, cells were digested using 90% HNO<sub>3</sub> until total evaporation and reconstituted in 1ml 1% HNO<sub>3</sub>. Digested solution was filtered through a 0.45 µm filter before Pt content was measured using 7700 X ICP-MS. All data was evaluated using Agilent Masshunter Workstation software.

#### 4.2.5.2 CLSM study

2 x 10<sup>4</sup> cells HSC2 cells were cultured on 8 Chambered # 1.0 Borosilicate Cover glass system (Lab Tek). After 48 h incubation medium was replaced with pH 5 acetate buffer with and without sialidase for 2 h. Sialidase is an enzyme which hydrolyses the terminal SA deposit of the cell surface carbohydrate chain<sup>19</sup>. Then cells were washed twice with PBS and incubated with pH 7.4 and pH 6.5 medium (5.5 mM glucose concentration) containing Alexa 647 labeled 5-BPA-DACHPt/m and PBA-DACHPt/m (500mM on a Pt basis). Fluorescence imaging of the live cells were done after 3, 6 and 9 h post incubation using CLSM. Quantification of micelles was done by measuring mean fluorescence intensity after subtracting background.

In a separate experiment, HSC2 cells (2 x 10<sup>4</sup> cells /200 µl) were plated on 8 Chambered # 1.0 Borosilicate Cover glass system (Lab Tek). After 48 h incubation, medium was replaced with pH 7.4 and pH 6.5 cell culture medium with 5.5 mM glucose concentration, which is comparable to blood glucose concentration containing Alexa Fluor 647-labeled PBA-DACHPt/m or 5-BPA-DACHPt/m (500 mM on a DACHPt basis). Fluorescence imaging of the live cells was done at 3-, 6- and 9-h after incubation by using CLSM (Zeiss LSM780, Carl Zeiss, Germany) Cells were also stained with LysoTracker green DND-26 before imaging for marking the late endosomes/lysosomes.

#### 4.2.6 *In vitro* cytotoxicity

HSC2 cells were plated and incubated for overnight in 96 well plates ( $5 \times 10^3$  cells/50  $\mu\text{L}$ / well). After 24 h of incubation medium was replaced with varying concentration of oxaliplatin or DACHPt/m, PBA-DACHPt/m and 5-BPA- DACHPt/m. in pH 7.4 and pH 6.5 media (5.5 mM glucose concentration) for 8 h and then replaced with fresh medium after washing two times with PBS. Cells were further incubated for 48 h and absorbance was measured 1 h after addition of 10  $\mu\text{L}$  of cell counting kit-8 (Dojindo) using Tecan microplate reader at 450 nm.  $\text{IC}_{50}$  value was calculated from linear regression using dose response curves.

#### 4.2.7 Effect of micelles on CSCs *in vitro*

HSC2 cells ( $5 \times 10^5$  /well) were plated in 6 well plates and incubated for 48 h. Cells were further incubated for 24 h with 48 h  $\text{IC}_{50}$  value of drugs, *i.e.* 110  $\mu\text{M}$  of DACHPt/m, PBA-DACHPt/m, 5-BPA-DACHPt/m and 10  $\mu\text{M}$  Oxaliplatin. After 24 h incubation cells were collected using accutase to preserve the surface receptors. Cell counting was done after collection to ensure consistent amount of cells for each staining sample. After collection cells were washed with 2% FBS containing PBS. Unspecific binding was blocked using Blocking One solution for 25 min; cells were washed and incubated in 50 $\mu\text{l}$  of primary antibody CD44v9 in PBS for 45 min on ice. After further washing two times cells were resuspended in 50 $\mu\text{l}$  Secondary antibody (Alexa 488 conjugated) and incubated for 30 min in dark on ice. Finally, cells were stained with DAPI, washed and suspended in 1ml PBS (containing 2% FBS). Cells were then analyzed using Flow cytometry (Becton Dickinson, Franklin Lakes, NJ, USA) and FlowJo software.

#### 4.2.8 *In vivo* blood circulation

To evaluate the blood circulation of the fluorescent labeled micelles, right earlobe of 6-week-aged BALB/c nu/nu mice (anesthetized with 2.5% isoflurane using a NARCOBIT-E anesthesia unit) was observed using CLSM. Images were recorded continuously for the first 10 min, followed by intermittent recordings in 5 min intervals for 6 h. Mice were injected with 5-BPA-DACHPt/m<sub>Alexa647</sub> and DACHPt/m<sub>Alexa555</sub> or PBA-DACHPt/m<sub>Alexa647</sub> and DACHPt/m<sub>Alexa555</sub> via tail vein in 60 sec, starting after 10 sec had elapsed from the start of observation. *In vivo* images were recorded using a Nikon A1R CLSM system attached to an upright ECLIPSE FN1 equipped with a x20 lens. Excitation lasers of 560 nm and 640 nm, emission filters of 595/50 nm and 700/75 nm were used, respectively.

#### 4.2.9 *In vivo* tumor accumulation and biodistribution

We evaluated the capacity of 5-BPA-DACHPt/m to deliver payload by measuring Pt content in HSC2 subcutaneous (SC) tumor model. Six weeks old female BALB/c nu/nu mice were inoculated with ( $1 \times 10^6$  cells/ 100  $\mu$ l) on left flank. Three weeks after inoculation mice were injected with oxaliplatin (5mg/Kg), DACHPt/m, PBA-DACHPt/m and 5-BPA-DACHPt/m at 5mg/Kg on a DACHPt basis. After 1, 4, 8, 24 and 48 h of drug injection mice were sacrificed and tumors and organs (spleen, liver, kidney) were harvested. Plasma was separated from blood, collected from inferior vena cava after centrifugation. Tumors, blood component and organs were weighed and digested using 90% HNO<sub>3</sub>. After evaporating all 90% HNO<sub>3</sub>, dried sample was reconstituted in 1ml of 1% HNO<sub>3</sub> and Pt was then measured by 7700 X ICP-MS after filtering through a 0.45  $\mu$ m filter. All data were evaluated using Agilent Masshunter Workstation software. Calculation was done for % injected dose per gram tissue for tumor and organs. For blood component calculated value was relative to DACHPt/m.

#### 4.2.10 Antitumor activity and survival study

Antitumor assessment of 5-BPA-DACHpt/m was performed in a CSC rich head and neck tumor model. To prepare the orthotopic HSC2 tumor model  $5.0 \times 10^5$  cells/ 30  $\mu$ l (15  $\mu$ l serum free media and 15  $\mu$ l matrigel) was inoculated into the right lateral edge of the tongue of 6 weeks BALB/C nu/nu female mice. Mice were anesthetized for inoculation and during tumor volume measurement. 4 days after tumor implantation (day 0) mice were separated into five groups (n=8) and administered with PBS, oxaliplatin (8mg/Kg), DACHPt/m, PBA-DACHPt/m and 5-BPA-DACHPt/m (2mg/Kg DACHPt basis) through tail vein, 4 times on day 0, 2, 4 and 15. Antitumor activity was assessed by measuring tumor growth using slide caliper. Tumor volume was calculated by using equation:  $V=(a \times b^2)/2$ , here a is major axes and b is minor axes of tumor in mm. Tumor volume and body weight was measured for a period of 4 weeks and mice were followed for survival studies.

#### 4.2.11 Evaluation of CSCs after treatment

To determine the treatment effect on CSC population orthotopic HSC2 tumors were harvested 48 h after the 3<sup>rd</sup> injection of the treatment regimen. Collected tumors were fixed in optimal cutting temperature compound (OCT) and then cut into 10 $\mu$ m thickness sections using cryostat for further staining. Tissues were fixed for 1 min at room temperature with 4% paraformaldehyde immediately after sectioning and washed with PBS. Tissue samples were then incubated with 0.05% tween in PBS for 30 min at room temperature. After blocking for another 45 min with Blocking One solution, tumor sections were incubated with primary antibodies CD44v9 and involucrin for overnight at 4 °C. Tissue samples were washed with PBS twice and reacted in the dark with secondary antibodies alexa fluor 594 anti-rat and alexa fluor 488 anti-mouse for 60 min at room temperature. Finally, nuclei were stained with DAPI

for 5 min before mounting with cover glass and observed under CLSM. Fluorescence intensity was quantified using imageJ software to estimate expression of CSCs after treatment.

## 4.3 Result

### 4.3.1 Confirmation of SA cleavage from cell surface by sialidase treatment

To confirm removal of SA from the cell surface after sialidase enzymatic treatment cells were stained for N-acetylgalactosamine (GalNAc) with *Helix pomatia* agglutinin (HPA). The position of GalNAc in cell surface glycan chain is right after SA. So when the SA is successfully removed GalNAc will be exposed causing high staining of HPA lectin selective for GalNAc<sup>22</sup>. The optimum pH condition for sialidase treatment have been reported to be pH 5.0-5.1. So the cells were incubated with acetate buffer pH 5.0 containing sialidase for efficient cleaving of SA from the cell surface glycan chain.

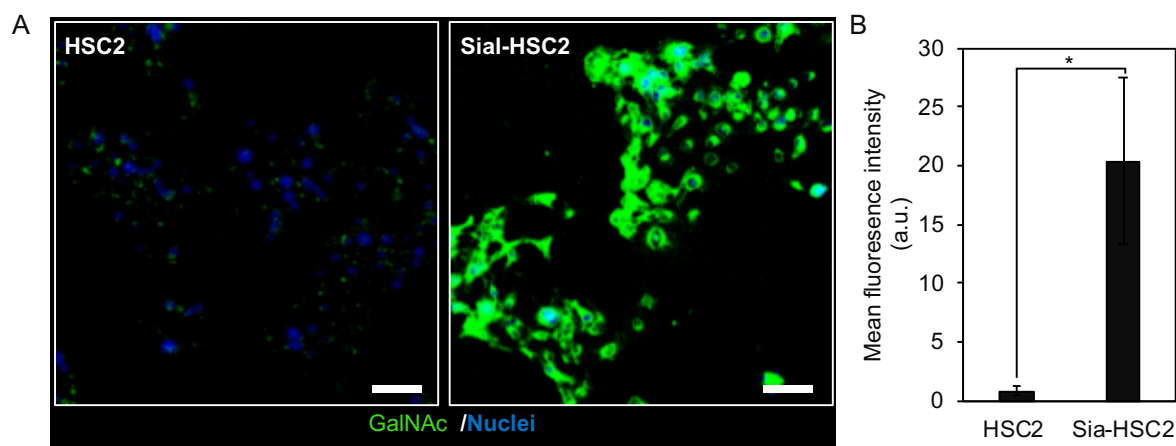


**Figure 1.** Staining of GalNAc after SA was cleaved enzymatically with sialidase to expose GalNAc (green). **A)** Staining of GalNAc (green) and cell nuclei (blue) in HSC2 and sialidase treated HSC2 *in vitro*. **B)** Quantification of mean fluorescence intensity of GalNAc (green) in HSC2 with and without sialidase treatment *in vitro*. Data are presented as average  $\pm$  standard deviation (S.D.) (n=3). Scale bars = 100  $\mu$ m. \* $p < 0.005$  calculated by Student's t tests.

Control cells without sialidase treatment showed very little to no HPA staining (**Fig. 1A & B**). This confirmed HPA binding sugar GalNAc was covered by SA hindering any staining. While, cells that were treated with sialidase demonstrated relatively high amount of HPA staining (**Fig. 1A Sial-HSC2:green & B**) compared to non-treated cells (**Fig. 1A, HSC2**). Such elevated staining of GalNAc verifies cleaving of SA by sialidase enzyme.

### 4.3.2 Analysis of stemness in different pH

To evaluate the effect of pH on the amount of CSC population, HSC2 cells were incubated for 24 h in pH 7.4 and pH 6.5 media and stained with CD44v9 antibody (CSC marker). Cells were analyzed using flow cytometry and the fraction of CD44v9 positive cells were calculated (**Fig. 2 A & B**). Cells incubated in pH 6.5 media showed a tendency to express more CD44v9 positive cells. But there were no significant difference in the amount of CSC fraction between cells incubated at pH 7.4 and pH 6.5 media (**Fig. 2B**). Therefore, it can be concluded that there is no noteworthy change in the expression of CSCs during short incubation with low pH medium.

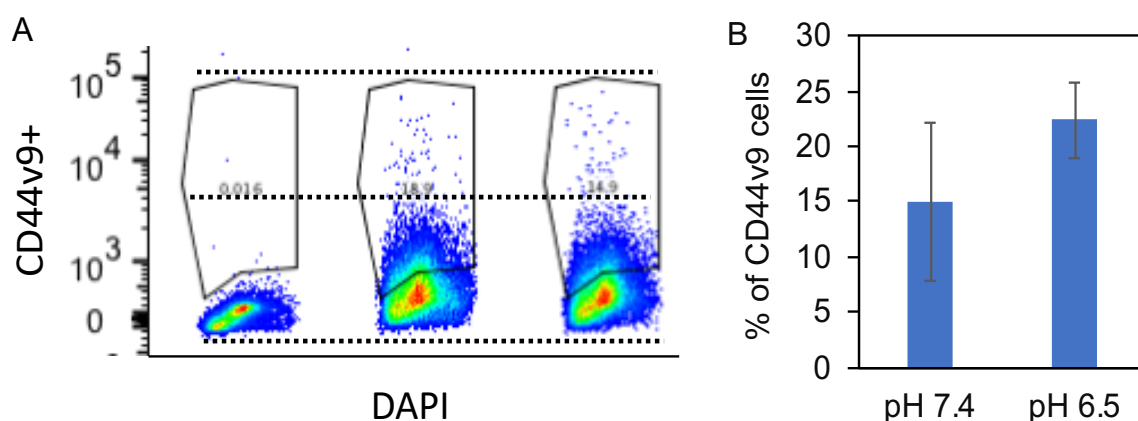


**Figure 2.** Effect of media pH on CSCs *in vitro*. **A.** Expression of CD44v9 on HSC2 cells measured by flow cytometry 24 h after media was replaced with new media having pH 6.5 and pH 7.4. **B.** Quantification of CD44v9 expression. Data are expressed as average  $\pm$  S.D.,  $n = 4$ .

### 4.3.3 *In vitro* Cellular uptake

#### 4.3.3.1 *Platinum internalization*

We evaluated the cellular uptake quantitatively by measuring internalized Pt by ICP MS to assess biological activity of ligand installed polymeric micelles in HSC2 cells (**Fig. 3 A,B**). The cellular uptake was evaluated at both physiological and intratumoral pH<sup>17</sup> (7.4 and 6.5 respectively) as 5-BPA was reported to demonstrate strong binding affinity to SA at lower pH<sup>23</sup>. We hypothesize due to this high binding of 5-BPA to SA cellular uptake of 5-BPA ligand would be more efficient. To prove our concept we incubated HSC2 cells with same concentration of oxaliplatin, DACHPt/m, PBA-DACHPt/m and 5-BPA-DACHPt/m at pH 7.4 and pH 6.5. After 1-, 6- and 9-h cells were washed with PBS to remove any unbound drug or micelles and collected. Internalization of oxaliplatin and micelles were quantitatively measured by ICP MS. In both pH condition oxaliplatin had fast cellular uptake. Oxaliplatin was taken up by cells in a continuous manner either through copper/organic cationic transporter or passive diffusion<sup>24</sup>. However, micelles are normally taken up slowly through endocytosis<sup>25</sup>. All the micelles had similar cellular uptake at physiological pH 7.4 (**Fig. 3A**) but 5-BPA-DACHPt/m demonstrated significantly higher internalization compared to other micelles at pH 6.5 (**Fig. 3B**). Such elevated cellular uptake of 5-BPA-DACHPt/m was probably due to greater engaging of 5-BPA to cell surface SA in acidic pH. If this high uptake was because of cell surface SA such improved uptake can be diminished by removing the SA from the cancer cell surface. To verify our hypothesis we performed another cellular uptake experiment using fluorescent labeled micelle and tracing their internalization using CLSM. Controlled experiments were performed by cleaving SA from the cancer cell surface.

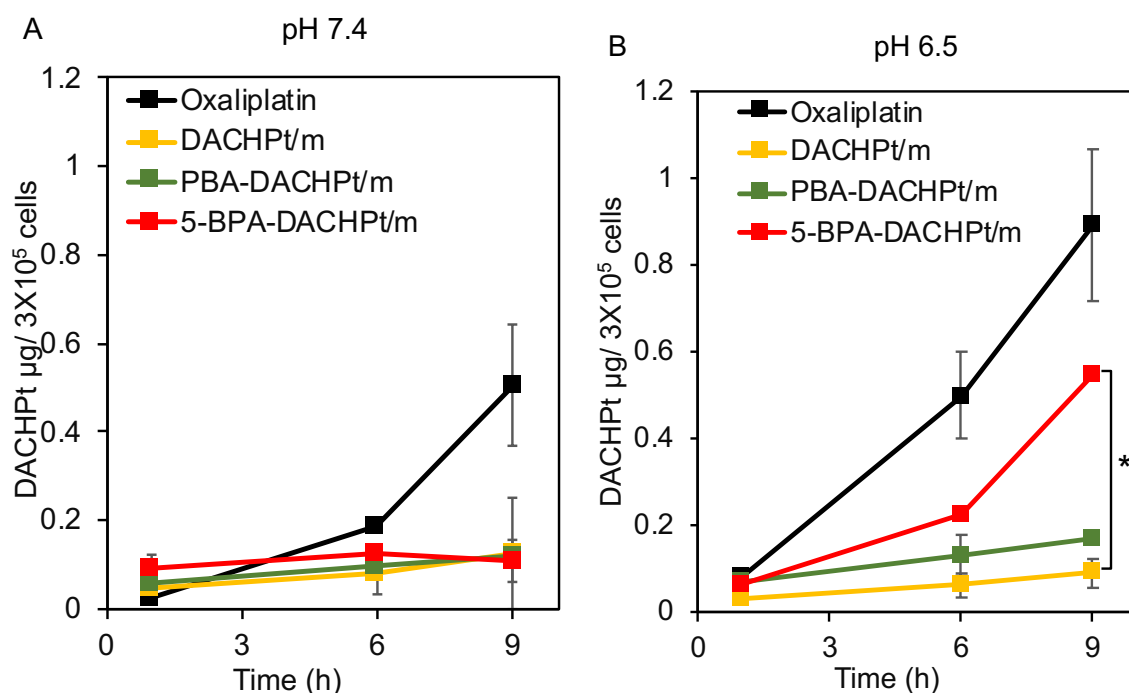


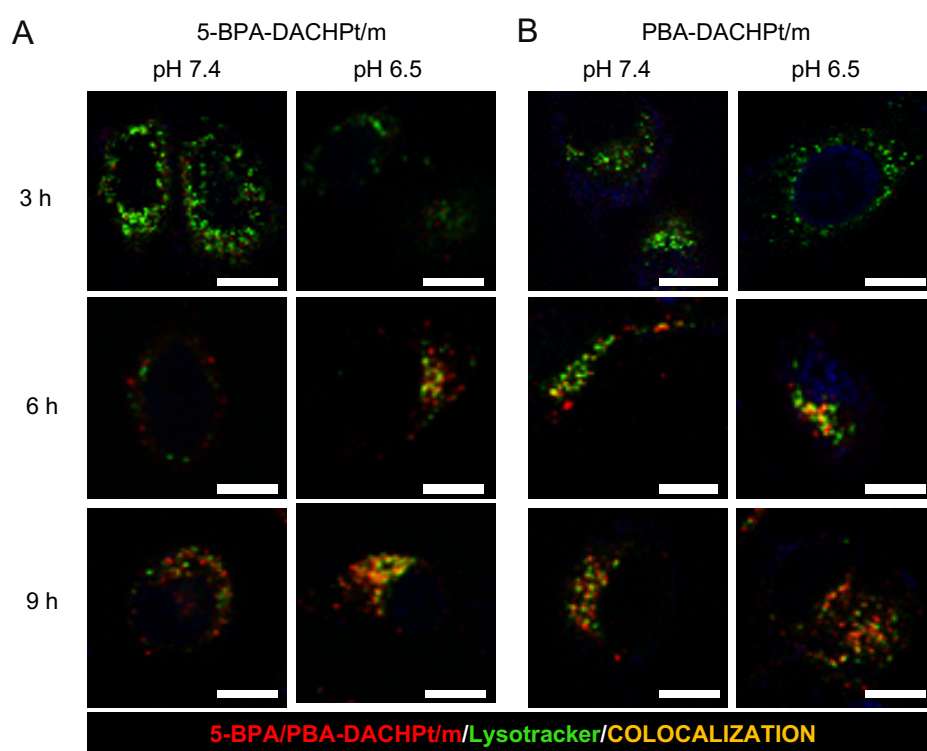
**Figure 3.** Intracellular delivery of micelles. A,B: *In vitro* intracellular Pt levels after incubation with free oxaliplatin or the micelles with HSC2 cells at **A)** pH 7.4 and **B)** pH 6.5. Data are expressed as average  $\pm$  S.D.,  $n = 3$ ,  $*p < 0.05$  calculated by Student's t tests.

#### 4.3.3.2 CLSM study of fluorescent labeled micelle

To verify if the high internalized Pt at pH 6.5 estimated during cellular uptake evaluation was due to the interaction between cell surface SA and 5-BPA ligand on the micelle surface, we then prepared alexa 647 labeled PBA-DACHPt/ $m_{\text{Alexa647}}$  and 5-BPA-DACHPt/ $m_{\text{Alexa647}}$ . First we demonstrated slow uptake of micelles (**Fig. 4A & B; red**) through endocytosis<sup>25</sup> at pH 7.4 and pH 6.5 by marking late endosomes/lysosomes using lysotracker (**Fig. 4A & B; green**). We then performed coordinated cellular uptake assessment by tracing fluorescent labeled micelles. Cells were incubated with 5-BPA-DACHPt/ $m_{\text{Alexa647}}$  and PBA-DACHPt/ $m_{\text{Alexa647}}$  and imaged using CLSM after 3-, 6- and 9-h (**Fig. 5A & B**). Controlled experiment was done by removing cell surface SA with sialidase treatment (**Fig. 5C & D**). Cellular uptake was quantified by measuring relative fluorescence intensity of micelles using

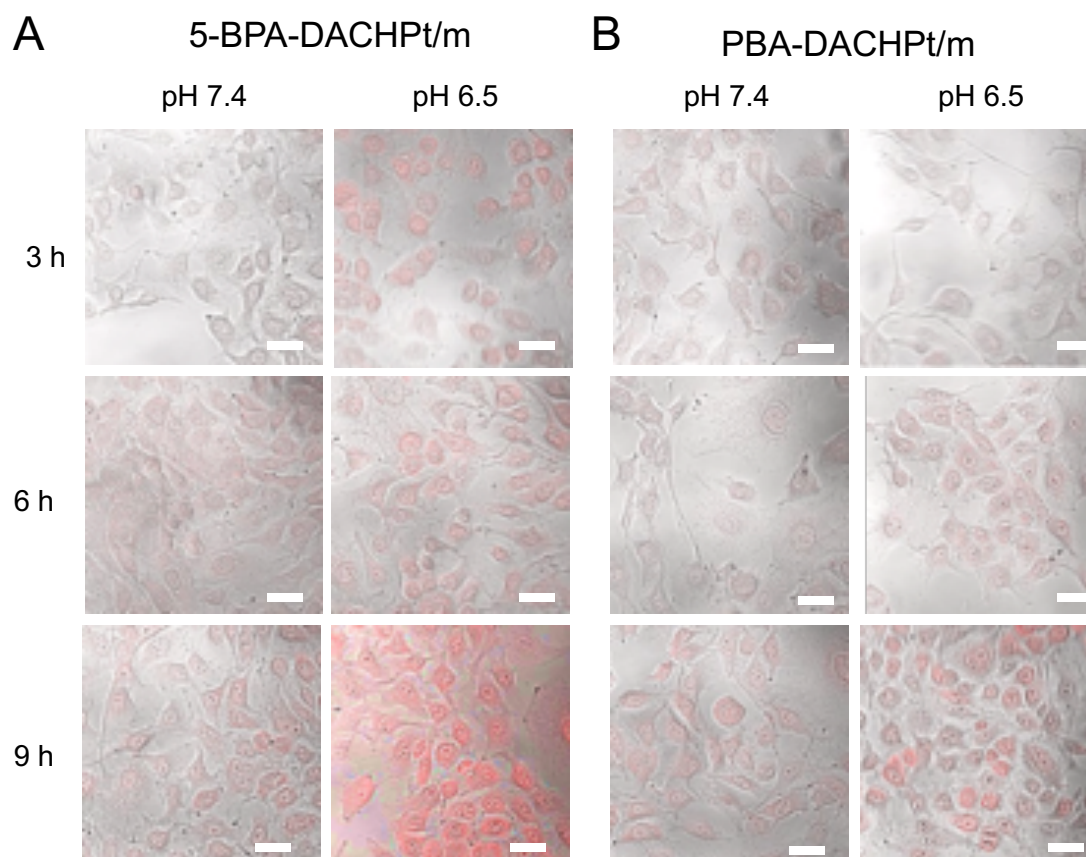


imageJ software. 5-BPA-DACHPt/m<sub>Alexa647</sub> demonstrated better cellular uptake compared to PBA-DACHPt/m<sub>Alexa647</sub> at pH 6.5 (**Fig. 5A, B & F**) but the uptake was similar at pH 7.4 (**Fig. 5A, B & E**). Such observation was identical to our previous cellular uptake experiment with quantification of internalized Pt (**Fig. 3A & B**). Furthermore, there was a reduction in cellular uptake of both 5-BPA-DACHPt/m<sub>Alexa647</sub> and PBA-DACHPt/m<sub>Alexa647</sub> when cells were treated with sialidase to cleave SA both at pH 7.4 and pH 6.5 condition (**Fig. 5C, D, E & F**). Thus, confirming both 5-BPA-DACHPt/m<sub>Alexa647</sub> and PBA-DACHPt/m<sub>Alexa647</sub> can engage with cell surface SA to elevate cellular uptake. After 9-h at pH 7.4 condition cellular uptake of sialidase treated and non-treated cells were comparable for both micelles probably due to unspecific uptake mechanism (**Fig. 5A, B, C, D & E**).



**Figure 4.** *In vitro* cellular transportation of A) 5-BPA-DACHPt/m and B) PBA-DACHPt/m in HSC2 cells. Fluorescent images of Lysotracker (green), 5-BPA-DACHPt/m and PBA-DACHPt/m (red), colocalization (yellow) after 3-, 6- and 9 h incubation at pH 7.4 and pH 6.5. Scale bar 10 μM.

Surprisingly, cells incubated with micelles at pH 6.5 continued to demonstrate ligand mediated uptake even at 9-h with 5-BPA-DACHPt/m<sub>Alexa647</sub> showing significantly higher uptake compared to PBA-DACHPt/m<sub>Alexa647</sub> (Fig. 5A,B & F). The uptake of 5-BPA-DACHPt/m at pH 6.5 was also notably higher compared to pH 7.4 (Fig. 5E & F). Both the micelle incubated at pH 6.5 demonstrated much lower uptake after 9 h with sialidase treated condition, confirming that this unusual high cellular uptake was attributed to SA expression on the cancer cell surface. Through this experiment we have successfully demonstrated the potential of improving drug delivery to cells in intratumoral acidic microenvironment through installing 5-BPA ligand on the micelle surface. As both the micelles demonstrated lower uptake in cells after cleaving of SA we theorized this unusual elevated uptake was due to greater interaction of 5-BPA ligand with cell surface SA in acidic pH.



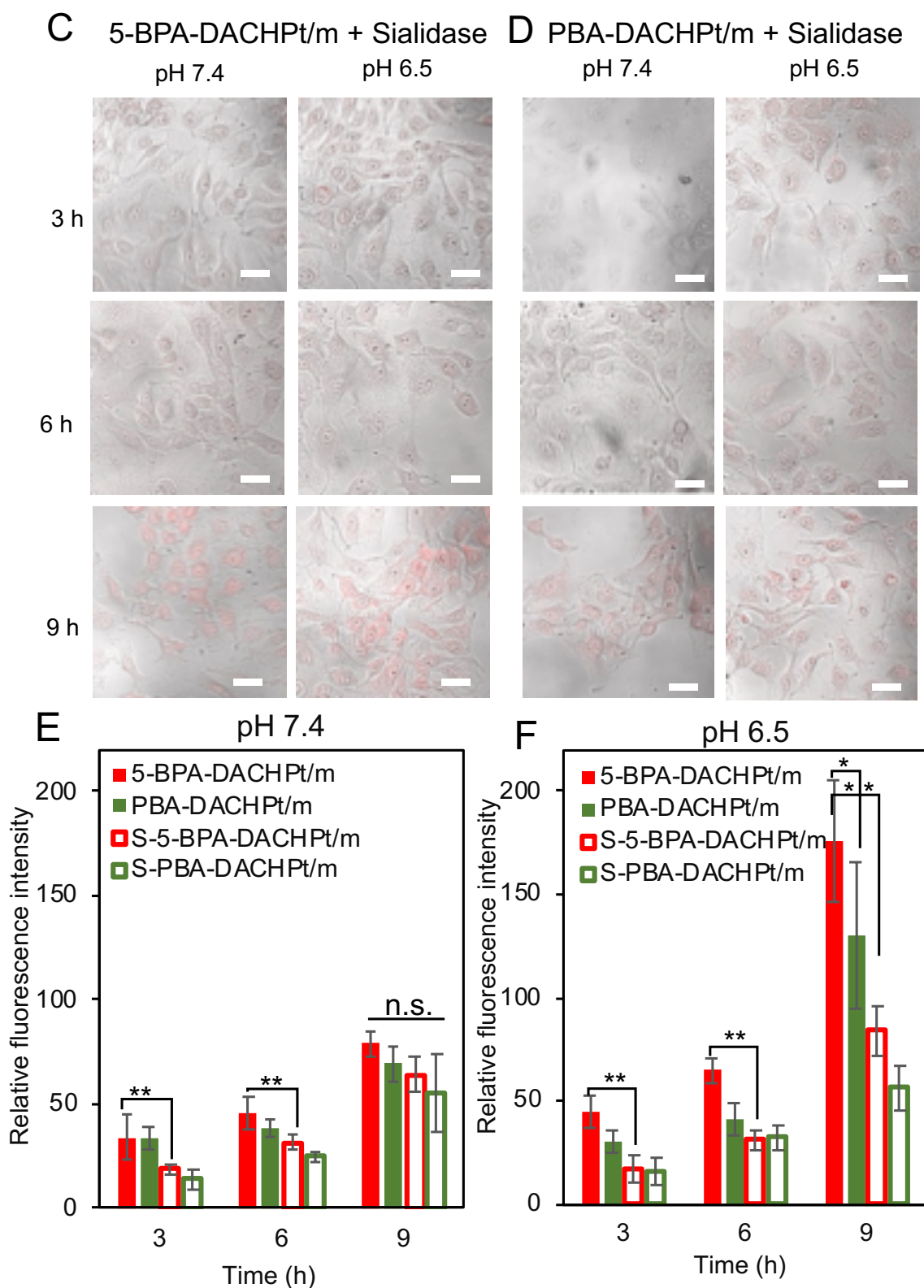


**Figure 5.** Cellular uptake of alexa fluor 647-labeled **A**) 5-BPA-DACHPt/m (red) or **B**) PBA-DACHPt/m (red) in HSC2 cells at 3-, 6- and 9-h at pH 7.4 and pH 6.5. Cellular uptake of Alexa

Fluor 647-labeled **C**) 5-BPA-DACHPt/m (red) or **D**) PBA-DACHPt/m (red) in HSC2 cells at 3-, 6- and 9-h at pH 7.4 and pH 6.5 after cleaving SA by sialidase. Scale bars in A-D = 100  $\mu$ m  
 E, F: Quantification of the uptake of fluorescent micelles at **E**) pH 7.4 and **F**) pH 6.5 into HSC cells with (open bar) and without (closed bar) sialidase treatment. Data are expressed as averages  $\pm$  S.D., n = 6, \* $p$  < 0.05, \*\* $p$  < 0.01.  $P$  values were calculated by Student's  $t$  test.

#### 4.3.4 *In vitro* cytotoxicity

To assess the ligand initiated enhanced cellular uptake and cytotoxicity of 5-BPA and PBA installed micelles we calculated the 50% growth inhibitory concentration ( $IC_{50}$ ) against HSC2 cells (**Table 1**). We have evaluated two ligand installed micelles PBA-DACHPt/m and 5-BPA-DACHPt/m along with non-ligand DACHPt/m and compared cytotoxic potency with clinically approved oxaliplatin which is the identical active as the DACHPt loaded in the micelle. After incubating the cells with varying concentration of free oxaliplatin, DACHPt/m, PBA-DACHPt/m and 5-BPA-DACHPt/m for 9h at pH 7.4 and pH 6.5 ; cells were washed and further incubated for 48 h. Finally, cell viability was measured using CCK8 assay. Free oxaliplatin demonstrated much lower  $IC_{50}$  values compared to the micelles (**Table 1**) as they are internalized very fast compared to micelles<sup>26</sup>. This high toxicity of oxaliplatin is supported by our high uptake of oxaliplatin in platinum internalization assay done quantifying Pt using ICP MS (**Fig. 3A & B**). Both PBA-DACHPt/m and 5-BPA-DACHPt/m exhibited much higher cytotoxicity compared to non-ligand micelle at pH 7.4 and pH 6.5. Thus, proving interaction between cell surface SA with the boronic acid ligands installed on the polymeric micelle surface. Cytotoxicity of PBA-DACHPt/m was identical in both pH probably due to similar binding affinity of PBA and SA at pH 6.5 and pH 7.4. On the contrary, 5-BPA-DACHPt/m exhibited significantly lower  $IC_{50}$  value at acidic pH 6.5 (**Table 1**) condition which correlated

with the higher cellular uptake of 5-BPA-DACHPt/m at pH 6.5 (**Fig. 5A & F**) due to better interaction of ligand with the cell surface SA at acidic pH<sup>23</sup>. This high cytotoxicity implies the probability of superior activity of the 5-BPA-DACHPt/m in *in vivo* acidic tumor microenvironment condition.

**Table 1.** *In vitro* cytotoxicity of micelles against HSC2 cell line

Drug	IC <sub>50</sub> (μM) <sup>a</sup>	
	pH 7.4	pH 6.5
Oxaliplatin	10 ± 1.5	9 ± 1.6
DACHPt/m	119 ± 31	178 ± 22
PBA-DACHPt/m	57 ± 13	64 ± 9
5-BPA-DACHPt/m	54 ± 5	38 ± 3

<sup>a</sup>Determined by CCK8 assay, n=4

#### 4.3.5 *In vitro* effect of micelle in CSCs

Assessment was done to evaluate the impact of micelles decorated with 5-BPA on CSCs. Especially on CD44v9 positive cells, which is a modified isoform of CD44 considered among the key markers of CSCs in epithelial cancers<sup>27</sup>. Furthermore, cells that are CD44v positive have been associated with resisted treatment and increased metastasis<sup>28</sup>. Moreover, these CD44v positive cells have been reported to express high fraction of SA<sup>6</sup> which can enhance the ligand mediated uptake of 5-BPA installed micelles. Cells were incubated with oxaliplatin, DACHPt/m, PBA-DACHPt/m and 5-BPA-DACHPt/m for 24h and then collected and investigated for CD44v9 positive cells by flowcytometry. As, CD44v9 have been reported as a sensitive marker for CSC population in HSC2 cell line<sup>3</sup>. All *in vitro* cultured HSC2 cells expressed CD44v9 positive fraction. Enhancement of CD44v9 positive fraction was observed after treatment with oxaliplatin (**Fig. 6A & B**), probably due to resistance of these cells to

cytotoxicity of oxaliplatin. Such elevation in CSCs in HSC2 cells was also reported upon treatment with free cisplatin<sup>29</sup>. On the other hand, treatment with micelles did not induce such increase in CD44v9 positive fraction (**Fig. 6A & B**) which suggests the micelles do not initiate any mechanism of active drug related detoxification in these cells.

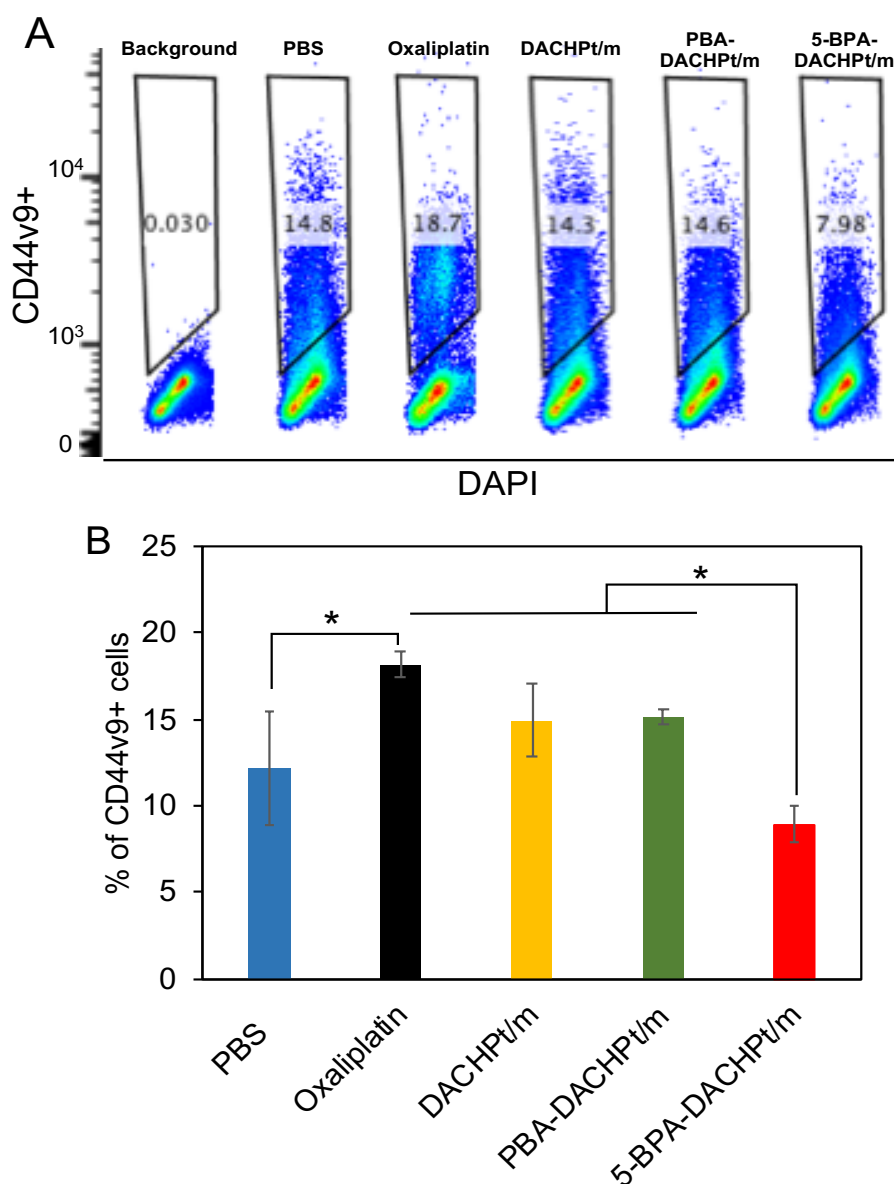


**Figure 6.** Effect of treatment on CSCs *in vitro*. **A)** Expression of CD44v9 on HSC2 cells measured by flow cytometry 24 h after treatment with PBS, free oxaliplatin, DACHPt/m, PBA-DACHPt/m or 5-BPA-DACHPt/m. **B)** Quantification of CD44v9 expression. Data are expressed as average  $\pm$  S.D.,  $n = 3$ ,  $*p < 0.05$  calculated by Tukey-Kramer method.

These CD44v9-positive cells have been reported to have elevated amount of glutathione (GSH) in the cytosol. Increased GSH plays a key role in hindering platinum drug delivery to nuclear DNA<sup>29</sup>. Researchers have also showed that such defense mechanism exerted by cytosolic GSH can be avoided by loading the platinum drug inside polymeric micelles and transporting the drug closer to the nuclear DNA<sup>29,26,30</sup>. Additionally, cells treated with 5-BPA-DACHPt/m demonstrated lowest fraction of CD44v9 positive cells (**Fig. 6A & B**). This could be due to augmented cytotoxicity of 5-BPA-DACHPt/m because of highly overexpressed SA on CD44v9 positive cells thus improving attachment of micelles. This further proves the rationale of targeting overexpressed SA in CSCs using 5-BPA as ligand .

#### 4.3.6 *In vivo* blood circulation of micelles

After 5-BPA-DACHPt/m micelle demonstrated better activity in *in vitro* studies next we focused on *in vivo* performance of micelle. First, we checked the stability of 5-BPA-DACHPt/m in blood compared to conventional clinically approved DACHPt/m. To trace the micelles in blood circulation using CLSM, we prepared alexa 555 labeled DACHPt/m and alexa 647 labeled 5-BPA-DACHPt/m and PBA-DACHPt/m. For this purpose ear lobe of 6-week-aged BALB/c nu/nu mice was fixed under CLSM under anesthesia. Then, fluorescent labeled 5-BPA-DACHPt/m<sub>Alexa647</sub> and PBA-DACHPt/m<sub>Alexa647</sub> micelles were co-injected with non-ligand DACHPt/m<sub>Alexa555</sub> to observe their blood circulation profile under CLSM and any possible interaction with endothelium or erythrocyte as both of them reported to have SA on their surface<sup>11</sup>. The circulation profile was compared with the non-ligand DACHPt/m<sub>Alexa555</sub>. Both 5-BPA-DACHPt/m<sub>Alexa647</sub> (**Fig. 7A, Red**) and PBA-DACHPt/m<sub>Alexa647</sub> (**Fig. 7B, Red**) showed similar blood circulation profile to non-ligand DACHPt/m<sub>Alexa555</sub> (**Fig. 7A & B: Green**). The circulation of micelles in blood was recorded for 6 h. During our observation period there was no attachment of 5-BPA-DACHPt/m<sub>Alexa647</sub> (**Fig. 7A, Red**) or PBA-

DACHPt/m<sub>Alexa647</sub> (**Fig. 7B, Red**) to the endothelium. We also did not observe any aggregation of erythrocytes as they have SA on the surface so there was a possibility of binding of boronic acid installed micelles on their surface. This could be due to the comparatively high concentration of glucose in blood (~5mM) and superior binding affinity of boronic acid to glucose in blood at pH 7.4. According to previous reports, expression of SA on erythrocytes is ~20 nmol/10<sup>9</sup> cells<sup>11</sup>. This amount is almost thousand fold lower compared to the amount of SA reported in cancer cells e.g. murine melanoma cells<sup>19</sup> (~1.1 nmol/10<sup>6</sup> cells)<sup>19</sup>. Hence, the high glucose in blood and higher binding affinity of boronic acid with glucose at pH 7.4 is probably instigating binding of glucose with the 5-BPA or PBA ligand installed on the surface of polymeric micelle.

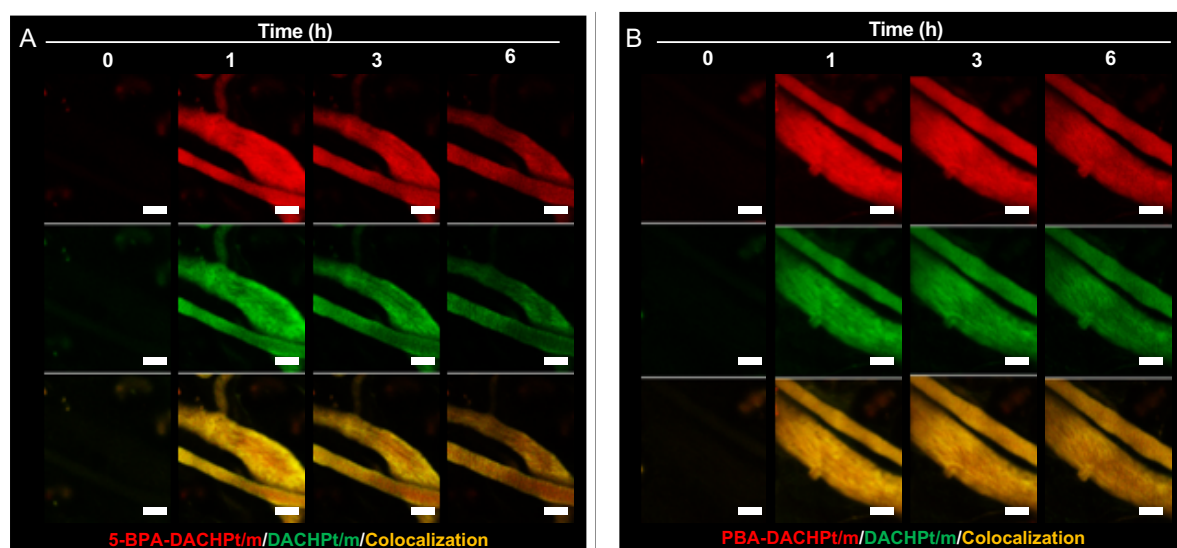


**Figure 7.** Effect of ligand on the *in vivo* performance. **A)** Blood circulation of alexa fluor 647-labeled 5-BPA-DACHPt/m (red) and alexa fluor 555-labeled DACHPt/m (green) after intravenous injection determined using intravital CLSM. Colocalization shown as yellow. **B)** Blood circulation of alexa fluor 647-labeled PBA-DACHPt/m (red) and alexa fluor 555-labeled DACHPt/m (green). Representative images were taken at 1-, 3- and 6 h after injection of micelles. Scale bars = 100  $\mu$ m.



### 4.3.7 Plasma clearance of micelles

We have also confirmed the prolong blood circulation of micelles by checking their plasma clearance profile through Pt content measurement at different time point using ICP MS. Mice were injected with free oxaliplatin (5 mg/kg), DACHPt/m, PBA-DACHPt/m and 5-BPA-DACHPt/m (at 5 mg/kg on DACHPt basis) via tail vein injection. After 1-, 4-, 8-, 24- and 48-h mice were sacrificed and blood was collected from inferior vena cava. Plasma was separated from blood component after centrifugation (rpm 1000). Plasma was digested to release Pt and measured by ICP MS. Calculation was done for % injected dose available per ml of plasma for each time point. Oxaliplatin was cleared out very quickly from the circulation, less than 1% injected dose was available only 1 h after injection (**Fig. 8**). The clearance of oxaliplatin mostly occurs through kidney. Platinum also irreversibly binds to plasma protein causing inactivation of more than 90% of the injected oxaliplatin. Such fast clearance doesn't allow enough time for the drug to accumulate in the tumor. On the other hand, all the micelles demonstrated long circulation profile in the blood and have almost identical plasma clearance profile. Almost more than 80% of the micelles were circulating 8 h after injection. We detected almost ~20% of the injected dose of micelles circulating in the blood even after 24 h (**Fig. 8**). Such long circulation profile is similar to our previously reported micelles<sup>19</sup>. The Pt level in plasma was significantly amplified for the DACHPt loaded polymeric micelles. Having a long circulation profile will allow the micelles to enter the tumor site for extended period of time thus improving the accumulation in tumor. All the micelles were cleared from the blood showing comparable profile after 48 h, only 1~2% of micelles were detected in the circulation (**Fig. 8**). As all the micelles, had almost identical plasma clearing profile ensuring installing 5-BPA or PBA ligand on the polymeric micelle surface does not affect their circulation in the blood due to interaction with SA expressed on the erythrocytes or other blood cells.

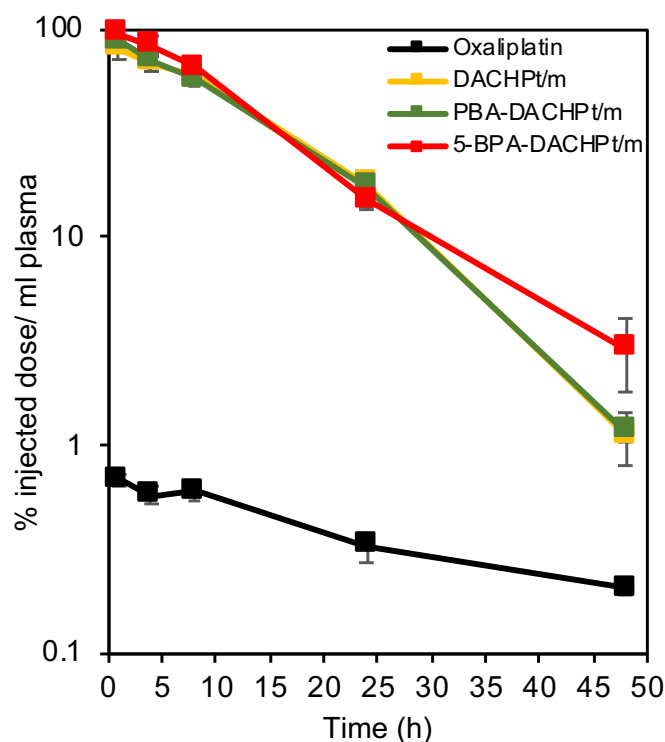


**Figure 8.** Plasma clearance of free oxaliplatin (5 mg/kg) and micelles DACHPt/m, PBA-DACHPt/m and 5-BPA-DACHPt/m (at 5 mg/kg on DACHPt basis) after intravenous injection.

#### 4.3.8 Interaction of the micelles with the cellular components of blood

We have also quantified Pt content in blood component (which is mainly composed of erythrocyte) collected after separating from plasma by centrifugation. Mice were injected with free oxaliplatin (5 mg/kg), DACHPt/m, PBA-DACHPt/m and 5-BPA-DACHPt/m (at 5 mg/kg on DACHPt basis) via tail vein injection. After 1-, 4-, 8-, 24- and 48-h mice were sacrificed and blood was collected from inferior vena cava. Blood components were collected after precipitation by ultracentrifuge (rpm 1000), weighed and digested using 90% HNO<sub>3</sub>. Amount of Pt was measured using ICP MS and calculated relative to DACHPt/m treated group at each time point. Amount of Pt measured in blood component from mice treated with DACHPt/m, PBA-DACHPt/m and 5-BPA-DACHPt/m at different time points did not demonstrate any

significant difference (**Fig. 9**). The measured Pt content can be taken as a parameter to observe any special interaction between the boronic acid ligands and SA present on erythrocyte. These results suggest there is no noteworthy interaction of PBA-DACHPt/m and 5-BPA-DACHPt/m with erythrocyte. This low interaction can be attributed to the high glucose concentration in blood (~5mM) and higher binding of boronic acid to glucose in blood pH 7.4. Researchers have previously reported almost thousand fold higher expression of SA on the surface of murine melanoma cells<sup>19</sup> (~1.1 nmol/10<sup>6</sup> cells) compared to erythrocytes<sup>11</sup> (~20 nmol/10<sup>9</sup> cells).

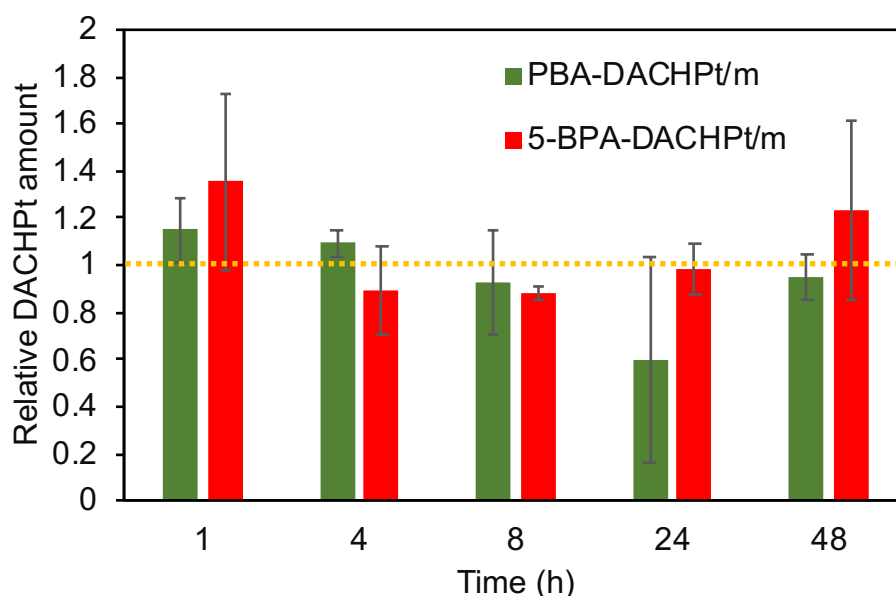


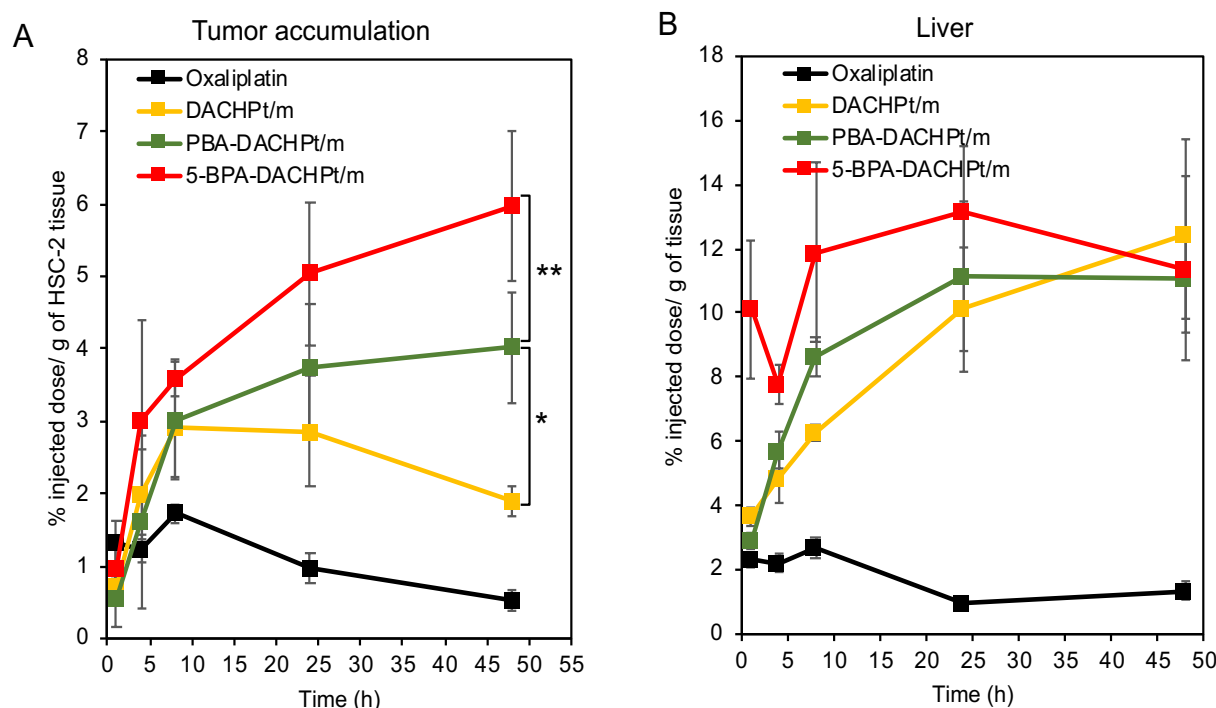
**Figure 9.** Quantification of the amount of DACHPt in the cellular components of blood after intravenous injection of micelles. The data were normalized to the amount of DACHPt from DACHPt/m at each time point. All the micelles have comparable level of DACHPt relative to DACHPt/m verifying no specific interaction with erythrocyte due to 5-BPA or PBA ligand.

#### 4.3.9 *In vivo* tumor accumulation and biodistribution

We quantified tumor accumulation and biodistribution of the DACHPt loaded micelles in SC HSC2 tumor model. After 24h of injection DACHPt/m and PBA-DACHPt/m showed similar

tumor accumulation with no substantial difference in accumulation, which was also same for PBA-DACHPt/m and 5-BPA-DACHPt/m (**Fig. 10A**). But there was a significant increase in the accumulation of 5-BPA-DACHPt/m after 24h when compared with non-ligand DACHPt/m. This can be due to the improved binding of 5-BPA with the cell surface SA in tumor. The difference in the accumulation became more evident after 48h of injection; the amount of DACHPt/m dropped inside the tumor but both 5-BPA and PBA installed micelles upheld their accumulation amount (**Fig. 10A**). At this point elevated accumulation trend of 5-BPA-DACHPt/m was significant compared to both DACHPt/m and PBA-DACHPt/m, this could be attributed to higher binding of 5-BPA to SA in intratumoral acidic pH to PBA. The amount of SA expression on HSC2 cells was measured to be  $\sim 1 \text{ nmol}/10^6 \text{ cells}$ , which is almost thousand fold higher compared to SA quantified in erythrocytes<sup>11</sup>. Moreover, the amount of glucose inside the tumor have been reported to be multiple fold lower compared to the healthy tissue<sup>31</sup> due to fast turnover of glucose to lactate as cancer cells follow the unprecedented aerobic glycolysis a process known as Warburg effect<sup>32</sup>. This phenomenon rationalizes the acidic pH inside tumor due to excessive lactic acid being constantly pumped out of the cells into the tumor microenvironment<sup>17</sup>. As we move from the healthy tissue to tumor there is a pH shift towards the acidic and the amount of glucose and SA also changes drastically so does their binding constant with 5-BPA which is inversely proportionate. Thus, the hypothesis is that the reduced binding of 5-BPA to glucose and amplified binding to overexpressed SA in intratumoral acidic pH would boost the attachment and retention of 5-BPA decorated micelles inside the tumor. This extended tumor withholding of 5-BPA-DACHPt/m will allow longer and greater accessibility of cytotoxic drug to cancer cells and augment chemotherapeutic efficiency of the drug. We have also quantified the amount of Pt in liver, spleen and kidney(**Fig. 10 B,C &D**). There was no significant difference in the accumulation in liver and spleen(**Fig. 10 B & C**). The kidney accumulation of 5-BPA-DACHPt/m was higher compared to other

micelles (**Fig. 10D**). SA has a very important role in renal function. Different parts of the kidney glomerular, podocytes and peritubular capillaries are all coated with glycocalyx<sup>33</sup>. The terminal carbohydrate of the glycocalyx is SA. The glycocalyx is normally expressed on the endothelium or endothelial cells of these parts. The endothelium is the mono layer of cells present in the inside lining of blood and lymphatic vessels. The kidney has three different kind of endothelial cells having unique features and functions (**Fig. 10E**)<sup>33</sup>. They are present in the glomerular, peritubular capillaries and both large and small vessels. The endothelium of all these sections are heavily covered in glycocalyx. As 97% glucose is reabsorbed by the kidney tubule there are region of very low glucose concentration<sup>34</sup>. Reduction in glucose concentration may potentially allow the 5-BPA-DACHPt/m to be attached to terminal SA of heavily glycocalyx coated endothelium. As the micelle is around 30 nm in size thus the probability of the micelle attachment location is in the vessel endothelium with dynamic changes in the concentration of glucose and blood flow.



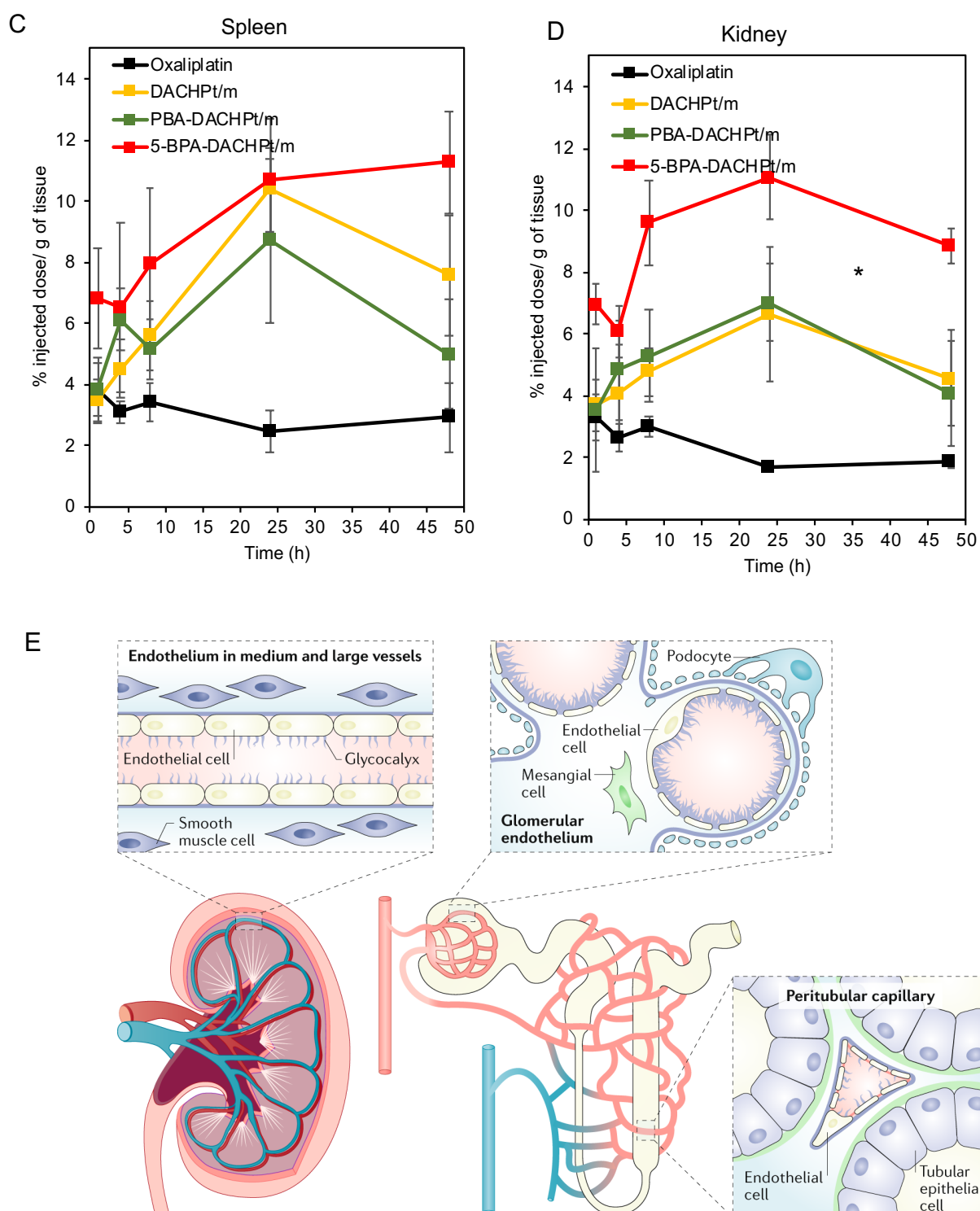


**Figure 10.** Tumor accumulation and biodistribution. Accumulation of free oxaliplatin (5 mg/kg) and micelles DACHPt/m, PBA-DACHPt/m and 5-BPA-DACHPt/m (at 5 mg/kg on DACHPt basis) in **A)** subcutaneous HSC2 tumor **B)** liver **C)** spleen and **D)** kidney after intravenous injection. **E)** Structure of kidney<sup>33</sup>. Data are expressed as averages  $\pm$  S.D.,  $n = 4$ ,

\* $p < 0.05$ , \*\* $p < 0.01$  calculated by Tukey-Kramer method.

#### 4.3.10 Antitumor activity and survival study

Researchers have previously reported about treatment resistant HSC2 xenograft tumor expressing high fraction of CD44v9 positive cells<sup>3</sup>. CD44v positive cells express higher amount of SA<sup>6</sup>, thus 5-BPA installed micelle should be more effective in treating this CSCs rich cancer model. Antitumor activity of 5-BPA-DACHPt/m was assessed in orthotopic tumor model by inoculating HSC2 cell into the right lateral edge of the tongue of mice. Mice were then given 4 intravenous injections of 8mg/kg dose basis oxaliplatin and 2mg/kg (DACHPt basis) micelles from 5 days after inoculation on day 0, 2, 4 and 15. For oxaliplatin maximum tolerated dose and micelle dose was selected based on our previous study<sup>35</sup>. Oxaliplatin did not show any inhibition of tumor growth as non-treated group even at such high dose (**Fig. 11A**) probably due to their fast clearance from the body and low tumor accumulation (**Fig. 10A**). Within 2 weeks after treatment the micelles demonstrated their tumor growth suppression ability compared to both oxaliplatin and non-treated group, which continued to grow conversely (**Fig. 11A**). After 3 weeks the superiority of 5-BPA-DACHPt/m compared to both DACHPt/m and PBA-DACHPt/m became evident as the variance in the tumor volume became significantly different (**Fig. 11A**) correlating with higher tumor accumulation and retention of 5-BPA-DACHPt/m (**Fig. 10A**). Tumor growth was followed for a month and the 5-BPA-DACHPt/m showed unprecedented tumor growth suppression capability. This antitumor benefit did not come as a cost of treatment side effect such as weight loss (**Fig. 11B**); but the mice did show reduction in body weight as the tongue tumor continued to grow and affected oral ingestion. These mice were also followed for survival until their demise.

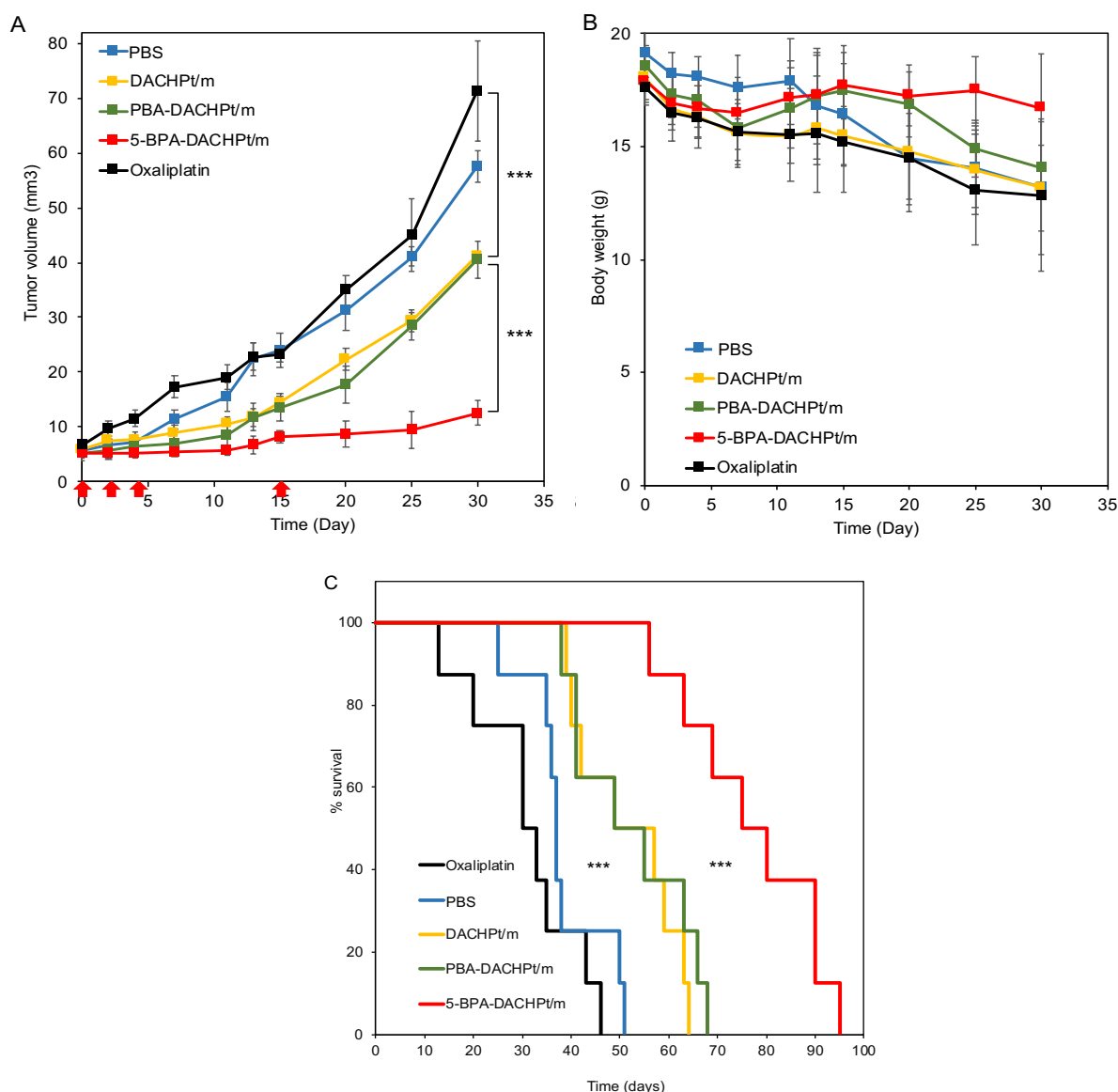


**Figure 11.** Effect of ligand on the *in vivo* performance. **A)** Antitumor activity against orthotopic HSC2 tumors after treatment with oxaliplatin (8 mg/kg), DACHPt/m, PBA-DACHPt/m and 5-BPA-DACHPt/m (at 2 mg/kg on DACHPt basis) injected on days 0, 2, 4 and 15 (arrows). Data are expressed as averages  $\pm$  S.D.,  $n = 8$ , \*\*\* $p < 0.001$  calculated by Tukey-Kramer method. **B)** Body weight of mice during treatment. **C)** Animal survival during treatment.  $n = 8$ , \*\*\* $p < 0.005$  calculated by Log-rank test.

All the micelles significantly improved survival of 50% mice by at least 2 weeks compared to control group and oxaliplatin treated group with 5-BPA-DACHPt/m improving



this time up to 7 weeks (**Fig. 11C**). The survival of the mice interrelated with their tumor growth which verifies the improved survival of 5-BPA DACHPt/m treatment was the extraordinary ability of the micelle to accumulate higher in acidic tumor and retain for extended period of time allowing loaded drug to have better efficacy. These results indicate the importance of controlling the binding affinity of boronic acid ligands for promoting the tumor targeting and antitumor efficacy of nanomedicines, denoting the potential of 5-BPA for generating effective anticancer approaches.

#### 4.3.11 *In vivo* assessment of CSCs

The concept of CSCs have been known to researchers for couple of decades. Recently, treatment resistance of CSCs are being hailed as the main culprit of cancer reoccurrences. These CSCs are concealed in special niches inside many tumors<sup>36</sup>. Their recognition and abolition still represent a big challenge. CSCs are blamed for the relapse of cancer after treatment and the focal point of CSC treatment is to extend the possible relapse time<sup>37,38</sup>. The CSCs treatment efficacy focuses on the remaining CSCs after the treatment<sup>39</sup>. For this purpose, treatment effect of 5-BPA-DACHPt/m on CSCs fraction was evaluated. HSC2 tumor reported to contain considerably high percentage of CD44v9 positive CSCs<sup>3</sup>. Thus, these cells may be more disposed to attach 5-BPA decorated on the micelle surface. To study the effect of 5-BPA-DACHPt/m on expression of CD44v9 positive cells we collected orthotopic HSC2 tumor after 3 treatment on day 0, 2 and 4. Collection was done 48 h after the 3<sup>rd</sup> injection and CD44v9 expression in tumors were investigated by immunohistochemistry. The tumor showed both involucrin positive area (**Fig. 12A, green**) which represents the differentiated cancer cell population and also CD44v positive area (**Fig. 12A, red**) representing CSCs in the tumor niche which have been reported previously in the same tumor<sup>3</sup>.

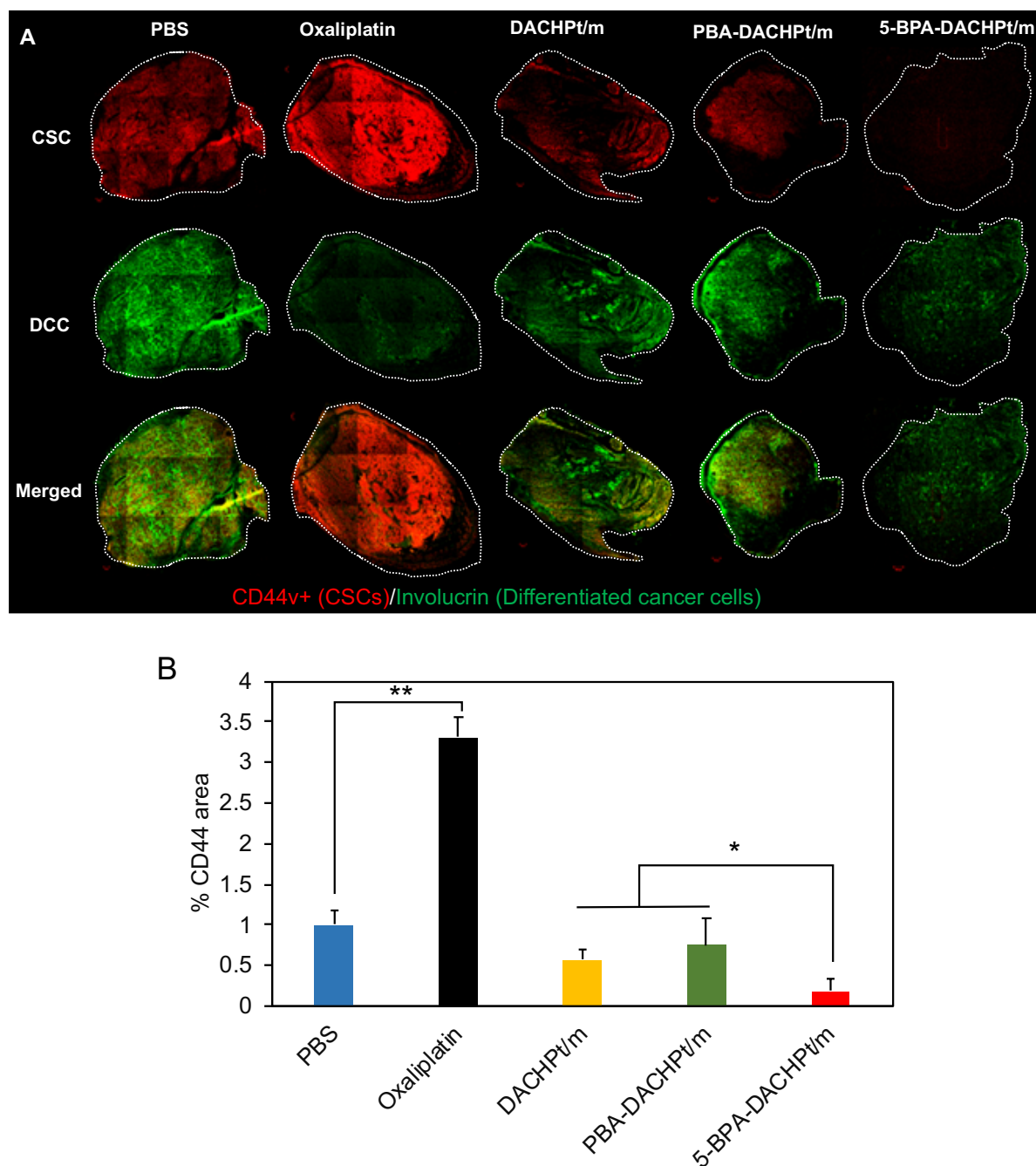


**Figure 12.** Ligand effect on CSC population *in vivo*. **A)** Distribution of CSCs (CD44v9; red) and differentiated cancer cells (involucrin; green) in tumors after treatment with oxaliplatin (8 mg/kg), DACHPt/m, PBA-DACHPt/m and 5-BPA-DACHPt/m (2 mg/kg) injected on days 0, 2 and 4. Tumors were removed 48 h after 3<sup>rd</sup> injection. **B)** Quantification of the CSC area. Data expressed as averages  $\pm$  S.D., n = 4, \*p < 0.05, \*\*p < 0.01 calculated by Tukey-Kramer method.

Tumors treated with oxaliplatin demonstrated enhanced fraction of CSCs (**Fig. 12A & B**), probably due to its inability to eliminate resistant CD44v9 positive cells. This increase is well related with the more aggressive tumor growth of oxaliplatin treated group compared to non-treated control group in the antitumor activity study (**Fig. 11A**). Such increase in CSC population in head and neck cancer have also been reported in patients after treatment with chemotherapeutic drug cisplatin<sup>3</sup>. All the micelle treated groups exhibited significantly low CD44v9 positive area compared to oxaliplatin treated group suggesting micelle treatment can efficiently subdue CSC percentage in the tumor (**Fig. 12A & B**). DACHPt/m and PBA-DACHPt/m treatment did not initiate any escalation in CD44v9 positive fraction in tumor as demonstrated by oxaliplatin treatment. But the treatment was not effective in reducing the CD44v9 positive fraction in tumor compared to non-treated control group. Whereas, treatment with 5-BPA-DACHPt/m efficaciously slashed the amount of CD44v9 positive fraction compared to control group (**Fig. 12A & B**). This well correlates with the high expression of SA in CD44v9 positive cells thus improving uptake of 5-BPA-DACHPt/m in these cells. Such reduction in CD44v positive cells was also seen in *in vitro* studies after treatment with 5-BPA-DACHPt/m.

## 4.4 Discussion

DACHPt (the parent complex of clinically approved oxaliplatin) loaded 5-BPA micelles have size around ~30 nm in diameter which is essential for deep penetration inside the tumor<sup>40</sup> and also allows the loaded drug to be released proximate to nucleus inside the cells allowing effective fatal DNA adduct formation with the Pt<sup>26</sup>. Such nanosized system also permits longer blood circulation (**Fig. 8**) thus allowing much higher accumulation in the tumor (**Fig. 10A**). On the contrary, free oxaliplatin has very fast clearance from the body with less than 1% of injected dose available just after 1h injection (**Fig. 8**) and restricted by severe toxicity concerns.

Furthermore, 5-BPA-DACHPt/m demonstrated much higher tumor retention over long period of time compared to non-ligand DACHPt/m (**Fig. 10A**) and avoiding any unspecific binding to endothelium (**Fig. 7A**) and blood component (**Fig. 9**). We have confirmed the extraordinary accumulation and retention of 5-BPA-DACHPt/m was ligand mediated and due to specific interaction between 5-BPA and SA on cancer cell surface through *in vitro* investigation. Firstly, we found 5-BPA-DACHPt/m are up taken by cells more in acidic pH condition (**Fig. 3B**) compared to other micelles which can be explained by high binding constant between 5-BPA and SA in low pH<sup>23</sup>. We verified such increased cellular uptake was ligand mediated by removing the target molecule from the cancer cell surface in this case SA using sialidase enzyme thus significantly reducing the cellular uptake (**Fig. 5A-D**). Such improved cellular uptake have permitted 5-BPA-DACHPt/m to be more cytotoxic in acidic pH environment after short incubation period (**Table 1**). Acidic pH is a common phenomenon in intratumoral microenvironment<sup>41</sup>. 5-BPA-DACHPt/m treatment have significantly reduced the amount of CD44v9 positive cell fraction of HSC2 cells *in vitro* compared to other treatments proving they can be effective in eliminating CSCs (**Fig. 6A & B**).

HNSCC tumor model HSC2 containing high fraction of CD44v9 positive cells have been reported to be treatment resistant<sup>3</sup>. Overcoming such resistance holds the key to treat such types of aggressive tumor. 5-BPA-DACHPt/m have effectively induced tumor growth suppression in resistant orthotopic HSC2 tumor model in mice (**Fig. 11A**). In line with previous report, treatment with free oxaliplatin triggered more aggressive tumor growth compared to the non-treated control group (**Fig. 11A**). Oxaliplatin treatment also induced reduction in body weight as side effect to toxicity (**Fig. 11B**). 50% of the mice treated with 5-BPA-DACHPt/m survived 7 weeks longer than nontreated and oxaliplatin treated group and 4 weeks longer than DACHPt/m and PBA-DACHPt/m treated group (**Fig. 11C**). We further explored the reason for such improvement in survival and discovered treatment with 5-BPA-DACHPt/m effectively

reduced fraction of CD44v9 positive CSCs in tumor micro distribution (**Fig. 12A & B**) such outcome can be rationalized by high amount of SA in CD44 positive cells thus allowing higher uptake of micelles otherwise difficult to treat cells. Therefore, these extensive cellular and animal studies validate the specific targeting ability of 5-BPA molecule as a ligand and the possibility of enhancing treatment efficiency of any nanomedicine by this simple ligand installing strategy.

## 4.5 Conclusion

To conclude, we have demonstrated the extraordinary ability of 5-BPA ligand to specifically target overexpressed SA in acidic tumor microenvironment. By installing 5-BPA on the surface of polymeric micelles loaded with chemotherapeutic drug we have demonstrated superior tumor growth suppression and improved survival in resistant CSCs rich orthotopic HSC2 tumor model. As, DACHPt/m are already undergoing clinical trials<sup>42</sup> improvement of treatment ability can be achieved by introducing cancer specific 5-BPA ligand on the surface of the polymeric micelle to challenge resistant CSCs rich tumors.

## 4.6 References

1. Leemans, C. R., Braakhuis, B. J. M. & Brakenhoff, R. H. The molecular biology of head and neck cancer. *Nat. Rev. Cancer* **11**, 9–22 (2011).
2. Al-Hajj, M., Wicha, M. S., Benito-Hernandez, A., Morrison, S. J. & Clarke, M. F. Prospective identification of tumorigenic breast cancer cells. *Proc. Natl. Acad. Sci.* **100**, (2003).
3. Yoshikawa, M. *et al.* XCT inhibition depletes CD44v-expressing tumor cells that are resistant to EGFR-targeted therapy in head and neck squamous cell carcinoma. *Cancer Res.* **73**, 1855–1866 (2013).
4. Prince, M. E. *et al.* Identification of a subpopulation of cells with cancer stem cell properties in head and neck squamous cell carcinoma. *Proc. Natl. Acad. Sci.* **104**, 973–

- 978 (2007).
5. Wang, M. *et al.* Eradication of CD44-variant positive population in head and neck tumors through controlled intracellular navigation of cisplatin-loaded nanomedicines. *J. Control. Release* **230**, 26–33 (2016).
  6. Barkeer, S., Chugh, S., Batra, S. K. & Ponnusamy, M. P. Glycosylation of Cancer Stem Cells: Function in Stemness, Tumorigenesis, and Metastasis. *Neoplasia (United States)* **20**, 813–825 (2018).
  7. Rillahan, C. D. *et al.* Global metabolic inhibitors of sialyl- and fucosyltransferases remodel the glycome. *Nat. Chem. Biol.* **8**, 661–668 (2012).
  8. Büll, C. *et al.* Targeting aberrant sialylation in cancer cells using a fluorinated sialic acid analog impairs adhesion, migration, and in vivo tumor growth. *Mol. Cancer Ther.* **12**, 1935–1946 (2013).
  9. Tatsuta, T., Satoh, T., Sugawara, S., Hara, A. & Hosono, M. Sialic acid-binding lectin from bullfrog eggs inhibits human malignant mesothelioma cell growth in vitro and in vivo. *PLoS One* **13**, e0190653 (2018).
  10. Loureiro, L. R. *et al.* Novel monoclonal antibody L2A5 specifically targeting sialyl-Tn and short glycans terminated by alpha-2–6 sialic acids. *Sci. Rep.* **8**, 12196 (2018).
  11. Miller, A., Sullivan, J. F. & Katz, J. H. Sialic Acid Content of the Erythrocyte and of an Ascites Tumor Cell of the Mouse. *Cancer Res.* **23**, 485–490 (1963).
  12. Rosen, S., Singer, M., Yednock, T. & Stoolman, L. Involvement of sialic acid on endothelial cells in organ-specific lymphocyte recirculation. *Science (80-. ).* **228**, 1005–1007 (1985).
  13. Cioffi, D. L., Pandey, S., Alvarez, D. F. & Cioffi, E. A. Terminal sialic acids are an important determinant of pulmonary endothelial barrier integrity. *Am. J. Physiol. Cell. Mol. Physiol.* **302**, L1067–L1077 (2012).
  14. Abe, Y. *et al.* Endothelial  $\alpha$ 2,6-Linked Sialic Acid Inhibits VCAM-1- Dependent Adhesion Under Flow Conditions. *J. Immunol.* **163**, 2867 LP – 2876 (1999).
  15. Büll, C. *et al.* Sialic acid blockade suppresses tumor growth by enhancing t-cell-mediated tumor immunity. *Cancer Res.* **78**, 3574–3588 (2018).
  16. Mi, P., Cabral, H. & Kataoka, K. Ligand-Installed Nanocarriers toward Precision Therapy. *Adv. Mater.* **1902604**, 1902604 (2019).
  17. Martin, G. R. & Jain, R. K. Noninvasive Measurement of Interstitial pH Profiles in Normal and Neoplastic Tissue Using Fluorescence Ratio Imaging Microscopy. *Cancer*

- Res.* **54**, 5670–5674 (1994).
18. Anderson, M., Moshnikova, A., Engelman, D. M., Reshetnyak, Y. K. & Andreev, O. A. Probe for the measurement of cell surface pH in vivo and ex vivo. *Proc. Natl. Acad. Sci.* **113**, 8177–8181 (2016).
  19. Deshayes, S. *et al.* Phenylboronic Acid-Installed Polymeric Micelles for Targeting Sialylated Epitopes in Solid Tumors. *J. Am. Chem. Soc.* **135**, 15501–15507 (2013).
  20. Otsuka, H., Uchimura, E., Koshino, H., Okano, T. & Kataoka, K. Anomalous binding profile of phenylboronic acid with N-acetylneuraminic acid (Neu5Ac) in aqueous solution with varying pH. *J. Am. Chem. Soc.* **125**, 3493–3502 (2003).
  21. Matsumoto, A. *et al.* Heterocyclic boronic acids display sialic acid selective binding in a hypoxic tumor relevant acidic environment. *Chem. Sci.* **8**, 6165–6170 (2017).
  22. Sanchez, J.-F. *et al.* Biochemical and Structural Analysis of *Helix pomatia* Agglutinin. *J. Biol. Chem.* **281**, 20171–20180 (2006).
  23. Matsumoto, A. *et al.* Heterocyclic boronic acids display sialic acid selective binding in a hypoxic tumor relevant acidic environment. *Chem. Sci.* **00**, 1–6 (2017).
  24. Kelland, L. The resurgence of platinum-based cancer chemotherapy. *Nat. Rev. Cancer* **7**, 573–584 (2007).
  25. Murakami, M. *et al.* Improving Drug Potency and Efficacy by Nanocarrier-Mediated Subcellular Targeting. *Sci. Transl. Med.* **3**, 64ra2-64ra2 (2011).
  26. Murakami, M. *et al.* *Improving Drug Potency and Efficacy by Nanocarrier-Mediated Subcellular Targeting.*
  27. Prince, M. E. *et al.* Identification of a subpopulation of cells with cancer stem cell properties in head and neck squamous cell carcinoma. *Proc. Natl. Acad. Sci. U. S. A.* **104**, 973–978 (2007).
  28. Yae, T. *et al.* Alternative splicing of CD44 mRNA by ESRP1 enhances lung colonization of metastatic cancer cell. *Nat. Commun.* **3**, (2012).
  29. Wang, M. *et al.* Eradication of CD44-variant positive population in head and neck tumors through controlled intracellular navigation of cisplatin-loaded nanomedicines. *J. Control. Release* **230**, 26–33 (2016).
  30. Miyano, K. *et al.* cRGD peptide installation on cisplatin-loaded nanomedicines enhances efficacy against locally advanced head and neck squamous cell carcinoma bearing cancer stem-like cells. *J. Control. Release* **261**, 275–286 (2017).
  31. Hirayama, A. *et al.* Quantitative metabolome profiling of colon and stomach cancer

- microenvironment by capillary electrophoresis time-of-flight mass spectrometry. *Cancer Res.* **69**, 4918–4925 (2009).
32. Vander Heiden, M., Cantley, L. & Thompson, C. Understanding the Warburg effect: The metabolic Requirements of cell proliferation. *Science* (80-. ). **324**, 1029–1033 (2009).
  33. Jourde-Chiche, N. *et al.* Endothelium structure and function in kidney health and disease. *Nat. Rev. Nephrol.* **15**, 87–108 (2019).
  34. Dominguez Rieg, J. A. & Rieg, T. What does sodium-glucose co-transporter 1 inhibition add: Prospects for dual inhibition. *Diabetes, Obes. Metab.* **21**, 43–52 (2019).
  35. Cabral, H., Nishiyama, N. & Kataoka, K. Optimization of (1,2-diamino-cyclohexane)platinum(II)-loaded polymeric micelles directed to improved tumor targeting and enhanced antitumor activity. *J. Control. Release* **121**, 146–155 (2007).
  36. Atashzar, M. R. *et al.* Cancer stem cells: A review from origin to therapeutic implications. *J. Cell. Physiol.* **235**, 790–803 (2020).
  37. Zhou, B. B. S. *et al.* Tumour-initiating cells: Challenges and opportunities for anticancer drug discovery. *Nat. Rev. Drug Discov.* **8**, 806–823 (2009).
  38. McDermott, S. P. & Wicha, M. S. Targeting breast cancer stem cells. *Mol. Oncol.* **4**, 404–419 (2010).
  39. Baccelli, I. & Trumpp, A. The evolving concept of cancer and metastasis stem cells. *J. Cell Biol.* **198**, 281–293 (2012).
  40. Cabral, H. *et al.* Accumulation of sub-100 nm polymeric micelles in poorly permeable tumours depends on size. *Nat. Nanotechnol.* **6**, 815–823 (2011).
  41. Estrella, V. *et al.* Acidity generated by the tumor microenvironment drives local invasion. *Cancer Res.* **73**, 1524–1535 (2013).
  42. Nishiyama, N., Matsumura, Y. & Kataoka, K. Development of polymeric micelles for targeting intractable cancers. *Cancer Sci.* **107**, 867–874 (2016).



# **Chapter 5**

## **PBA installed polymer as immunomodulator**

## Chapter 5: PBA installed polymer as immunomodulator

### Abstract

The ability of boronic acid conjugated polymer system to induce proliferation of T cells have been reported. 8-arm-PEG was used as a model polymer to verify the concept for availability of multiple binding sites. 5-BPA and PBA was conjugated to 8-arm-PEGs and remaining free amines were acetylated. *In vitro* proliferation assays was conducted using immortalized human T lymphocytes (Jurkat cells) and lymphocytes collected from mouse lymph nodes. In both cases, only boronic acid conjugated 8-arm-PEGs induced proliferation. Small molecules 5-BPA or PBA did not induce any proliferation. Evaluation of CD4 and CD8 positive cell population after incubation with polymers revealed changes in CD4 fraction with PBA-8-arm-PEG incubation.

## Chapter 5: PBA installed polymer as immunomodulator

### 5.1 Introduction

### 5.2 Experimental

#### 5.2.1 Materials

#### 5.2.2 Cell line and animals

#### 5.2.3 Conjugation of PBA and 5-BPA to 8-arm-PEG-amine

#### 5.2.4 *In vitro* proliferation of Jurkat cells

#### 5.2.5 *In vitro* proliferation of mouse T cells

#### 5.2.6 CD4 and CD8 staining of mouse T-cells

### 5.3 Result

#### 5.3.1 Characterization of polymers

#### 5.3.2 T cell proliferation assay

##### 5.3.2.1 Jurkat cells

##### 5.3.2.2 Mouse T cells

#### 5.3.3 Staining of CD4 and CD8

### 5.4 Discussion

### 5.5 Conclusion

### 5.6 References

## 5.1 Introduction

T cells also called T lymphocytes comprises with different subpopulations and play essential role in immune response. Each subpopulation have their distinctive functions and together they maintain a healthy immune system<sup>1</sup>. Researchers have long been trying to develop methods to activate and proliferate T cells as a possible treatment regimen for numerous diseases including

cancer<sup>2</sup>. T cells can be stimulated to activate and proliferate using mitogens. One mitogen from natural origin is lectin, with the ability to bind with sugars are known for their proliferative activity and have been investigated extensively<sup>3,4</sup>. Lectins have the ability to activate and proliferate T cells probably through interaction with surface glycan of T cell receptors (TCR)/CD3 complex that initiate a cascade of reaction involving activation of enzyme protein kinase C (PKC) and some particular PKC genes<sup>5</sup>. Such lectin activation of T cells have generated cells with extraordinary cytotoxic activity<sup>6</sup>. However, the toxicity and immunogenicity of lectin hinders the development of such studies. If injected into the body lectin can cause aggregation of erythrocytes by interacting with surface glycan or even bind to endothelium and inhibit transport of molecule across. Both of these can cause serious consequences and can be even fatal. This toxicity issue can be overcome by synthesizing polymer with lectin like properties.

PBA can form reversible covalent interactions with diol-containing molecules similar to lectin. In fact, sugars, such as the common monosaccharides (*e.g.* glucose), contain diols, and as a consequence, PBA have proven to be helpful molecular ligands for binding and detection, as synthetic lectins. While the binding of boron to diol-containing molecules is commonly promoted at basic pH, the binding constant between these agents drops at neutral and acidic pHs. On the other hand, the binding of boronic acids to N-acetylneuraminic acid or SA (the terminal sugar of the cell surface glycan chain) opposes this trend, and the binding constant between boronic acid compound and SA increases at acidic pHs. For example, complexes between PBA and sugars were shown to be stable at pH higher than their pKa, however, with pH lower than pKa only SA-PBA complexes were stable<sup>7</sup>. Researchers have previously synthesized PBA conjugated polymer and demonstrated their ability to induce lymphocyte aggregation and proliferation<sup>8,9,10</sup>.

In recognition of sugar moiety by lectin one of the key feature is their multiple binding

sites. Concanavalin A (Con A) a normally used lectin for the proliferation of T cells have four binding sites for a sugar chain<sup>11</sup>. The importance of multivalency have also been established by previous researchers<sup>10</sup>. Uchimura et al. synthesized a polymer with multiple PBA molecule which could induce proliferation of spleen lymphocytes collected from mice with elevated amount of IL-2 on the cell surface and demonstrated cytotoxic ability in combination with IL-2 treatment against YAC-1 cells. They hypothesize such proliferation phenomenon was observed probably owing to the interaction between cell surface SA of lymphocyte and PBA molecule. Thus, in this study I focus on developing PBA based polymer system to use as synthetic lectin that can be translated to *in vivo* application.

In this chapter, I have prepared PBA and 5-BPA conjugated 8-arm-PEG (Mw 40,000). I verified the ability of the PBA and 5-BPA conjugated polymers to induce proliferation in immortalized human T lymphocytes (Jurkat cells) at pH 7.4 and pH 6.5. In accordance with previous reports neither PBA or 5-BPA small molecule demonstrated such activation ability confirming the necessity of multivalent binding site for engaging cell surface glycan to induce proliferation. 8-arm-PEG-PBA also induced similar proliferation in T cells collected from mouse lymph nodes. Staining with CD4 and CD8 antibodies after polymer treatment revealed induction of CD4+ cells with 8-arm-PEG-PBA treatment in cells collected from both lymph nodes and thymus. Whereas, 8-arm-PEG-5-BPA treatment had small but significant impact on CD8+ cells collected from thymus only. Thus confirming the potential of boronic acid polymers to use as synthetic lectin to induce *in vitro* T cell proliferation.

## 5.2 Experimental

### 5.2.1 Materials

5-Boronopicolinic acid (5-BPA) was obtained from Santa Cruze Biotechnology, Inc (Texas, United States). 3-carboxy phenylboronic acid (PBA), 4-(4,6-dimethoxy-1,3,5-triazin-2-yl)-4-methylmorpholinium chloride n-hydrate (DMT-MM), triethylamine (TEA, >99%) and dimethyl sulfoxide (DMSO) (>99%) were obtained from Wako Pure Chemical Co., Inc. (Osaka, Japan). 8-arm-poly(ethylene glycol)-amine (8-arm-PEG; Mw = 40,000) was purchased from Sigma-Aldrich Co. (ST. Louis, MO). Cy5 NHS ester was obtained from Lumiprobe (Florida, USA). Roswell Park Memorial Institute medium (RPMI 1640) and Dulbecco's modified eagle's medium (DMEM) was obtained from Sigma-Aldrich Co. (ST. Louis, MO). Fetal bovine serum (FBS) was purchased from Dainippon Sumitomo Pharma Co., Ltd. (Osaka, Japan). Phosphate-buffered saline (PBS) was purchased from Wako Pure Chemical Industries Ltd. (Osaka, Japan). MEM Non-essential amino acids, penicillin streptomycin, sodium pyruvate, HEPES buffer solution and 2-mercaptoethanol was purchased from Life Technologies (California, USA). FITC rat anti-mouse CD4 (clone: GK 1.5), alexa fluor 647 rat anti-mouse CD8a (clone: 53-6.7) was obtained from BD Biosciences (California, USA). Anti-mouse CD16/32 antibody (clone: 93) was purchased from Biolegend (California, USA).

### 5.2.1 Cell line and animals

Jurkat cells (immortalized human T lymphocytes) were purchased from Cell Bank, Riken BioResource Center (Tsukuba, Japan). Jurkat cells were maintained in RPMI 1640 media containing 10% of fetal bovine serum (FBS) and 1% of penicillin streptomycin in a humidified atmosphere containing 5% CO<sub>2</sub> at 37°C. T cells collected from mice were maintained in RPMI 1640 media containing 10% of fetal bovine serum (FBS), 1% of penicillin streptomycin, 1%

of L-glutamine, 1% of MEM Non-essential amino acids, 1% of sodium pyruvate and 0.1% of 2-mercaptoethanol in a humidified atmosphere containing 5% CO<sub>2</sub> at 37°C. Female, 6-week-old BALB/c wild type mice were purchased from Charles River Japan (Kanagawa, Japan). All experiments were performed in accordance with the Guidelines for the Care and Use of Laboratory Animals as stated by The University of Tokyo.

### 5.2.3 Conjugation of 5-BPA and PBA to 8-arm-PEG (40k)-amine

8-arm-PEG<sub>40K</sub>-amine was dissolved in buffer pH 8.4 and one equivalent of Cy5 NHS was dissolved in DMSO and added to the polymer (**Fig. 1**). Reaction was carried out overnight and then dialyzed against DMSO and then distilled water. Finally, the polymer was freeze dried. 10 fold molar excess of 5-BPA and PBA were activated using DMT-MM in DMSO and added to a reaction mixture of 8-arm-PEG<sub>40K</sub>-amine with TEA and reacted for 24 h. Polymer was then purified by dialysis first against DMSO and then distilled water and lyophilized to obtain powder (**Fig. 1**). Conjugation of 5-BPA and PBA was confirmed by <sup>1</sup>H-NMR measured in D<sub>2</sub>O at 25°C. Any free amine was capped using acetic anhydride and further dialyzed and lyophilized to obtain 5-BPA-Cy5-8-arm-PEG<sub>40K</sub>-Ac and PBA-Cy5-8-arm-PEG<sub>40K</sub>-Ac.

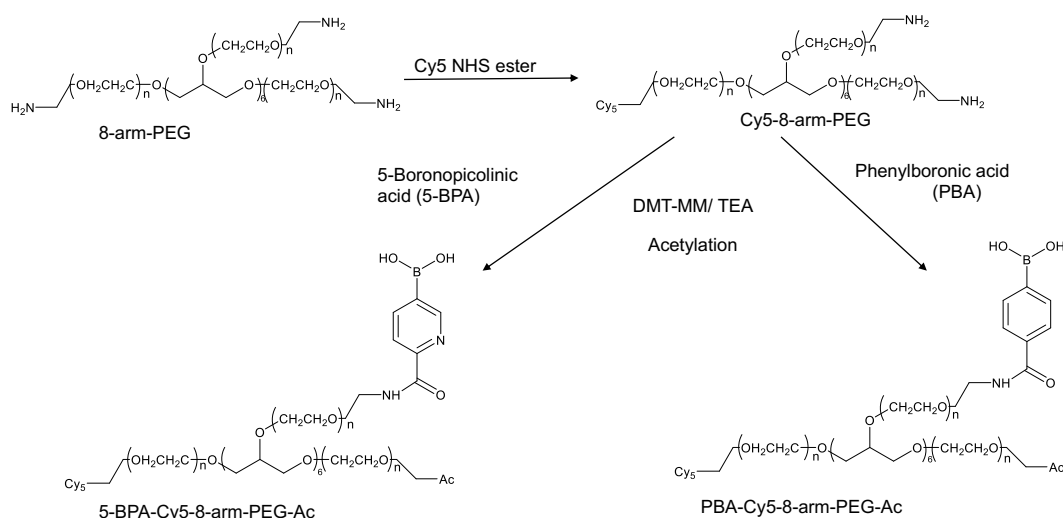


**Figure 1.** Synthesis scheme of 5-BPA and PBA conjugation to 8-arm-PEG

### 5.2.4 *In vitro* proliferation of Jurkat cells

Proliferation of Jurkat cells (immortalized human T lymphocyte cells) was assessed after incubation with different concentration of 5-BPA, PBA and conjugated 8-arm PEG<sub>40K</sub>. Experiment was performed at pH 7.4 and pH 6.5.  $2 \times 10^4$  Jurkat cells were plated in 96 well plate. After 24 h of incubation cells were exposed to varying concentration of 5-BPA or PBA small molecules or 5-BPA or PBA conjugated 8-arm-PEG<sub>40K</sub>. After further incubation for 48 h, 10  $\mu$ l cell counting kit 8 (CCK-8) was added to each well. 1 h after addition of CCK-8 absorbance was measured at 450 nm using Tecan Microplate Reader: Tecan infinite 200. % proliferation of cells were calculated relative to control group that was incubated with media only at pH 7.4 and pH 6.5

### 5.2.5 *In vitro* proliferation of mouse T cells

T lymphocytes collected from BALB/c wild (female; age 6 weeks;) type mice were also evaluated through above mentioned experiment. Single cell suspensions were prepared by passing lymph nodes through a 40  $\mu$ m mesh.  $2 \times 10^5$  cells from lymph nodes were plated in 96 well plates. Cells were cultured in RPMI-1640 media containing 50ml FBS, 5 ml Penicillin/Streptomycin, 5ml HEPES(1M), 5ml Sodium pyruvate (100mM), 5ml non-essential amino acids and 500  $\mu$ l 2-mercaptoethanol. After overnight incubation PBA and 8-arm-PBA was added and further incubated for 48 h. Finally, 10  $\mu$ l of CCK-8 was added to each well and absorption was measured at 450 nm using Tecan Microplate Reader: Tecan infinite 200. % proliferation of cells were calculated relative to control group that was incubated with media only.



### 5.2.6 CD4 and CD8 staining of mouse T-cells

Thymus and lymph nodes were collected from 13 weeks female BALB/c wild type mice. Single cell suspensions were prepared by passing lymph nodes and thymus through a 40  $\mu\text{m}$  mesh. Cells were collected in media and washed twice before cell counting.  $1.5 \times 10^5$  cells from lymph nodes and  $2.5 \times 10^6$  cells from thymus were plated in 24 well plates. Cells were allowed to settle down for 3 h and then incubated for 48 h with PBA and 5-BPA conjugated 8-arm-PEG. Cells were stained twice, first right after collection and then again after 48 h incubation with 5-BPA or PBA conjugated polymers to observe any change in CD4 and CD8 sub population. Any unspecific binding was blocked by incubating cells with anti-mouse CD16/32 (clone: 93) (1:100) for 20 min. CD16/32 antibody is specific for Fc $\gamma$ R III/II and can be used to block unspecific staining of antibodies. Cells were then washed with PBS (with 2% FBS) and incubated with alexa fluor 647 anti-mouse CD8a (clone: 53-6.7) and FITC anti-mouse CD4 (clone: GK 1.5) antibody (1:200) for 50 min. Finally cells were stained with DAPI for 5 min and washed with PBS (with 2% FBS) 2 times and resuspended in 1ml PBS (with 2% FBS). CD4 and CD8 staining was evaluated using Flow cytometry (Becton Dickinson, Franklin Lakes, NJ, USA) and analysis of positive staining cells were done using FlowJo software after appropriate gating.

## 5.3 Result

### 5.3.1 Characterization of polymers

8-arm PEG conjugating boronic acid derivatives provides the possibility for multivalent binding to glycoproteins of cells (**Fig. 2A**). As previous studies have demonstrated the importance of multiple binding site for synthesizing synthetic lectin<sup>12</sup>. We hypothesize by using a PEG with multiple arm will allow several conjugated boronic acid to bind with the cell

surface SA of the T cells and induce proliferation. Conjugation of 5-BPA and PBA was done using coupling reagent DMT-MM through formation of amide bond between the carboxylic acid group of boronic acids and amine group of 8-arm-PEGs. As, the conjugation efficiency was not 100% any remaining amine group was capped through acetylation reaction. The conjugation of 5-BPA and PBA was calculated by proton ratio of  $-\text{OCH}_2\text{CH}_2$  ( $\delta = 3.7$  ppm) in PEG and  $-\text{H}$  present in pyridine ring ( $\delta = 7.2$  ppm, 8.1 ppm, 8.8 ppm) of 5-BPA (**Fig. 2B**) and benzene ring ( $\delta = 7.5$  ppm, 7.8 ppm, 7.9 ppm, 8.1 ppm) of PBA (**Fig. 2C**) in the  $^1\text{H}$ -NMR spectra. Conjugation efficiency was 65% and 78% respectively.

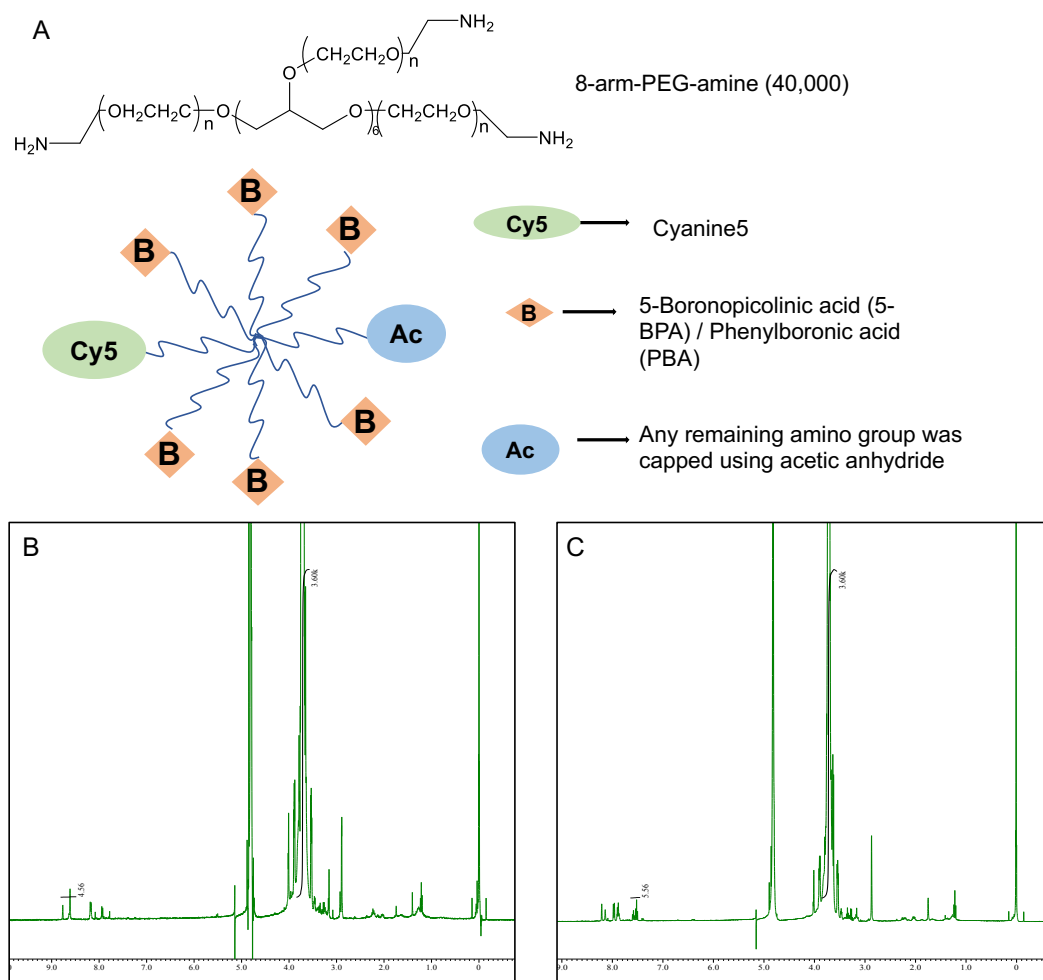


**Figure 2.** A) Design strategy of 8-arm PEG conjugating boronic acid derivatives.  $^1\text{H}$ -NMR spectra of **B)** 5-BPA-Cy5-8-arm-PEG<sub>40K</sub> and **C)** PBA-Cy5-8-arm-PEG<sub>40K</sub> measured in  $\text{D}_2\text{O}$  at  $25^\circ\text{C}$ .

## 5.3.2 T cell proliferation assay

### 5.3.2.1 Jurkat cells

The ability of lectin to induce proliferation of human lymphocytes was first observed by Nowell<sup>13</sup>. He found phytohaemagglutinin (PHA) from *Phaseolus vulgaris* induces aggregation of erythrocytes and induced proliferation of lymphocytes. Since then there have been numerous studies of activation of T cells using lectin<sup>14</sup>. As boronic acid have weak but similar binding to glycans, thus use of boronic acid conjugated polymer as synthetic lectin to induce proliferation of T cells have been explored<sup>12</sup>. To verify the ability of boronic acid polymer to activate T cells initial experiments were carried out using jurkat cell line. Jurkat cells are immortalized human T lymphocytes and were developed four decades ago by Gillis & Watson to study T-cell receptors (TCRs)<sup>15</sup>. They discovered jurkat cells can be stimulated with PHA to produce interleukin-2 (IL-2). Thus, jurkat cell line is being used as an model for *in vitro* studies of human T cells<sup>16</sup>. To assess if PBA and 5-BPA conjugated 8-arm-PEG can induce proliferation of jurkat cells we evaluated them against free small molecule PBA and 5-BPA. We incubated the cells with 8-arm-PEG-5-BPA, 8-arm-PEG-PBA, 5-BPA and PBA molecule at pH 7.4 and pH 6.5 for 48 h. We performed the experiment in two different pH as the binding of boronic acid derivatives are different<sup>17</sup>. At pH 7.4 both 8-arm-PEG-5-BPA and 8-arm-PEG-PBA induced three times higher cell proliferation compared to control (no treatment, only media) (**Fig 3A**). Whereas, neither of the small molecules 5-BPA or PBA showed any increase in proliferation (**Fig 3B**). This could be due to the multivalency properties exert by the multiple boronic acid conjugated 8-arm-PEGs. Such phenomenon was also observed previously with a long chain polymer with PBA conjugation<sup>12</sup>. The % proliferation at pH 6.5 was also significantly higher for both 8-arm-PEG-5-BPA and 8-arm-PEG-PBA (**Fig 4A**) but comparatively lower than pH 7.4 condition.

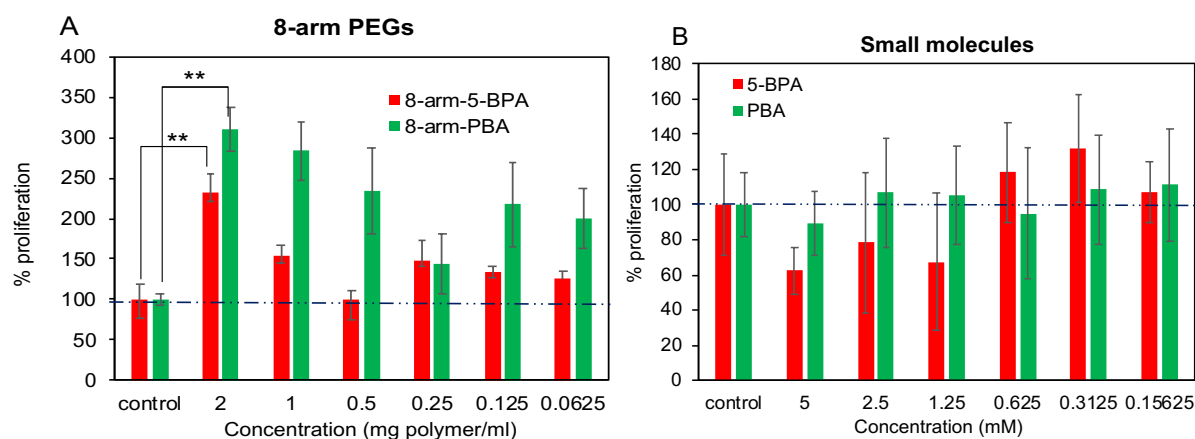


**Figure 3.** *In vitro* proliferation of Jurkat cells at pH 7.4 after stimulation with **A)** 8-arm-PEG-5-BPA & 8-arm-PEG-PBA and **B)** 5-BPA and PBA for 48 h. Data are presented as average  $\pm$  standard deviation (S.D.) (n=3).  $**p < 0.01$  calculated by Student's t tests.

Cells tend to die at pH 6.5 condition. Similar to pH 7.4 experiment neither of the small molecules 5-BPA or PBA showed any increase in proliferation (**Fig 4B**). From this experiment we can verify that both 8-arm-PEG-5-BPA and 8-arm-PEG-PBA have the ability to induce proliferation of jurkat cells. It is essential to have multiple boronic acid binding site to induce T cell proliferation.

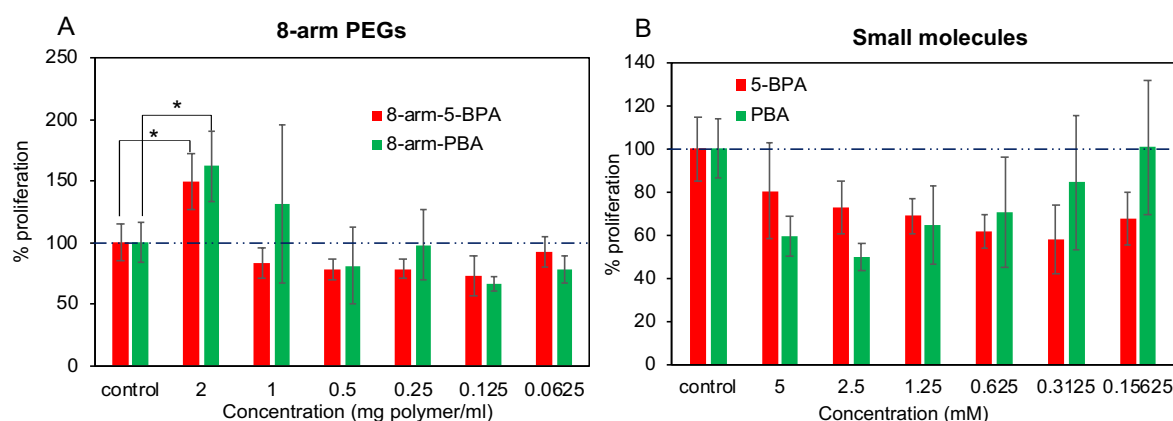


**Figure 4.** *In vitro* proliferation of Jurkat cells at pH 6.5 after stimulation with **A)** 8-arm-PEG-5-BPA & 8-arm-PEG-PBA and **B)** 5-BPA and PBA for 48 h. Data are presented as average  $\pm$  standard deviation (S.D.) (n=3).  $*p < 0.05$  calculated by Student's t tests.

### 5.3.2.2 Mouse T cells

Motivated by the ability of boronic acid conjugated polymers ability to induce higher proliferation in jurkat cells we assessed if such activation can also be observed in cells collected from mice lymph nodes. For this purpose we collected lymph nodes of wild type BALB/c mice . We incubated the lymphocytes with 8-arm-PEG-PBA and PBA molecule at pH 7.4. We only performed the experiment using 8-arm-PEG-PBA as it showed better proliferation compared to 8-arm-PEG-5-BPA in jurkat cell assay. Increase in % proliferation after stimulation with 8-arm-PEG-PBA was identical to our jurkat cell assay almost three times compared to control (no treatment, only media) (**Fig. 5**). As expected, the small molecule PBA again did not demonstrate such proliferation ability like the polymer (**Fig. 5**). Thus, our preliminary experiments confirm the ability of 8-arm-PEG-PBA to induce proliferation in cells collected from mice. Moreover, the importance of having multiple binding site for prompting such activation was also well evidenced.

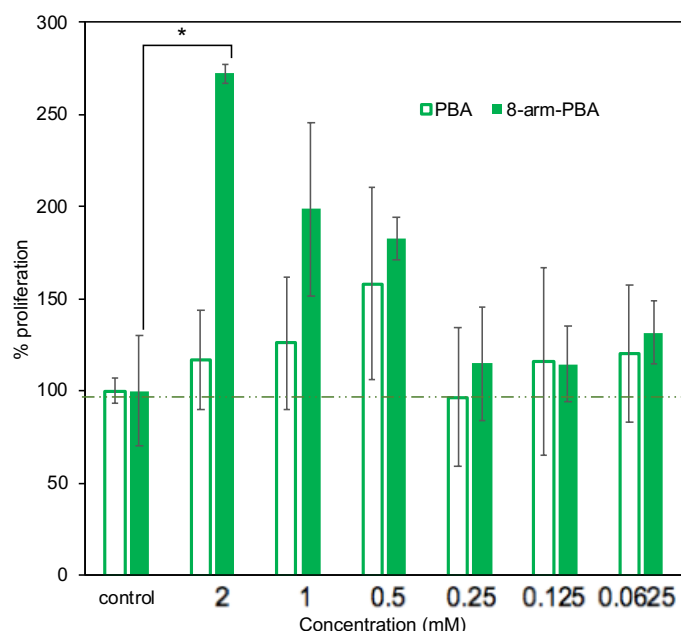


**Figure 5.** *In vitro* proliferation of lymphocytes after stimulation with 8-arm-PEG-PBA and PBA for 48 h. Data are presented as average  $\pm$  standard deviation (S.D.) (n=3). \* $p < 0.05$

calculated by Student's t tests.

### 5.3.3 Staining of CD4 and CD8

Through our jurkat cell and mouse lymphocyte assay it is quite evident that boronic acid conjugated 8-arm-PEGs exerts lectin like behavior and can induce proliferation. To better understand what kind of T cell sub-population they are affecting we evaluated cells collected from mouse thymus and lymph nodes for CD4 and CD8 population. First evaluation was done right after collection to quantify the amount of CD4 and CD8 positive cells in thymocytes and lymphocytes. The ratio of CD4<sup>+</sup> and CD8<sup>+</sup> cells were 2:1 in cells collected from lymph nodes and most of the cells accounted for were double negative (**Fig. 6A**). Whereas, the ratio of CD4<sup>+</sup> and CD8<sup>+</sup> cells was almost 1:1 and most of the cells accounted for were double positive (**Fig. 6B**). The ratio values were similar to that of already reported in mice<sup>18</sup>. We optimized the protocol for staining cells with CD4 and CD8 antibodies and analysis by flow cytometry.

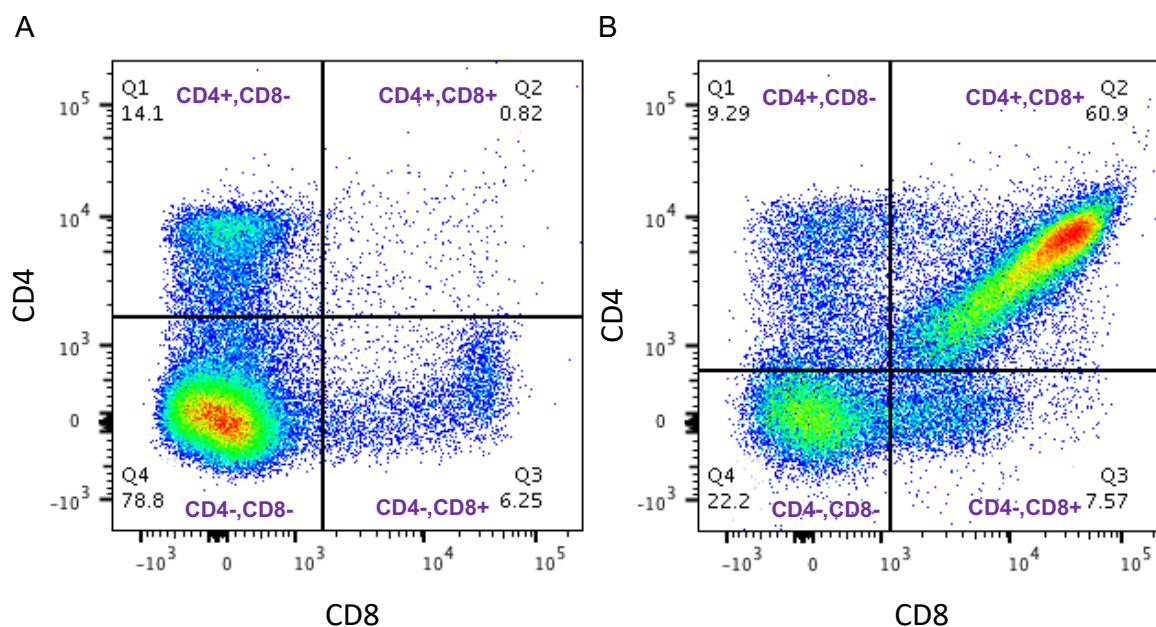


**Figure 6:** Evaluation of CD4 and CD8 positive cells collected from mice **A)** lymph nodes and **B)** thymus right after collection before treatment with boronic acid conjugated polymers.

The optimized protocol was followed to analyze cell fraction after polymer treatment. Then we incubated the cells with 8-arm-PEG-5-BPA & 8-arm-PEG-PBA for 48 h and evaluated for CD4 and CD8 positive cells. 8-arm-PEG-PBA treated cells collected from lymph node and thymus demonstrated more than 50% CD4+ staining cells (**Fig. 7A & B, green bar**). There were around 10% and 20% double positive staining in lymph node and thymus cell population respectively (**Fig. 7A & B, green bar**). On the contrary, cells collected from lymph nodes and treated with 8-arm-PEG-5-BPA were mostly double negative (**Fig. 7A, red bar**) but cells collected from thymus showed small but significant amount of CD8+ staining (**Fig. 7B, red bar**). This study suggests depending on the structure of boronic acid molecule conjugated polymers might interact with specific subpopulation to exert an affect. Matsumoto et al. also demonstrated different binding ability of different boronic acids depending on the glycan<sup>19</sup>. Specific reason for such altered staining is not clear and more in depth studies need to carry out to understand the mechanism.

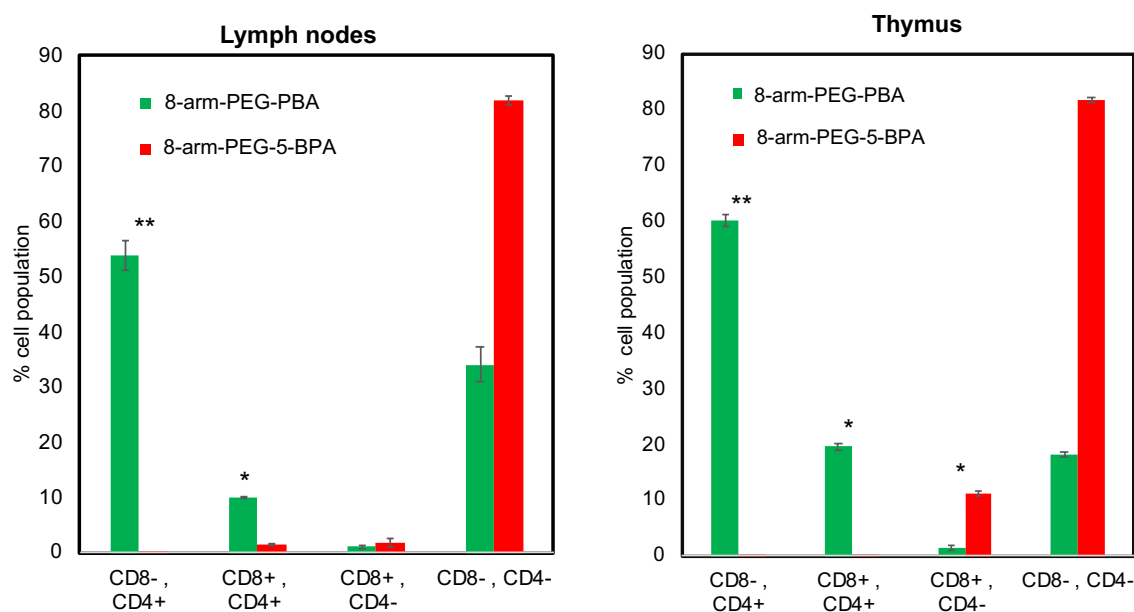


**Figure 7:** Evaluation of CD4 and CD8 positive cell in mouse **A)** lymphocytes and **B)** thymocytes after incubation with 8-arm-PEG-5-BPA & 8-arm-PEG-PBA for 48 h. Data are presented as average  $\pm$  standard deviation (S.D.) (n=3). \* $p < 0.01$  and \*\* $p < 0.001$  calculated

by Student's t tests.

## 5.4 Discussion

The ability of 8-arm-PEG-PBA and 8-arm-PEG-5-BPA to induce T cell proliferation was validated using immortalized human T lymphocytes (Jurkat cells) at pH 7.4 and pH 6.5. The activation ability demonstrated by the polymers were not replicated by small molecule PBA or 5-BPA verifying the necessity of multiple binding site for engaging cell surface glycan to induce proliferation similar to several binding pockets of lectin. T cells collected from mouse lymph nodes also demonstrated 3 fold higher proliferation upon incubation with 8-arm-PEG-PBA but not with free PBA. 8-arm-PEG-PBA treatment also showed significantly higher induction of CD4<sup>+</sup> in cells collected from both lymph nodes and thymus. On the contrary, thymus cells that were treated with 8-arm-PEG-5-BPA demonstrated significant impact on CD8<sup>+</sup> cells.

## 5.5 Conclusion

To conclude it was confirmed that boronic acid conjugated polymer system can behave like a mitogen and induce proliferation T cells. Higher proliferation in both Jurkat cells and mouse T cells confirms potential of boronic acid conjugated polymer system for *in vitro* T cell expansion. More studies need to be conducted to understand the mechanism fully. Different effect on CD4 and CD8 fraction instigated by 5-BPA and PBA conjugated polymer certifies the importance of boronic acid structure in such phenomenon. Thus our preliminary studies suggest 5-BPA or PBA conjugated polymers have the potential to work as synthetic lectin to induce *in vitro* T cell proliferation.



## 5.6 References

1. Hwang, J.-R., Byeon, Y., Kim, D. & Park, S.-G. Recent insights of T cell receptor-mediated signaling pathways for T cell activation and development. *Exp. Mol. Med.* (2020). doi:10.1038/s12276-020-0435-8
2. Waldman, A. D., Fritz, J. M. & Lenardo, M. J. A guide to cancer immunotherapy: from T cell basic science to clinical practice. *Nat. Rev. Immunol.* (2020). doi:10.1038/s41577-020-0306-5
3. Sharon, N. Lectins: Carbohydrate-specific Reagents and Biological Recognition Molecules. *J. Biol. Chem.* **282**, 2753–2764 (2007).
4. Carvalho, E. V. M. M., Oliveira, W. F., Coelho, L. C. B. B. & Correia, M. T. S. Lectins as mitosis stimulating factors: Briefly reviewed. *Life Sci.* **207**, 152–157 (2018).
5. Isakov, N., Mally, M. I. & Altman, A. Mitogen-induced human T cell proliferation is associated with increased expression of selected PKC genes. *Mol. Immunol.* **29**, 927–933 (1992).
6. Yau, T., Dan, X., Ng, C. C. W. & Ng, T. B. Lectins with potential for anti-cancer therapy. *Molecules* **20**, 3791–3810 (2015).
7. Otsuka, H., Uchimura, E., Koshino, H., Okano, T. & Kataoka, K. Anomalous binding profile of phenylboronic acid with N-acetylneuraminic acid (Neu5Ac) in aqueous solution with varying pH. *J. Am. Chem. Soc.* **125**, 3493–3502 (2003).
8. Miyazaki, H. *et al.* Boronate-Containing Polymer as Novel Mitogen for Lymphocytes. *Biochem. Biophys. Res. Commun.* **195**, 829–836 (1993).
9. Uchimura, E., Otsuka, H., Okano, T., Sakurai, Y. & Kataoka, K. Totally synthetic polymer with lectin-like function: induction of killer cells by the copolymer of 3-acrylamidophenylboronic acid with N,N-dimethylacrylamide. *Biotechnol. Bioeng.* **72**, 307–314 (2001).
10. Otsuka, H., Ikeya, T., Okano, T. & Kataoka, K. Activation of lymphocyte proliferation by boronate-containing polymer immobilised on substrate: The effect of boron content on lymphocyte proliferation. *Eur. Cells Mater.* **12**, 36–42 (2006).
11. Ando, Y. *et al.* Concanavalin A-mediated T cell proliferation is regulated by herpes virus entry mediator costimulatory molecule. *Vitr. Cell. Dev. Biol. - Anim.* **50**, 313–320 (2014).
12. Uchimura, E., Otsuka, H., Okano, T., Sakurai, Y. & Kataoka, K. Totally synthetic polymer with lectin-like function: Induction of killer cells by the copolymer of 3-

- acrylamidophenylboronic acid with N,N-dimethylacrylamide. *Biotechnol. Bioeng.* **72**, 307–314 (2001).
13. Nowell, P. C. Phytohemagglutinin: An Initiator of Mitosis in Cultures of Normal Human Leukocytes. *Cancer Res.* **20**, 462 LP – 466 (1960).
  14. Kilpatrick, D. C. Mechanisms and assessment of lectin-mediated mitogenesis. *Appl. Biochem. Biotechnol. - Part B Mol. Biotechnol.* **11**, 55–65 (1999).
  15. Gillis, S. & Watson, J. Biochemical and biological characterization of lymphocyte regulatory molecules. V. Identification of an interleukin 2-producing human leukemia T cell line. *J. Exp. Med.* **152**, 1709–1719 (1980).
  16. Abraham, R. T. & Weiss, A. Jurkat T cells and development of the T-cell receptor signalling paradigm 01 2017/5/1. **4**, 1–8 (2017).
  17. Matsumoto, A. *et al.* Heterocyclic boronic acids display sialic acid selective binding in a hypoxic tumor relevant acidic environment. *Chem. Sci.* **8**, 6165–6170 (2017).
  18. Lin, S.-Y., Ardouin, L., Gillet, A., Malissen, M. & Malissen, B. The Single Positive T Cells Found in CD3- $\zeta/\eta$ -/- Mice Overtly React with Self-Major Histocompatibility Complex Molecules upon Restoration of Normal Surface Density of T Cell Receptor-CD3 Complex. *J. Exp. Med.* **185**, 707–716 (1997).
  19. Matsumoto, A. *et al.* Supplementary Information Heterocyclic Boronic Acids Display Sialic Acids Selective Binding under Hypoxic Tumor Relevant Acidic Environment.

# Chapter 6

## Conclusion

## Chapter 6: Conclusion

### 6.1 Conclusion

The main benefit of nanocarriers is that it can deliver loaded anticancer drug to specific site like tumor while avoiding unspecific systemic targeting. Polymeric micelle, i.e. core-shell structure formed by self-assembly of block copolymers is one group of NPs, that have received much attention due to their ability to carry a wide range of molecule in the core, improve blood circulation and avoid recognition by reticuloendothelial system<sup>1</sup>. Their selective and increase accumulation to tumor is attributed to the enhanced permeability and retention (EPR) effect<sup>2</sup>. The targeting of polymeric micelle can be even more selective by installing ligand molecules directly on the micelle surface, for recognizing receptors or antigens present on cancer cells<sup>3</sup>. Sialic acid a compound from sialoglycan group is the terminal sugar of the glycan chain surrounding eukaryotic cell surface. Sialylated antigens occur more frequently than oncogene markers, making them a universal target for ligand-mediated targeting of nanocarriers. Thus development of ligand installed polymeric micelle is essential.

In **Chapter 2**, elevated expression of sialic acid in different *in vitro* cultured murine and human cancer cell lines were confirmed. Relatively high expression of sialic acid in tumor tissue compared to normal tissue was verified. 5-BPA molecule demonstrated higher binding to cancer cell surface sialic acid in acidic pH 6.5 compared to pH 7.4. 5-BPA conjugated model polymer retained the binding affinity to sialic acid. Finally, superiority of 5-BPA as a ligand molecule over PBA was validated using Cy5 dye labeled 5-BPA-8-arm-PEG and PBA-8-arm-PEG through *in vitro* and *in vivo* assessment. 5-BPA-8-arm-PEG demonstrated enhanced cellular uptake at intratumoral pH condition (pH 6.5) and higher tumor accumulation compared to PBA-8-arm-PEG while keeping the similar accumulation in different organs. Thus, proving the rationale of using 5-BPA as a ligand on the surface of polymeric micelles.

In **Chapter 3**, PEG-*b*-PLGA block copolymers with narrow weight distribution and degree of polymerization of 40 were synthesized. 5-BPA was conjugated to the end terminus of PEG-*b*-PLGA using a shorter PEG as spacer through click chemistry. Fluorescent dye labeled PEG<sub>10K</sub>-*b*-PLGA were prepared to construct fluorescent micelle. Before construction of micelles presence of boron diol on 5-BPA and PBA conjugated block-copolymer was confirmed. Finally, DACHPt loaded polymeric micelles were constructed with 50% 5-BPA or PBA on the surface of individual micelles. All the micelles were measured to be around 30 nm in size with narrow size distribution. Drug loading efficiency and surface charge of all the micelles were also comparable. Therefore, it was deemed equitable to compare these micelles for their biological activity to determine the effectiveness of ligand installation.

Biological activity of micelles were studied extensively through cellular and animal experiments in **Chapter 4**. Cellular uptake of the micelles by measuring internalized Pt demonstrated increased uptake of 5-BPA-DACHPt/m at pH 6.5. Similar augmented uptake of 5-BPA-DACHPt/m was also replicated during CLSM studies using fluorescent labeled micelles. Such enhanced cellular uptake of 5-BPA-DACHPt/m was confirmed to occur due to interaction with cell surface sialic acid by removing sialic acid through sialidase treatment. 5-BPA-DACHPt/m demonstrated lower IC<sub>50</sub> value and better efficiency in eliminating CSC population *in vitro*. *In vivo* blood circulation and plasma clearance of all the micelles was almost identical. Nevertheless, 5-BPA-DACHPt/m demonstrated significantly higher tumor accumulation and retention compared to PBA-DACHPt/m and non-ligand DACHPt/m. Such improved accumulation of 5-BPA-DACHPt/m was translated during antitumor studies with improved tumor growth suppression. Consequently, producing better survival of animals probably by eliminating CSC population.

Potential of boronic acid conjugated polymer system as a mitogen to induce T cell proliferation was explored in **Chapter 5**. 5-BPA and PBA were conjugated to 8-arm-PEGs for

their multivalent binding sites. 5-BPA and PBA conjugated to 8-arm-PEGs induced proliferation of immortalized human T lymphocytes (jurkat cell), but such phenomenon did not occur with small molecules. T cells collected from mouse lymph nodes also demonstrated 3 fold higher proliferation upon incubation with 8-arm-PEG-PBA but not with free PBA. 8-arm-PEG-PBA treatment showed significantly higher induction of CD4<sup>+</sup> in cells collected from both lymph nodes and thymus. On the contrary, thymus cells that were treated with 8-arm-PEG-5-BPA demonstrated significant impact on CD8<sup>+</sup> cells. Therefore, signifying potential of boronic acid conjugated polymers as synthetic lectin to induce *in vitro* T cell proliferation.

## 6.2 Future Perspectives

Our results proved that, by installing 5-BPA on the surface of polymeric micelles, we can increase the tumor targeting ability, which can improve suppression of tumor growth and survival in CSCs rich tumor model. Our results also support specific binding ability of 5-BPA to SA in intratumoral acidic pH. Combination of overexpression of SA, scarcity of glucose and acidic pH condition in tumor microenvironment could make 5-BPA as an excellent ligand for selective targeting of cancer cells. Our findings also showed the unique ability of PBA conjugated polymers in inducing T cell proliferation *in vitro*. Future direction for 5-BPA as a ligand to target SA in cancer for developing antitumor therapy and PBA installed polymer as a immunomodulator are outlined separately.

### 6.2.1 5-BPA installed polymeric micelle

5-BPA can be a potent ligand for tumor targeting, as validated through the modification of small molecules, polymers and polymeric micelles loading anticancer drug. Moreover, I demonstrated through extensive cellular and animal studies that 5-BPA-DACHPt/m improved

tumor targeting and antitumor efficacy due to specific interaction of 5-BPA with SA at intratumoral acidic pH. DACHPt loaded polymeric micelles (NC-4016) is undergoing phase I clinical trials for treating solid tumors and lymphoma (Study NCT01999491)<sup>4</sup> after demonstrating better performance in a xenograft model of gastric cancer<sup>5</sup>. We hypothesize by installing 5-BPA ligand on the surface of DACHPt loaded micelle to specifically target cancer cells can further improve the treatment outcome. Our smart ligand system not only improved delivery of cytotoxic drugs, but also were effective in eliminating resistant CSCs, thus improving animal survival significantly. As overexpression of SA and acidic tumor microenvironment are common features of tumors, 5-BPA molecule as a ligand will have broad application for diagnosis and therapy of cancer and other applications in the field of bioengineering.

### 6.2.2 PBA installed polymer as immunomodulator

The ability of our boronic acid-conjugated polymer systems for inducing T cell proliferation suggest the prospective of such synthetic lectin to induce proliferation of T cells *in vitro*. Lectins have the ability to activate and proliferate T cells probably through interaction with surface glycan of T cell receptors (TCR)/CD3 complex that initiate a cascade of reaction involving activation of enzyme protein kinase C (PKC) and some particular PKC genes<sup>6</sup>. Such lectin activation of T cells have generated cells with extraordinary cytotoxic activity<sup>7</sup>. There are beads (ThermoFisher) and culture plates (BD Biosciences) coated with anti-CD3 antibodies available in the market for the stimulation of T cell proliferation. As, boronic acids are recognized as synthetic lectin they possibly binds to the TCR/CD3 to exert proliferation of T cells similar to lectin. I perceive the potential of developing *in vitro* culture systems coated with boronic acid conjugated polymer which can lead to more efficient and cost-effective technique for culturing T cells, as well as potential for developing novel immunotherapeutic approaches

against cancer.

## 6.3 References

1. Cabral, H., Miyata, K., Osada, K. & Kataoka, K. Block Copolymer Micelles in Nanomedicine Applications. *Chem. Rev.* **118**, 6844–6892 (2018).
2. Matsumura, Y. & Maeda, H. A. A new concept for macromolecular therapeutics in cancer-chemotherapy - mechanism of tumoritropic accumulation of proteins and the antitumor agent Smancs. *Cancer Res* **46**, 6387-6392. (1986).
3. Mi, P., Cabral, H. & Kataoka, K. Ligand-Installed Nanocarriers toward Precision Therapy. *Adv. Mater.* **1902604**, 1902604 (2019).
4. Varela-Moreira, A. *et al.* Clinical application of polymeric micelles for the treatment of cancer. *Mater. Chem. Front.* **1**, 1485–1501 (2017).
5. Yamamoto, Y. *et al.* Effect of combined treatment with the epirubicin-incorporating micelles (NC-6300) and 1,2-diaminocyclohexane platinum (II)-incorporating micelles (NC-4016) on a human gastric cancer model. *Int. J. Cancer* **135**, 214–223 (2014).
6. Isakov, N., Mally, M. I. & Altman, A. Mitogen-induced human T cell proliferation is associated with increased expression of selected PKC genes. *Mol. Immunol.* **29**, 927–933 (1992).
7. Yau, T., Dan, X., Ng, C. C. W. & Ng, T. B. Lectins with potential for anti-cancer therapy. *Molecules* **20**, 3791–3810 (2015).



## Publications

### Original articles

1. **T. Khan**, K. Igarashi, A. Tanabe, T. Miyazawa, S. Fukushima, Y. Miura, Y. Matsumoto, T. Yamasoba, A. Matsumoto, H. Cabral and K. Kataoka. *Structural Control of Boronic Acid Ligands Enhances Intratumoral Targeting of Sialic Acid to Eradicate Cancer Stem-Like Cells*. ACS ABM (2020)
2. O. Schäfer, T. Miyazaki, L. Braun, L. Capeloa, **T. Khan**... K. Kataoka, H. Cabral and M. Barz. *Block-Sequence of Reactive Triblock Copolypept(o)ides Dictates Self-Assembly and Intratumoral RNAi*. (Submitted).
3. JD. Martin, M. Panagi, A. Hosoi, **T. Khan**... T. Stylianopoulos and H. Cabral. *Microenvironment Normalizing Schedule of Glucocorticoid Steroids Potentiates Immune Checkpoint Blockade in Metastatic Triple Negative Breast Cancer*. (in preparation)
4. C. Qin, X. Hou, **T. Khan**, N. Nitta; M. Yanagawa, Y. Sakurai, M. Suzuki, S. Masunaga, H. Tanaka, Y. Sakurai, H. Takahashi. I. Aoki, H. Yanagie and H. Cabral. *Enhanced MRI-Guided Gadolinium Neutron Capture Therapy by Polymeric Nanocarriers Promoting Tumor Accumulation and Intracellular Delivery*. ChemNanoMat. (2020).
5. JD. Martin, M. Panagi, C. Wang, **T. Khan**, M. Martin, C. Voutouri, K. Toh, P. Papageorgis, F. Mpekris, C. Poldorou, G. Ishii, S. Takahashi, N. Gotohda, T. Suzuki, M. Wilhelm, V. Melo, S. Quader, J. Norimatsu, R. Lanning, M. Kojima, M. Stuber, T. Stylianopoulos, K. Kataoka and H. Cabral.. *Dexamethasone Increases Cisplatin-Loaded Nanocarrier Delivery and Efficacy in Metastatic Breast Cancer by Normalizing the Tumor Microenvironment*. ACS Nano (2019).
6. G. Lo Huang, A. Tao, T. Miyazaki, **T. Khan**, T. Hong, Y. Nakagawa and H. Cabral. *PEG-Poly(1-Methyl-L-Tryptophan)-Based Polymeric Micelles as Enzymatically Activated Inhibitors of Indoleamine 2,3-Dioxygenase*. Nanomaterials (2019).

7. A. Matsumoto, A.J. Stephenson-Brown, **T. Khan**, T. Miyazawa, H. Cabral, K. Kataoka and Y. Miyahara. *Heterocyclic Boronic Acids Display Sialic Acids Selective Binding under Hypoxic Tumor Relevant Acidic Environment*. Chem. Science (2017).

## Conferences

### Domestic proceedings

1. **T. Khan**, A. Matsumoto, H. Cabral and K. Kataoka. The 34<sup>th</sup> Annual meeting of the Japan Society of the Drug Delivery System, Nagasaki, Japan, June 2018 (Poster).

### International proceedings

1. **T. Khan**, A. Matsumoto, H. Cabral and K. Kataoka. Biomaterials International , Tokyo, Japan, July 2018 (Poster).
2. **T. Khan**, K. Igarashi, A. Matsumoto, H. Cabral and K. Kataoka. 32nd International Microprocesses and Nanotechnology Conference , Hiroshima, Japan, October 2019 (Oral presentation).

## Awards

Young authors travel award MNC 2019.

## Patent

A. Matsumoto, T. Miyazawa, Y. Miyahara, H. Cabral, **T. Khan**, K. Miyata,, ボロン酸によるシアル酸認識と医学応用 .Application number: 13B177006-1, Application date: 平成 29 年 7 月 20 日.

